Novel Configurations of Atomic beam and Laser Beam for Micro and Nanolithography

by
Kamlesh Mukundrao Alti

Department of Physics
Indian Institute of Technology Guwahati,
Guwahati – 781039, India.
July, 2005.

Novel Configurations of Atomic beam and Laser Beam for Micro and Nanolithography

A Thesis Submitted
in Partial Fulfillment of the Requirements
for the Award of the Degree of
DOCTOR OF PHILOSOPHY

by
Kamlesh Mukundrao Alti

To the
Department of Physics
Indian Institute of Technology Guwahati,
Guwahati – 781039, India.
July, 2005.

Dedicated to

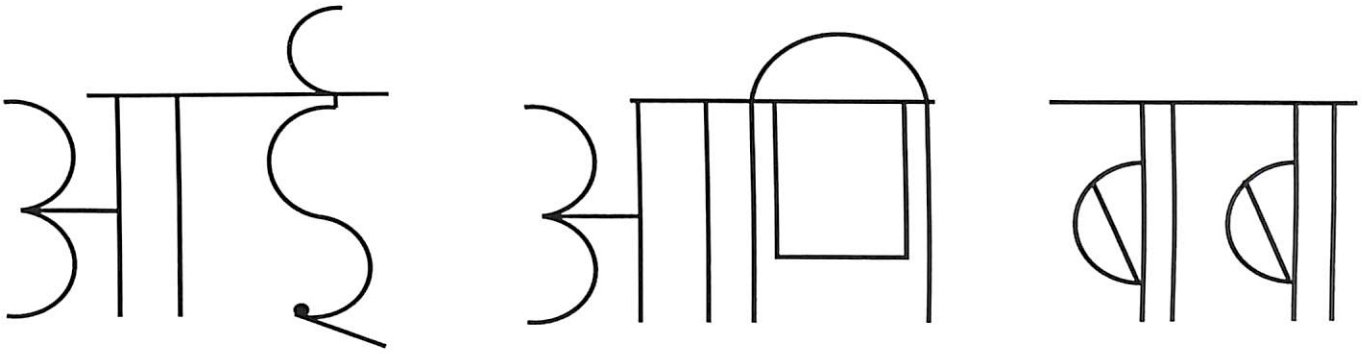

Mom and Dad

Indian Institute of Technology Guwahati
Department of Physics
North Guwahati, Guwahati-781039, Assam State, INDIA
Phone: +91 361 2582705, 2690321 to 328 (extn. 2705), Fax: +91 361 2690762
Dr. Alika Khare
Associate Professor
E-mail: alika@iitg.ernet.in, k_alika@yahoo.com

Certificate

It is certified that work contained in the thesis entitled "**NOVEL CONFIGURATIONS OF ATOMIC BEAM AND LASER BEAM FOR MICRO AND NANOLITHOGRAPHY**" by **Mr Kamlesh Mukundrao Alti** (Roll no. 01612101), a student in the Department of Physics, Indian Institute of Technology Guwahati, for the award of degree of Doctor of Philosophy, has been carried out under my supervision and that this work has not been submitted elsewhere for a degree.

Date: July 14, 2005

Dr Alika Khare 14/7/05
(Thesis Supervisor)
Associate Professor
Department of Physics
I I T Guwahati

Acknowledgements

I am greatly indebted to Dr. Alika Khare for the support she has extended to me throughout my work towards this thesis, and for her informed guidance and advice. We have many insightful conversations during the development of the ideas in this thesis. Her patience and willingness to discuss the minutiae of the different obstacles I encountered while working on this project were invaluable.

I am very much benefited from the critical comments on this work by all the doctoral committee members; Dr. Charudutt Kadolkar, Dr. M. K Nandy and Dr. P. K. Giri.

I am thankful to Dr. Pratima Agarwal for allowing me to use thermal evaporation unit for thin film deposition.

I am thankful to Mr. Sidananda Sarma, Mr. Chandan Borgohain, Mr. Lokesh Chakraborty, Mr. Atul Deka, Mr. Basab Bijoypurkayastha and Mr. Madan Deka for their technical assistance.

I like to thank Head of Department of Mechanical Engineering for allowing me to use optical microscope facility and to all the members of Mechanical workshop for helping me in designing and fabricating the components used in the experiments. I also like to thank Head of Central Instruments Facility for providing EDAX facility.

I am deeply indebted to all the faculties of Physics department, Nagpur university, for motivating me to took research career in Physics.

My special thanks goes to Mr. Ardhendu Sekhar Patra, Mr. Susanta Das, Mr. Purnananda Nandi, Mr. Santanu Sinha, Mr. Pramod Nayak, Mr. Amal Medhi and to all immediate seniors and juniors of the Department of Physics, IIT Guwahati for their cooperation, timely help and support they have rendered me throughout my stay in IIT campus.

My close friends, Prafull and Devendra who always stood by my side asking over and over again "Is it over? What are you doing in Guwahati from the past four years?"

This thesis is dedicated to my parents, Saroj and Mukund Alti, who have always supported me in my endeavors, always given me the strength and encouragement to follow my dreams, and have never left me in doubt of their love for me.

Abstract

Present work mainly focus on two lithographic techniques viz; selective laser ablation lithography and atom lithography using dipole force.

The work on atom lithography using dipole is on simulation of atomic trajectories under dipole force using semi-classical technique for various configuration of atomic beams and light fields to focus down the atomic beam at sub-micron level. Through these studies new configuration of light fields and atomic beams were proposed for their applications in the field of microlithography and nanolithography. We proposed the use of square arrays of multiple atomic lens produced by interference of four nearly collinear optical beams in atom lithography using dipole force. This configuration is useful in writing large number of micro-periodic structures in square arrays in a single step via atom lithography. A novel configuration of microscopic square arrays of atomic beams (matrix of micro-ovens) in presence of TEM_{00} mode laser, acting as a atomic lens, is proposed for atom lithography via dipole force for obtaining sub $\lambda/2$ periodic structures.

Application of dipole force in the isotopic separation was also proposed. As an example, a scheme for the enrichment of U^{235} using dipole force generated by a red detuned TEM_{00} mode of laser with respect to U^{235} transition is discussed

Atom lithography technique needs fairly collimated atomic beam. Therefore we have developed a new technique of generation of cold atomic beam having low divergence using

laser ablation without using any collimation optics. The axial velocities and divergence of atomic beam was studied as a function of laser energy.

Selective laser ablation technique is demonstrated for obtaining one and two dimensional periodic structures ranging from micron to sub-micron level using high power multiple laser beam interferometry in a single shot. The advantage of this technique over other technique is also discussed.

The proposed configuration of matrix of micro-ovens for obtaining large number of periodic atomic beams is experimentally realized via selective laser ablation lithography in one as well as two dimension for the first time.

Table of Contents

List of Figures

List of Tables

Chapter 1

Introduction

Materials prepared in the form of periodic structure arrays of nanometer dimensions displays interesting distinguish behavior as compared to their bulk counterparts [1, 2]. Quantum confinement of electrons in nanostructured materials leads to remarkable changes in their quantum states [3] which subsequently changes the electronic and optical properties of the material. The periodic submicron- nano arrays of materials of desirable electronic properties [4, 5] leads to the shrinking of chips [6], increasing the capabilities of data storage devices [7], giant magneto-resistive materials [8] and gas sensors [9]. The nanostructures with desirable optical properties can lead to photonic devices [10, 11], optical switches [12], optoelectronic devices [13] and continuously tunable organic laser [14] with 1-d periodic lines of required material.

A number of lithographic techniques have been explored for fabrication of periodic structures of nano dimension for tailoring electronic, magnetic and optical properties of materials for the fabrication of efficient devices with improved spatial resolutions and fast temporal response. An overview of existing lithographic techniques is given below for engineering the materials of nanometer dimensions.

1.1 Lithographic techniques

Various lithographic techniques are optical lithography, electron and ion beam lithography, X-ray lithography, scanning probe lithography and laser interference lithography. Atom lithography via dipole force is another upcoming scheme for writing the whole periodic structure in a single step. Atomic scale lithography is reported recently [15] for the fabrication of single electron device.

1.1.1 Optical lithography

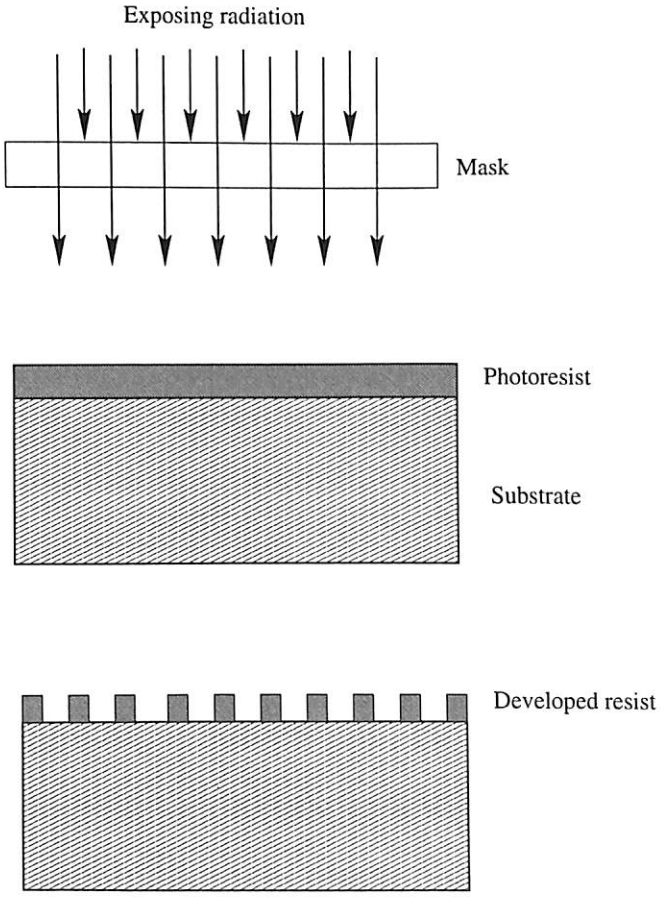

Figure 1.1: Basic steps of optical lithography

The optical lithography [16–18] refers to a lithographic process that uses visible or ultraviolet light to form patterns on the photo-resist through printing. Printing is the process

of projecting the image of the pattern onto the wafer surface using a light source and a photo mask. There are three types of printing - contact, proximity, and projection printing. Fig. 1.1 depicts the basic principle of optical lithography. The basic steps involved in optical lithography process are exposure of photoresist to radiation (Visible, UV, X-rays) via mask followed by development of resist through etching and washing.

The resolution of optical lithography technique is limited to the order of wavelength of the radiation as well as to the numerical aperture (NA) of the optics used for this lithographic technique. Another major limitation besides resolution in optical lithography is the depth of focus. Using a lens with a higher NA will result in better resolution of the image, but as the depth of focus of a lens is inversely proportional to the square of the NA, so improving the resolution by increasing the NA reduces the depth of focus of the system. To improve the resolution by this technique, the use of shorter wavelength is necessary. The short wavelength light sources are expensive. New lasers towards short wavelength are required to be developed or an synchrotron is required for EUV or X-ray lithography [19] for smaller dimension. Moreover the optics required for UV and X-ray lithography is an area of research [20] even today.

1.1.2 Electron and Ion beam lithography

Electron beam lithography (EBL) [21] and Ion beam lithography (IBL) [22] are used commercially for writing down to sub-100 nm. The schematics of EBL/IBL is shown in Fig. 1.2. It uses a focused high energy beam of electrons/ions for the material removal/deposition for imprinting the circuit pattern. The actual EBL or IBL system is very complicated as compared to that of shown in the schematic of Fig. 1.2. It consists of an electron/ion source, an electron/ion column that 'shapes' and focuses the electron/ion beam onto the substrate and a mechanical stage that positions the wafer under the electron/ion

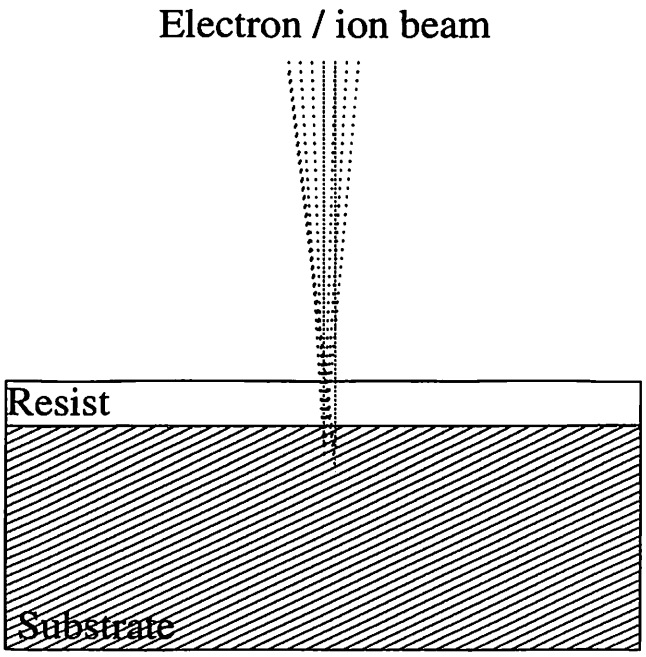

Figure 1.2: Electron lithography

beam for the pattern writing.

These techniques offers higher patterning resolution than optical lithography because of the shorter wavelengths of the charged particles used. The resolution of these techniques are limited due to chromatic aberration, space charge effect of beam and electron scattering in the resist. There are also chances of damaging the substrate in these type of lithographic systems because of the involvement of high energy (10-50 keV) charged particles beam.

1.1.3 Scanning probe lithography

Advent of scanning probe microscopy (SPM) has opened up a new era of scanning probe lithography [23]. In scanning probe lithography (SPL), cantilever of scanning tunneling microscope (STM) or the atomic force microscope (AFM) is used to pattern nanometer-scale features.

STM probe [24] can be used to make patterns on Self-Assembled Monolayer (SAM)

by applying voltage pulse and therefore removing molecules at the nanometer scale. The vacancy created after removal of molecules can be filled with new kind of molecules by applying voltage pulse to STM probe in liquid containing new molecules. STM lithography can also be done by removing atoms via supplying tension impulses.

Just as a pen is used for writing on a paper's surface, it is possible to write on a surface with a tip of atomic force microscope which can result into surface modifications at the nanometer scale [25, 26]. Surfaces can be modified by physically scratching it or by directly depositing molecules onto it by using electric fields with the help of AFM cantilever. AFM lithography can also be obtained using conductive tips and sample in order to produce nano-oxidation. This process is based on negatively biasing the tip with respect to the substrate under ambient conditions. With the proper tip voltage, the substrate can be locally oxidized, and by moving the tip in contact mode or non-contact mode across the surface, a line can be written.

Resolution of these techniques depends on scan rate and bias voltage. The processing speed of SPM lithography is too slow for implementation in actual device construction. There have been some efforts to construct parallel processing SPM devices with multi-tip cantilevers [27]. These techniques are material selective and expensive. This limits their implementation at the commercial level.

1.1.4 Atom lithography using dipole force

Atom lithography using dipole force [28–31] is a new upcoming technique which can overcome some of the limitations of already existing techniques. It offers massive parallelism without using any material mask. This technique uses the dipole force [32, 33] for focusing the atomic beam down to tens of nanometer in a periodic one-, two-,and three-dimensional structures [34, 35]. This technique has an advantage of producing complicated structures

without using any physical masks [36, 37] in a single step. As the de Broglie wavelength of neutral atoms is very small (<0.1 nm for thermal atomic beam), this lithographic technique has the potential for high resolution. Moreover, the low energy atomic beam used in this lithography does not damage the substrate.

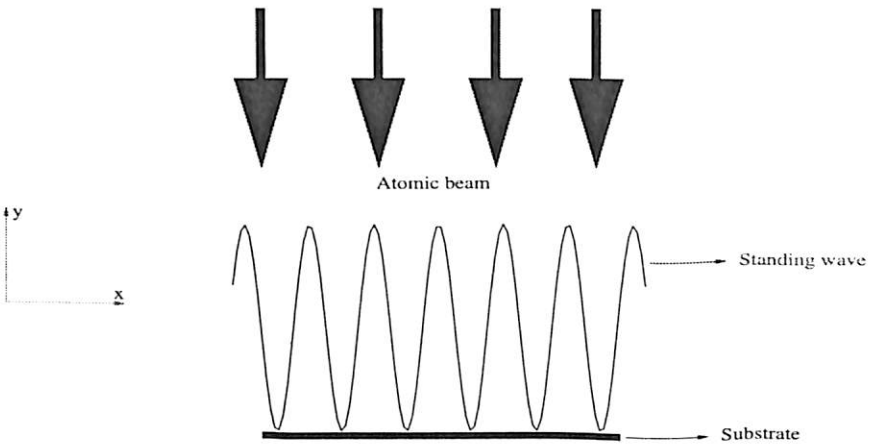

Figure 1.3: Basic principle of atom lithography using dipole force in presence of standing wave

An atom in a radiation field experiences two kinds of forces. The radiation pressure force resulting from the absorption, followed by the random spontaneous emission of photons. The magnitude of this force is limited by the rate of spontaneous emission and saturates as the laser intensity increases. This dissipative spontaneous force is responsible for laser cooling [33]. Ashkin [38] was the first to demonstrate the trapping and acceleration of micron size particles. Subsequently, he also reported atomic-beam deflection by resonance radiation pressure [39]. The second kind of force is called as the conservative or dipole force, originates from the interaction of neutral atom with an near resonant, non uniformly distributed laser field. From a pure classical point of view, an atom placed in the radiation field experiences induced dipole moment $\mathbf{p} \propto \mathbf{E}$; $\mathbf{E}$ being electric field associated with the field which results into an interaction potential $U = -\mathbf{p}.\mathbf{E}$. This interaction potential gives rise to the conservative force $\mathbf{F} = -\nabla U$. The magnitude of this force depends on the in-

tensity gradient and amount of detuning and the direction of force depends on the sign of detuning. With the proper configuration of the atomic beam and the laser beam, the trajectories of the atoms can be manipulated so as to focus down the atoms in the periodic nano size structures of desired geometry. The intensity gradient acts as the atomic lens as well as mask and so no additional material mask is required.

Bjorkholm et al. [40] reported the focusing of sodium atomic beam in presence of TEM_{00} mode laser in 1978 for the first time experimentally. Subsequently, they reported [41] a minimum spot size of 28 μm using the same configuration. Aberration problem due to large thickness of atomic lens in their work was overcome by Sleator et al. [42]. They created a cylindrical atomic lens based on the large period standing wave produced by bouncing the laser beam off a glass substrate under very small angle of incidence and successfully focused down the beam of metastable helium atoms down to 4 μm with such lens. The idea of using the standing wave was further developed by Timp et al. [43], where the atomic beam of sodium was launched perpendicular to the standing wave of near resonant radiation field of wavelength λ as shown in Fig. 1.3. Each period of standing wave acts as the cylindrical lens to focus the atomic beam. This results into the grating structure of sodium on the substrate with periodicity $\lambda/2$ (294.3±0.3 nm). Since then, there have been large number of experimental reports on the focusing of atomic beams of chromium [44–48], cesium [49], aluminium [50], ytterbium [51] and iron [52, 53] using dipole force generated by cw optical standing wave. R. Gupta et al. [54] and J. J. McClleland [55] reported the formation of two dimensional arrays of chromium having lattice spacing 212 nm by using the standing waves formed by two orthogonally polarized light. The width of the structure reported by the author was in the range of 80 nm. The dependence of the laser power onto the width of the structure and focusing depth was also discussed [55, 56]. S.J.Rehse et al. [57] have discussed the possibilities to obtain nanostructures of gallium and indium us-

ing this technique. Periodicity of standing wave configuration is always limited to $\lambda/2$. The idea of using polarization gradient masks [58, 59] in atom lithography has been introduced to achieve periodicity down to $\lambda/8$. Periodicity lesser than $\lambda/2$ can also be achieved by switching the detuning of the light field during deposition [60]. It is shown that the material selective characteristics of atom-light interaction can be used for structural doping [61]. Focusing of atomic beam of cesium via dipole force with a pulsed standing wave is also reported [62, 63]. As the pulsed laser can be conveniently converted to short wavelength range via harmonic generators it offers advantages in the application of atom lithography with elements having blue or UV resonance lines thereby reducing the periodicity of the writing. Formation of periodic gratings of atomic density was also observed as a result of interference of atoms diffracted by pulsed optical standing wave [64] having minimum periodicity equal to $\lambda/4$.

Theoretical simulations of trajectories under the dipole force is necessary to understand the process as well as to access the optimum parameters of atom-light interaction for the deposition of required nano structures. The trajectories of atoms under the given configuration of atomic beam as well as the light beam under the dipole force can be computed [65] either by semi-classical approach or by solving the Bloch equations [32] under quantum mechanical formulations. The atomic trajectories via dipole force have been reported for TEM_{00} mode of laser [66], for standing wave configuration with the Gaussian envelop for chromium [67] and He [68] atoms and for Laguerre Gaussian and Bessel light beams for rubidium atoms [69]. Simulations can be performed by Monte Carlo wavefuntion method [70–72] to keep track of wavefuntion during atom-photon interaction. It has the advantage of calculating the diffusion effect caused by spontaneous emissions. C. J. Lee [73] has reported the quantum mechanical analysis of the atom lithography via dipole force. They have performed the simulation by considering the wave nature of atom in

standing wave and analyzed the various broadening effects on the width of the focused atomic spot.

Although Semi-classical approach for atomic trajectories is very fast and helps in visualizing the trajectories under dipole force for various atomic configurations and light fields, but it cannot calculate the modification in trajectories due to the spontaneous emission and consequent diffusion. These classical trajectories using semi-classical approach are valid for far off-resonance detuning and where the internal complexity of the atoms can be ignored.

As the invention of laser cooling enabled to cool the atomic beam in the transverse direction, the use of such 2-d laser cooled neutral atomic beam as a lithographic tool is gaining interest. In this technique, the substrate (gold or silicon) coated with a resist of self-assembling monolayer (SAM) of alkanethiols or organosilicon (which acts as a resist), is exposed to manipulated atomic beam under dipole force. Due to exposure, the resist is selectively inactivated and the pattern can be transferred to the underlying film by an etching process. This technique has been demonstrated first by K.K. Berggren et al. [74] using metastable argon atoms. Since then there have been number of reports on this particular lithography technique using transversely cooled cesium [49], metastable helium [75–77] and barium [78] atomic beam for the production of periodic structures on the resist.

Atom lithography using dipole force is emerging as a promising technique for the generation of precise periodic nanostructures without using any mask in a single step. New configurations of atomic beam and light beam are required to be explored for reducing the periodicity and the size of nano structures via this lithographic technique.

1.1.5 Laser interference lithography

Laser interference lithography (LIL) technique [79–83] is another coming up technique to perform the periodic writing in a single shot with uniformity over a large area. There are two types of laser interference lithographic techniques, viz; based on photoresist and direct write LIL or Selective laser ablation lithography (SLAL).

Laser interference lithography based on photoresist

The schematics of LIL based on photoresist is depicted in Fig. 1.4. A photoresist-coated substrate is positioned at the point of intersection of two coherent light beams. The plane of intersection of two coherent light beam forms a standing wave due to interference, having sinusoidal intensity distribution. Therefore, on exposure of photoresist with this interference pattern yields a periodic line-space pattern whose period, is determined by the wavelength of light (λ), and the angle of intersection of the beams. This lithographic technique

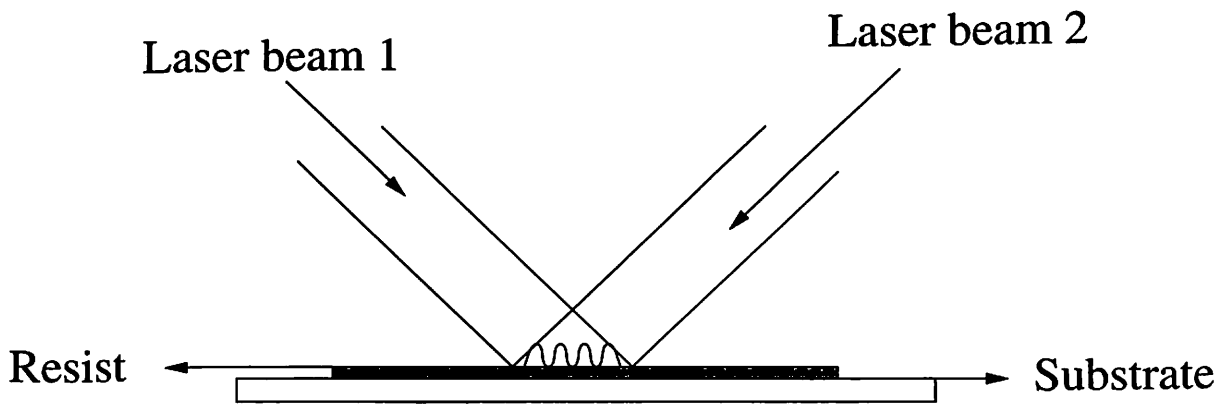

Figure 1.4: Basic principle of laser interference lithography

can be used to write the periodic [79–81] as well as non-periodic [82] patterns in one and two dimensions. The minimum periodicity obtained from LIL technique is always limited to $\lambda/2$. Use of photoresist makes this process multi-step where all the protocols of optical lithography has to be followed.

Selective laser ablation lithography

Selective laser ablation lithography (SLAL) is another new technique [83–85] utilizing the high power laser. This is a direct write lithographic technique. This technique has the capability of producing periodic micro and nano structures in a single step utilizing only a single shot of pulsed high power laser. SLAL involves selective ablation of material of

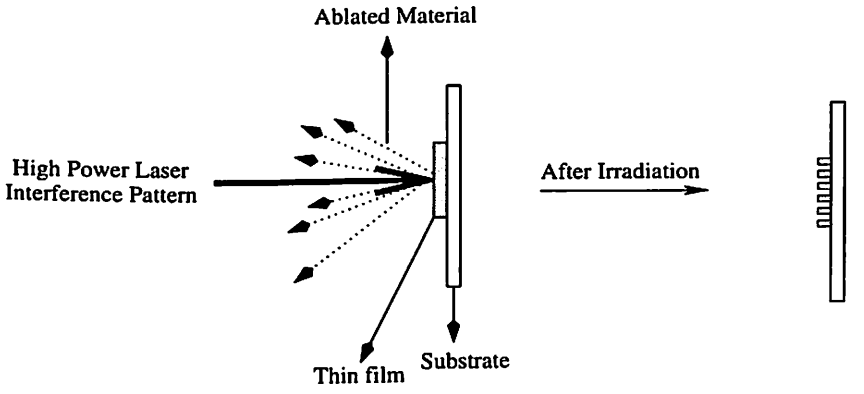

Figure 1.5: Basic principle of direct write laser interference lithography

thin film by high power laser via mask [84] or interference pattern [83, 85] leaving the unexposed portion of the thin film unaffected. Thus the desired pattern is imaged onto the the thin film of material as shown in Fig. 1.5.

Y. Nakata et al. [85] have reported the one and two dimensional periodic structure formation on the thin film by selectively ablating it with the interference pattern formed by femtosecond laser. The interference pattern in this case was highly delocalized. We have reported [83] the formation of periodic lines onto the copper thin film by exposing the thin film with the interference pattern formed by Michelson interferometer. In this technique, the two interfering beams were nearly collinear and hence the transportation of the pattern at the complex location, for example under vacuum, is convenient compared to earlier report [85]. Moreover the spatial frequency of the pattern can be controlled on line by the mirror tilt. The minimum periodicity obtained using this technique is restricted

to $\lambda/2$ but the structure size can be of nanometer scale. This is a single-step single-shot technique making it one of the simplest and fastest technique of lithography.

1.2 Techniques for generation of atomic beam

One of the major requirement of atom lithography discussed in Sec. 1.1.4 is collimated atomic beam. We review here some of the techniques to generate the atomic beam.

1.2.1 Thermal Oven

Thermal oven [86–88] is commonly used technique for generating thermal atomic beam of low melting point materials. It involves heating of the material above its melting point with the help of heating coils, this leads to evaporation of material and formation of divergent beam of constituent atoms. Typical configuration of oven in shown in Fig. 1.6. The divergence and flux of such beams depends on the length (L), diameter (l) of the nozzle and the temperature of the oven. Atomic beam coming from such apparatus have very large divergence and relatively very low particle flux owing to the thermal evaporation. This technique is restricted to materials of low melting points only.

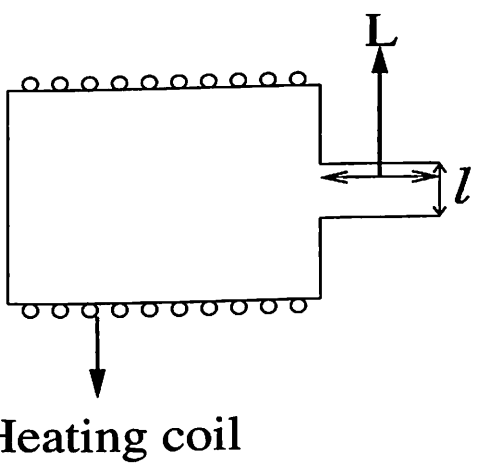

Figure 1.6: Typical geometry of oven

1.2.2 Discharge source

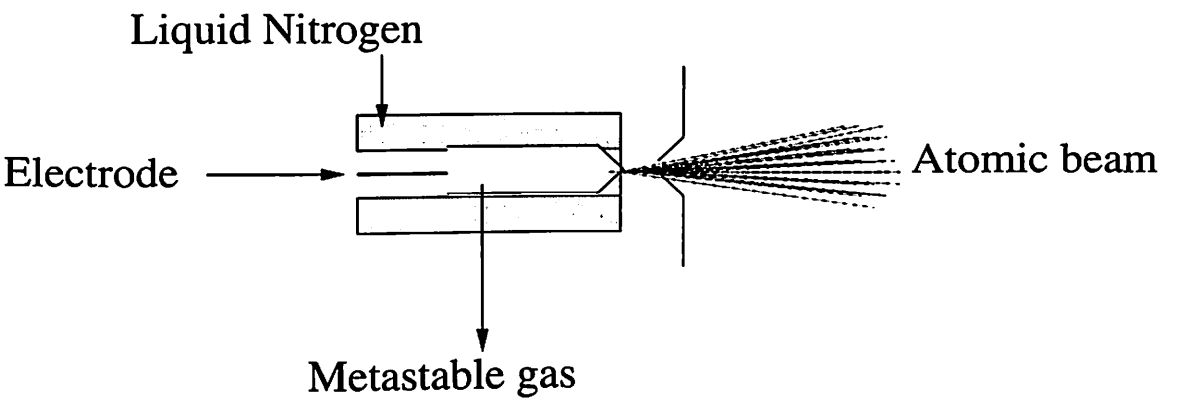

Figure 1.7: Discharge source for atomic beam generation

Metastable state atomic beam of rare gas is prepared usually using a gas discharge source [89, 90]. The basic principle of discharge source is depicted in Fig. 1.7. It involves the partial excitation of rare gas atoms to one of its metastable state by the electrical discharge. The source is then cooled with liquid nitrogen to reduce the axial velocity of the atoms. These metastable rare gas atoms are of interest in the area of quantum optics, atom optics and lithography.

1.2.3 Laser ablation

Processing of materials via pulsed laser ablation [91, 92] has wide spectrum applications. It is used in mechanical industries [93, 94], thin film deposition [95–103], fabrication of waveguide [104], light emitting diodes [105], nanostructure fabrication [106, 107], determination of isotopic ratios [108, 109], medical surgery [110], lithography [83–85] and for the production of atomic beam [111–118]. The laser ablation is gaining importance in all these applications because of its potential to process almost any material precisely with the minimum damage to the surroundings. With the proper choice of the target material, environment and the laser parameters, the morphology and the stoichiometry of the thin

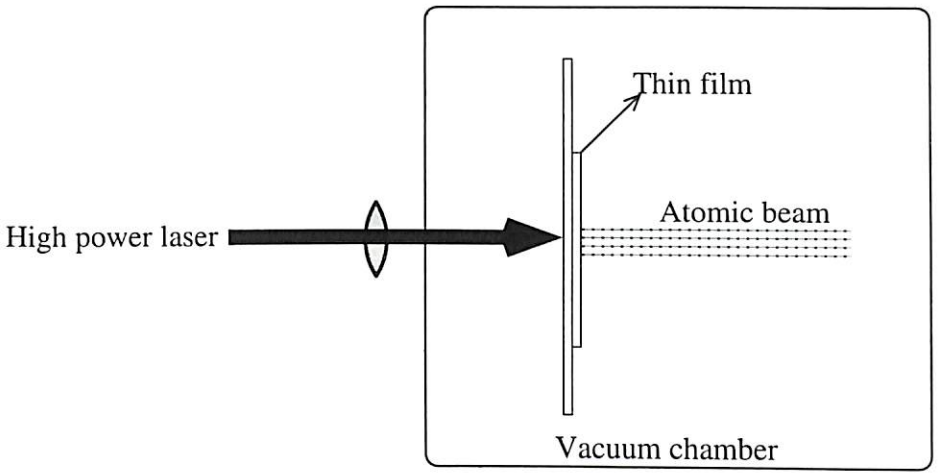

Figure 1.8: Atomic beam generation by focused laser ablation of thin film

film deposited via laser ablation can be controlled [119, 120]. Whenever a solid target or a thin film is exposed to a focused high power laser, ablation of the material and plasma formation takes place. The physical process involves in laser ablation are very complicated [95, 121–123]. It involves initially coupling of laser energy to the target, vaporization and plasma formation, resulting into removal of material from the target, propagation and interaction with the surrounding environment and cooling and finally recombination of the plasma. With the target of monoatomic species placed in vacuum, the laser ablation may results into the generation of atomic and ionic beam. There have been several reports on the generation of neutral atomic beam via laser ablation of targets of Bi, Cr, and Hg [111], Ba [124], Al [112, 113, 117], Cu [112, 114], Na [115], Si [116] and U [118] in the thermal to super-thermal range. The schematics of experimental set-up for the generation of atomic beam via rear side laser ablation of thin film is shown in Fig. 1.8. The focal intensities are of the order of or more than $10^8 W/cm^2$ at the target. At such higher intensities, the initial emission of vaporized material and plasma formation is hemispherical [125–128] and hence the atomic beams so generated have very large divergence ranging from few tens of degrees to 150^0. For the precise application viz; micro-nano lithography, the col-

limated atomic beam is required. We have reported for the first time [129] the generation of the fairly collimated atomic beam by using an unfocused laser beam. The unfocused laser beam have low intensities and therefore the ionization of the ablated material as well as divergence is low and so the atomic flux are expected to be higher. The advantage of technique of production of atomic beam via laser ablation is manifold. The experimental set-up required is simple (Fig. 1.8), the process is single step. It has the ability to generate the atomic beam of almost any material irrespective of the melting point. The pulsed beam is generated with the pulse duration ranging from few microseconds to sub-milliseconds. By controlling the laser intensities, the neutral velocities can be achieved in the range of cold to thermal to super-thermal with the equally high flux.

1.3 Present work

In the present work, we have proposed some of the novel configurations of atomic beam and light beam for micro and nanolithography. We have also developed the selective laser ablation via laser interference pattern for one and two dimensional lithography as well as for the generation of multiple atomic beams having periodicity of the order of λ. Generation of low divergence slow pulsed atomic beam of Indium via rear side ablation of thin film is also reported in this thesis.

The detail semi-classical derivation of dipole force is given in Chap.2.

In Chap.3, we present the results obtained from the simulation of atomic trajectories for various light field configurations. A new light field configuration is introduced for microfabrication using atom lithography. A novel concept of using multiple periodic atomic beams (MPAB) or Matrix of Micro Ovens (MMO) traveling in TEM_{00} mode of laser beam is proposed and the simulated lithographic patterns of periodicity less than $\lambda/2$ are discussed. As an application of dipole force to other field, an idea of using TEM_{00} mode of

laser for the isotopic separation of uranium is also proposed.

In Chap.4, experimental set ups for the generation of low divergence cold indium atomic beam via rear side laser ablation of thin film, measurement of axial velocity of atomic beam and ablation dynamics of indium thin film at different laser energies are discussed. The experimental set-up developed for the selective laser ablation via two beam and four beam high power laser interference pattern is discussed for the direct lithography and for the generation of multiple atomic beams in one and two dimensions.

In Chap.5, The results of generation and characterization of indium atomic beam via rear side laser ablation of thin film are discussed.

In Chap.6, Results obtained for selective laser ablation lithography in one and two dimension on Indium thin films are presented. Also, for the first time, we report the formation of arrays of multiple atomic beams in one and two dimension using rear side selective laser ablation of Indium thin film. This configuration of atomic beams obtained experimentally matches with the configuration for atom lithography using dipole force as proposed in Chap.3.

Chap.7 contains conclusion of all the theoretical and experimental results and future scope of the this work.

Chapter 2

Atom-photon interaction

This chapter contain the detail semi-classical derivation for the dipole force [32]. Consider a two level single atom, as shown in Fig. 2.1, at rest, at the origin 0, with two discrete non-degenerate states, the ground state $|a>$ and the first excited state $|b>$, having energy separation of $\hbar w_0$ between them and natural width Γ. Let a monochromatic field $\mathbf{E}_e$(0,t), with frequency ω_L, amplitude $\mathbf{E}_0$ given by

$$\mathbf{E_e}(0,t) = \mathbf{E_0}\cos(w_L t) \tag{2.1}$$

is incident on the atom.

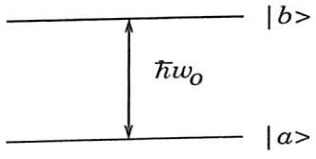

Figure 2.1: Two level atom

Hamiltonian of this atom+radiation system is given by

$$H = H_A - \mathbf{d}.\mathbf{E_e}(0,t) \tag{2.2}$$

Where H_A is the Hamiltonian of the atom and $\mathbf{d}$ is the electric dipole moment of the atom. Here we have neglected the states of quantized vacuum field, because for solving equation of motion for atom the states of the quantized vacuum field are of no interest.

2.1 Optical Bloch equations

The evolution equation for atomic density matrix σ is given by

$$\dot{\sigma} = -\frac{i}{\hbar}[H, \sigma] \tag{2.3}$$

Substituting the expression for H in Eq. 2.3, we get

$$\dot{\sigma} = -\frac{i}{\hbar}[H_A - \mathbf{d}.\mathbf{E_e}(0,t), \sigma] \tag{2.4}$$

Solving this equation for each component of $\dot{\sigma}$ and including the effect of spontaneous emission in terms of damping parameter, we get four equations [32].

$$\dot{\sigma}_{aa} = -i\Omega_1 \cos(w_L t)(\sigma_{ba} - \sigma_{ab}) + \Gamma\sigma_{bb} \tag{2.5}$$

$$\dot{\sigma}_{ab} = iw_0\sigma_{ab} - i\Omega_1 \cos(w_L t)(\sigma_{bb} - \sigma_{aa}) - \frac{\Gamma}{2}\sigma_{ab} \tag{2.6}$$

$$\dot{\sigma}_{ba} = -iw_0\sigma_{ba} + i\Omega_1 \cos(w_L t)(\sigma_{bb} - \sigma_{aa}) - \frac{\Gamma}{2}\sigma_{ba} \tag{2.7}$$

$$\dot{\sigma}_{bb} = i\Omega_1 \cos(w_L t)(\sigma_{ba} - \sigma_{ab}) - \Gamma\sigma_{bb} \tag{2.8}$$

Where Ω_1 is the Rabi frequency given by $\Omega_1 = -\frac{2\mathbf{d}_{ab}.\mathbf{E}_0}{\hbar}$, where $\mathbf{d}_{ab} =< a|\mathbf{d}|b >=< b|\mathbf{d}|a >$. These equations are called as Optical Bloch equations (OBE). Eq. 2.5 and 2.8 described the rate of change of populations of levels $|a >$ and $|b >$ respectively and Eq. 2.6 and 2.7

the rate of change of coherences. From Eq. 2.5 and 2.8

$$\begin{aligned} \dot{\sigma_{aa}} + \dot{\sigma_{bb}} &= 0 \\ \sigma_{aa} + \sigma_{bb} &= \text{Constant} = 1 \text{ (Normalization condition)} \end{aligned} \tag{2.9}$$

The dipole $\mathbf{d}$, which is purely non-diagonal in the basis $\{ |a>, |b> \}$, may be written as

$$\begin{aligned} \mathbf{d} &= \mathbf{d}_{ab}(|b><a| + |a><b|) = \mathbf{d}_+ + \mathbf{d}_- \\ \mathbf{d}_\pm &= \mathbf{d}_{ab} l_\pm \\ l_+ &= |b><a| \\ l_- &= |a><b| \end{aligned} \tag{2.10}$$

$l_\pm$ are raising and lowering operators from $|a>$ to $|b>$ and from $|b>$ to $|a>$. Also writing $\cos(w_L t) = \frac{1}{2}[e^{iw_L t} + e^{-iw_L t}]$. With these, the second term of R.H.S of Eq. 2.2 can be written as

$$-\mathbf{d}.\mathbf{E_0}\cos(w_L t) = \frac{1}{2}\hbar\Omega_1[l_+ e^{-iw_L t} + l_- e^{iw_L t} + l_- e^{-iw_L t} + l_+ e^{iw_L t}] \tag{2.11}$$

The first two terms of Eq. 2.11 describe processes where the atom rises from $|a>$ to $|b>$ by absorbing a photon or falls down from $|b>$ to $|a>$ by emitting a photon. These processes are resonant and are much more important than the non resonant processes associated with the last two terms in Eq. 2.11. We will neglect the last two terms. This approximation is called rotating wave approximation.

$$\therefore -\mathbf{d}.\mathbf{E_0}\cos(w_L t) = \frac{1}{2}\hbar\Omega_1[l_+ e^{-iw_L t} + l_- e^{iw_L t}] \tag{2.12}$$

To suppress any time dependence in the coefficients of the equations, following new variables are introduced.

$$\hat{\sigma}_{ab} = \sigma_{ba} e^{iw_L t} \qquad \hat{\sigma}_{ba} = \sigma_{ab} e^{-iw_L t} \tag{2.13}$$

$$\hat{\sigma}_{aa} = \sigma_{aa} \qquad \hat{\sigma}_{bb} = \sigma_{bb} \tag{2.14}$$

Which leads to following Optical Bloch equations.

$$\dot{\hat{\sigma}}_{aa} = -i\frac{\Omega_1}{2}(\hat{\sigma}_{ba} - \hat{\sigma}_{ab}) + \Gamma\hat{\sigma}_{bb} \tag{2.15}$$

$$\dot{\hat{\sigma}}_{bb} = i\frac{\Omega_1}{2}(\hat{\sigma}_{ba} - \hat{\sigma}_{ab}) - \Gamma\hat{\sigma}_{bb} \tag{2.16}$$

$$\dot{\hat{\sigma}}_{ab} = -i\delta_L\hat{\sigma}_{ab} - i\frac{\Omega_1}{2}(\hat{\sigma}_{bb} - \hat{\sigma}_{aa}) - \frac{\Gamma}{2}\hat{\sigma}_{ab} \tag{2.17}$$

$$\dot{\hat{\sigma}}_{ba} = i\delta_L\hat{\sigma}_{ba} + i\frac{\Omega_1}{2}(\hat{\sigma}_{bb} - \hat{\sigma}_{aa}) - \frac{\Gamma}{2}\hat{\sigma}_{ba} \tag{2.18}$$

Where δ_L is the detuning given by $\delta_L = \omega_L - \omega_0$.

2.1.1 Steady state solutions of Optical Bloch Equations

It is convenient to write optical Bloch equations in terms of three variables defined by

$$u = \frac{1}{2}(\hat{\sigma}_{ab} + \hat{\sigma}_{ba}) \tag{2.19}$$

$$v = \frac{1}{2i}(\hat{\sigma}_{ab} - \hat{\sigma}_{ba}) \tag{2.20}$$

$$w = \frac{1}{2}(\hat{\sigma}_{bb} - \hat{\sigma}_{aa}) \tag{2.21}$$

Using these variables, optical Bloch equations can be rewritten as

$$\dot{u} = \delta_L v - \frac{\Gamma}{2} u \tag{2.22}$$

$$\dot{v} = -\delta_L u - \Omega_1 w - \frac{\Gamma}{2} v \tag{2.23}$$

$$\dot{w} = \Omega_1 v - \Gamma w - \frac{\Gamma}{2} \tag{2.24}$$

$$\tag{2.25}$$

Steady state solution of above equations are

$$u_{st} = \frac{\delta_L}{\Omega_1} \frac{s}{1+s} \tag{2.26}$$

$$v_{st} = \frac{\Gamma}{2\Omega_1} \frac{s}{1+s} \tag{2.27}$$

$$w_{st} = \frac{1}{2} \frac{s}{1+s} - \frac{1}{2} \tag{2.28}$$

$$\tag{2.29}$$

Where s is called saturation parameters and is given by

$$s = \frac{\frac{\Omega_1^2}{2}}{\delta_L^2 + \frac{\Gamma^2}{4}} \tag{2.30}$$

2.2 Mean radiative force on an atom

To find the mean radiative force $\mathbf{F}$ on an atom, placed in a radiation field, we need to consider the translation degrees of freedom. Considering Hamiltonian

$$H = \frac{\mathbf{P}^2}{2M} + H_A + H_R - \mathbf{d}\left[\mathbf{E}_e(\mathbf{R}, t) + E_\perp(\mathbf{R})\right] \tag{2.31}$$

Where $\mathbf{P}$ and $\mathbf{R}$ are the momentum and the position of the center of mass of the atom, M is the atomic mass and H_R is the Hamiltonian of quantum radiation field. $\mathbf{E_e}(\mathbf{R}, t)$ and $\mathbf{E}_\perp(\mathbf{R})$ are external field and quantum radiation field respectively evaluated at the center of mass R of the atom.

2.2.1 Equation of motion

Heisenberg equations for $\mathbf{R}$ and $\mathbf{P}$ are given by

$$\dot{\mathbf{R}} = \frac{\partial H}{\partial \mathbf{P}} = \frac{\mathbf{P}}{M} \tag{2.32}$$

$$\dot{\mathbf{P}} = M\ddot{\mathbf{R}} = \frac{\partial H}{\partial \mathbf{R}} = \sum_{j=x,y,z} d_j \nabla_R \left[E_{ej}(\mathbf{R}, t) + E_{\perp j}(\mathbf{R}) \right] \tag{2.33}$$

Taking average of Eq. 2.33

$$M < \ddot{\mathbf{R}} >= \sum_j < d_j \nabla_R \left[E_{ej}(\mathbf{R}, t) + E_{\perp j}(\mathbf{R}) \right] > \tag{2.34}$$

As the de Broglie wavelength of the atom is very small compared to wavelength of driving field, one can construct the wave packet having very small dimensions compared to optical field. Therefore operator $\mathbf{R}$ can be replaced by it's mean value $< \mathbf{R} >= \mathbf{r_G}$. The last term of Eq. 2.34, which represents the contribution of the gradient of the quantum radiation field at $\mathbf{r_G}$, is zero, as the source field is even in $\mathbf{r}$. Rewriting Eq. 2.34, we get

$$M\ddot{\mathbf{r}}_\mathbf{G} = \sum_j < d_j > \nabla E_{ej}(\mathbf{r_G}, t) \tag{2.35}$$

$M\ddot{\mathbf{r}}_\mathbf{G}$ is the force that governs the motion of the center $\mathbf{r_G}$ of the atomic wave packet and it is expressed as a function of driving field evaluated at this point.

To find the average value of d_j

$$\begin{aligned} < d_j > &= Tr(\sigma \mathbf{d}) = (\mathbf{d}_{ab})_j(\sigma_{ab} + \sigma_{ba}) \\ &= (\mathbf{d}_{ab})_j(\hat{\sigma}_{ab}e^{iw_L t} + \hat{\sigma}_{ba}e^{-iw_L t}) \\ &= 2(\mathbf{d}_{ab})_j(u\cos(w_L t) - v\sin(w_L t)) \end{aligned} \tag{2.36}$$

2.2.2 Time scales

There exit two different time scales for the evolution of internal and external degrees of freedom. The internal degrees of freedom of the atom evolve appreciably over time scales of the order of $T_{int} = \Gamma^{-1}$. Considering atoms of very small velocity v, which during T_{int}, travels over a distance $vT_{int} = v\Gamma^{-1} << \lambda$, λ being the wavelength of light.

External degrees of freedom of the atom evolve over the time scales of the order of $T_{ext} = \frac{\hbar}{E_{rec}}$, where $E_{rec} = \frac{\hbar^2 k^2}{2M}$ is the recoil energy of the atom when it absorbs a photon. For most of the allowed transition $\hbar\Gamma >> E_{rec}$ which results in the fact that $T_{int} << T_{ext}$. This means that, if $\mathbf{r_G}$=0 initially, the mean dipole $< \mathbf{d} >$ has the time to reach the steady state regime calculated before, before $\mathbf{r_G}$ has changed appreciably under the influence of mean radiative force given by Eq. 2.35.

2.2.3 Dipole force

To calculate the mean radiative force exerted on an atom initially at rest at 0, $< d_j >$ in Eq. 2.36 has to be replaced by its steady state value

$$< \mathbf{d} >_{st} = 2(\mathbf{d}_{ab})\,[u_{st}\cos(w_L t) - v_{st}\sin(w_L t)] \tag{2.37}$$

From this equation physical meaning of u_{st} and v_{st} can be interpreted. u_{st} is the component of $< \mathbf{d} >_{st}$ in phase with $\mathbf{E_e}$ and v_{st} is the component of $< \mathbf{d} >_{st}$ in quadrature with $\mathbf{E_e}$. Near the origin 0, where the atom is located, the driving field is written as

$$\mathbf{E_e}(\mathbf{r}, t) = \mathbf{e}E_0(\mathbf{r}) \cos(w_L t + \phi(\mathbf{r})) \tag{2.38}$$

Where $\mathbf{e}$ is the polarization vector. Amplitude $E_0(\mathbf{r})$ and phase $\phi(\mathbf{r})$ of this field vary in space, with the condition $\phi(\mathbf{r}) = 0$ at $\mathbf{r} = 0$ and t=0.

$$\therefore \nabla E_{ej} = e_j \left[\cos(w_L t)\nabla E_0 - \sin(w_L t)E_0 \nabla\phi\right] \tag{2.39}$$

Where ∇E_{ej} and hence ∇E_0, $\nabla\phi$ and E_0 are calculated at $\mathbf{r} = 0$. So finally Eq. 2.35 in terms of Eq. 2.37 and Eq. 2.39 can be written as

$$\mathbf{F} = \sum_j \overline{< d_j > \nabla E_{ej}} \tag{2.40}$$

$$= (\mathbf{e}.\mathbf{d}_{ab}) \left[u_{st}\nabla E_0 + v_{st}E_0 \nabla\phi\right] \tag{2.41}$$

Thus $\mathbf{F}$ has two components. The first term of Eq. 2.41

$$\mathbf{F_{react}} = (\mathbf{e}.\mathbf{d}_{ab})u_{st}\nabla E_0 \tag{2.42}$$

called as dipole or gradient force since it depends on intensity gradient of the external field. This force is a conservative force. The second term is given by

$$\mathbf{F_{dissip}} = (\mathbf{e}.\mathbf{d}_{ab})v_{st}E_0 \nabla\phi \tag{2.43}$$

is called dissipative force. This force is responsible for laser cooling.

In terms of Rabi frequency

$$\mathbf{F}_{\mathbf{react}} = -\hbar\Omega_1 u_{st}\alpha \tag{2.44}$$

$$\alpha = \frac{\nabla\Omega_1}{\Omega_1} \tag{2.45}$$

$$\mathbf{F}_{\mathbf{dissip}} = -\hbar\Omega_1 v_{st}\beta \tag{2.46}$$

$$\beta = \nabla\phi \tag{2.47}$$

Substituting the expression for u_{st} in Eq. 2.44, expression for dipole force will become

$$\mathbf{F} = \frac{-\hbar\Gamma^2\delta_L\nabla(\frac{I}{2I_{sat}})}{\Gamma^2(1+\frac{I}{I_{sat}})+4{\delta_L}^2} \tag{2.48}$$

Where, δ_L is the detuning parameter, Γ is the natural line width, I is the intensity of laser and I_{sat} is the saturation intensity. Eq. 2.48 can be solved numerically for the modified atomic trajectories in presence of near resonant non-homogeneous radiation field. With the careful choice of the parameters of radiation field, atomic beam and duration of interaction of atoms with the field, the atomic beam can be focused to write the periodic nanostructures of desired geometry.

Chapter 3

Simulation results

3.1 Introduction

This chapter contains the simulation studies of atomic trajectories under dipole force for various light fields and atomic beam configurations. Light configurations includes standing wave, TEM_{00} mode of laser. A new configuration of using square arrays of multiple atomic lens produced by interference of four nearly collinear optical beams for atom lithography using dipole force is proposed. A novel configuration of multiple periodic atomic beams (MPAB) traveling in TEM_{00} mode of laser is explored for the first time to generate the structure via dipole force with periodicity below $\lambda/2$. The collimated as well as divergent rubidium atomic beams are considered for simulation of atomic trajectories via dipole force using Eq. 2.48 for rubidium transition $5S^2{}_{1/2}$ - $5P^2{}_{3/2}$, as shown in Fig. 3.1. The natural linewidth of this transition is 6 MHz. Apart from the nano lithography, the dipole force can also be applied for isotopic separation. We have also worked out the trajectories of various isotopes of uranium via dipole force to demonstrate its application in isotopic separation.

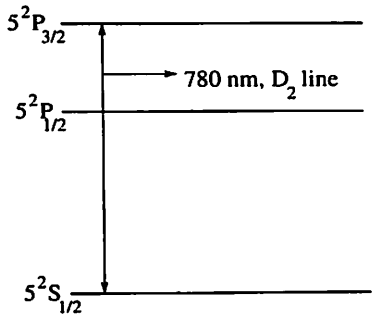

Figure 3.1: Energy level diagram of rubidium

3.2 TEM_{00} mode of laser

Most simplest light configuration is TEM_{00} mode of a laser. Gaussian variation of intensity in the transverse plane of TEM_{00} laser beam acts as a single atomic lens for the focusing of atomic beam to a single spot. Intensity distribution of TEM_{00} mode laser traveling along y direction is defined by

$$I = \frac{I_0 w_0^2}{w(y)^2} \exp[-2(x^2 + z^2)/w(y)^2] \tag{3.1}$$

Where

$$w(y) = w_0(1 + (\frac{y}{y_0})^2)^{1/2} \tag{3.2}$$

is the beam size at a distance y from the location of beam waist ($2w_0$) as depicted in Fig. 3.2 and y_0 is the Rayleigh length given by

$$y_0 = \frac{w_0^2 \pi}{\lambda} \tag{3.3}$$

Where λ is the wavelength of laser.

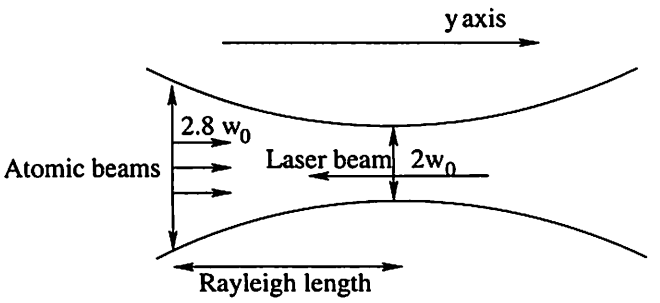

Figure 3.2: Launching position of atoms with respect to Gaussian laser beam

3.2.1 Boundary conditions

The collimated as well as divergent one-dimensional cold and thermal atomic beams of rubidium were considered for simulations of trajectories via dipole force using Eq. 2.48 in counter propagating TEM_{00} mode of laser. The direction of propagation of rubidium atomic beam is taken along y axis and that of laser beam along -y axis as shown in Fig. 3.2. The atoms were assumed to enter in the field at a Rayleigh distance with respect to the location of beam waist (w_0=50 μm) of laser (see Fig. 3.2). From Eq. 2.48 equations of motion of atoms in x and y direction are given by

$$m(\frac{\partial^2 x}{\partial t^2}) = \frac{2x\hbar\delta_L}{\frac{w(y)^2[1+(\frac{y}{y_0})^2]}{I_0 exp[-2(x^2)/w(y)^2]} + \frac{\Gamma^2}{I_{sat}(\Gamma^2+4\delta_L^2)}} \qquad m(\frac{\partial^2 y}{\partial t^2}) = 0 \tag{3.4}$$

Eqs. 3.4 are computed simultaneously for rubidium atomic beams (collimated as well as divergent) for following initial boundary conditions. For collimated atomic beams two initial boundary conditions at t=0 are

$$\frac{\partial x}{\partial t} = v_x = 0 \qquad \frac{\partial y}{\partial t} = v_y = 17 \text{or} 1700 \text{m/s} \tag{3.5}$$

Other two boundary conditions are x and y coordinates at t=0, depicting the distribution of atoms in the atomic beam at the launching position, given by

$$x = N\delta_x \qquad y = y_0 \tag{3.6}$$

Where N=-10,-9,-8,....,8,9,10 and $\delta_x = 1\mu m$, giving 21 atoms in the beam with 1 μm spacing between the adjacent atom.

For divergent atomic beam, instead of Eq. 3.5, two initial boundary conditions at t=0 are

$$v_x = v\sin(X(0.0025)) \qquad v_y = v\cos(X(0.0025)) \tag{3.7}$$

Where X=-2,-1,1,2 and v=17 or 1700 m/s. The other three boundary conditions are same as given by Eq. 3.6 apart from the difference that now from each location 5 atoms are launched in coaxial cones, therefore the total number of atoms in the beam are now 5 times more with a maximum cone angle (or θ_{dmax}) of 5 mrad.

3.2.2 Results and discussion

The rubidium trajectories are computed for cold as well as thermal beams traveling in TEM_{00} mode of laser with peak intensity, I_0, equal to 16.5 W/m^2, which corresponds to saturation intensity of rubidium transition (Fig. 3.1), for red detuning δ_L=-200 MHz. The computed rubidium trajectories of cold rubidium atomic beam in TEM_{00} mode of laser for red detuning is shown in Fig. 3.3a for first focal spot. Interaction time required for focusing the atomic beam is 35.88 μs. Fig. 3.3b shows the effect of longer interaction time of atoms with laser beyond the first focus. Atomic trajectories in this case show multiple focusing and defocusing depending on the interaction time.

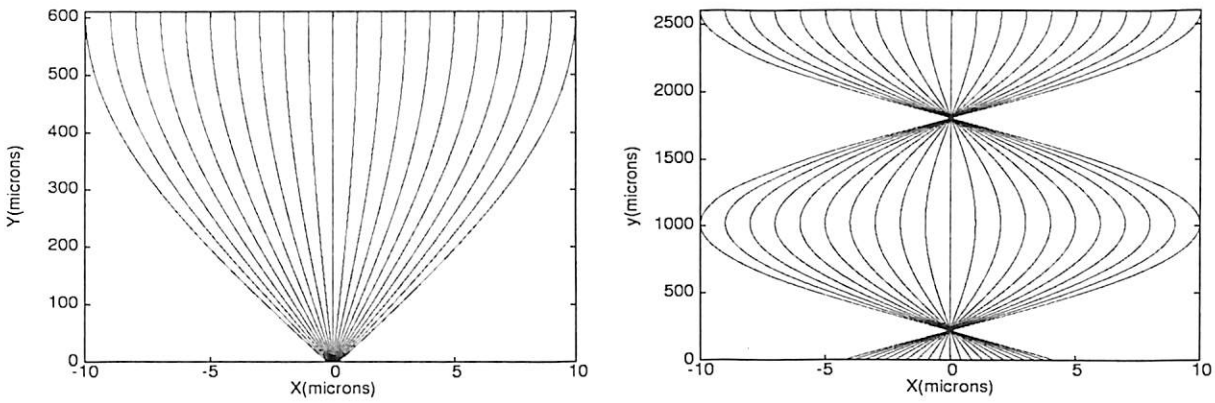

(a) (b)

Figure 3.3: Trajectories of initially collimated cold rubidium atomic beam in TEM_{00} mode of laser showing (a). First focal spot and (b). Multiple focusing due to longer interaction time of atomic beam with laser.

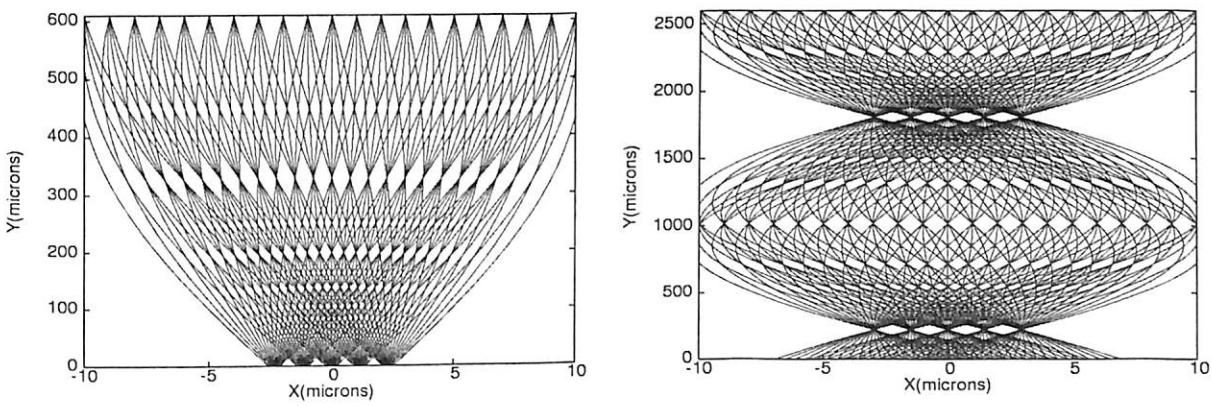

(a) (b)

Figure 3.4: Trajectories of initially divergent cold rubidium atomic beam in TEM_{00} mode of laser showing (a). First focal spot and (b). Multiple focusing due to longer interaction time of atomic beam with laser.

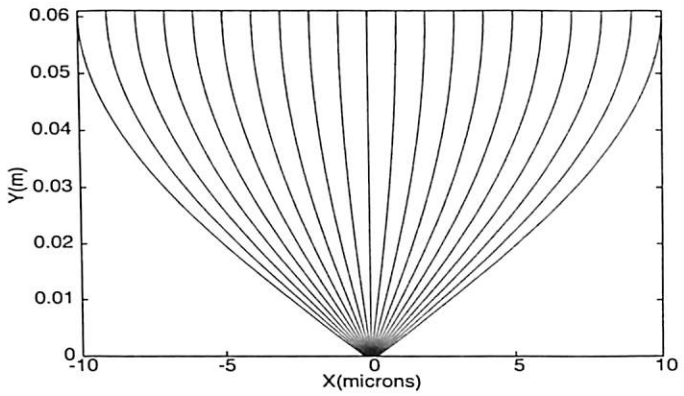

Figure 3.5: Trajectories of initially collimated thermal rubidium atomic beam showing first focal spot for the same interaction time as with cold atomic beam.

The collimated atomic beam is an ideal case, therefore effect of divergence of atomic beam was studied for same interaction time. Fig. 3.4a shows the first focal spot of the initially divergent (θ_{dmax} = 5 mrad) cold rubidium atomic trajectories in TEM_{00} mode of laser. The focus spot size is increased in this case as compared to collimated atomic beam due to the initial divergence of the atom. Multiple focusing effect for longer interaction time of atoms with the laser is shown in Fig. 3.4b.

Fig. 3.5 shows the first focal spot of thermal (1700 m/s) rubidium atoms for the same interaction time (35.88 μs) as that required for cold rubidium atoms. Therefore interaction time for the focusing of the atomic beam is independent of it's axial velocity.

3.3 Standing wave configuration

The TEM_{00} mode of laser beam gives only one single focus spot of atoms of micron dimensions. Therefore a light configuration which gives multiple periodic atomic lenses is needed for periodic writing. Standing wave of light is one such configuration which gives series of periodic microlenses with period $\lambda/2$, as shown in Fig. 3.6. The atomic beam is launched perpendicular to standing wave and focus down into the grating structure by each

period of standing wave, which acts as a cylindrical atomic lens. Intensity distribution of a one-dimensional standing wave can be taken as

$$I = I_0 \cos^2(kx) \tag{3.8}$$

Where $k = \frac{2\pi}{\lambda}$.

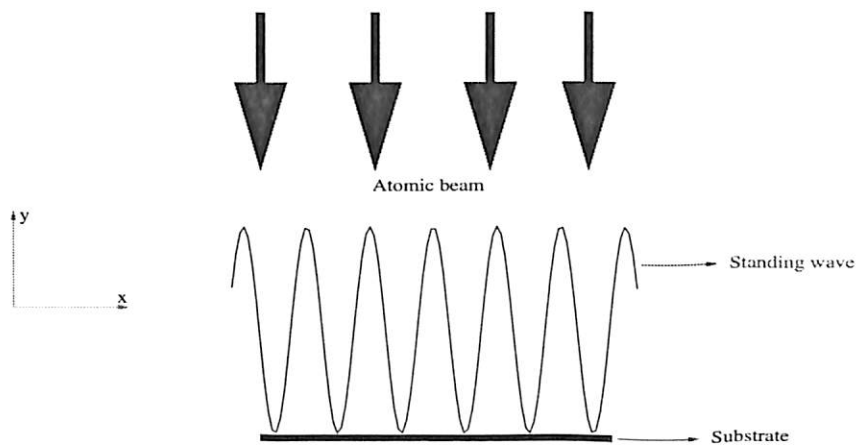

Figure 3.6: Launching position of atoms with respect to Standing wave

3.3.1 Boundary conditions

The collimated as well as divergent cold and thermal one-dimensional atomic beam of rubidium were considered for simulations of trajectories via dipole force. The direction of propagation of rubidium atomic beam is taken along -y axis while the standing wave is along x axis as shown in Fig. 3.6. From Eq. 2.48, equations of motion of atoms in x and y directions are given by

$$m(\partial^2 x/\partial t^2) = \frac{\hbar\Gamma^2\delta_L \frac{I_0}{I_{sat}} \cos(kx)\sin(kx)}{\Gamma^2(1 + \frac{I_0\cos(kx)^2}{I_{sat}}) + 4\delta_L^2} \qquad m(\partial^2 y/\partial t^2) = 0 \tag{3.9}$$

Eqs. 3.9 are computed simultaneously for rubidium atomic beams (collimated as well as divergent). For collimated atomic beams two initial boundary conditions at t=0 are

$$\frac{\partial \mathrm{x}}{\partial \mathrm{t}} = v_x = 0 \qquad \frac{\partial y}{\partial t} = v_y = 17/\mathrm{or}/1700\mathrm{m/s} \tag{3.10}$$

Other two boundary conditions are x and y coordinates at t=0, which are given by

$$\mathrm{x} = N\delta_x \qquad y = y_0 \tag{3.11}$$

Where N=1,2,3,....,90 and δ_x=13 nm. For divergent atoms two initial boundary conditions for t=0 modified to

$$\mathrm{v_x} = v\sin(X(0.0025)) \qquad v_y = v\cos(X(0.0025)) \tag{3.12}$$

Where X=-2,-1,1,2 and v=17 or 1700 m/s. The other two boundary conditions are same as given by Eq. 3.11 apart from the difference that now from each location 5 atoms are launched in coaxial cones, such that the total number of atoms are now 450 with a maximum cone angle (or θ_{dmax}) of 5 mrad.

3.3.2 Results and discussion

The computed trajectories of cold (17 m/s) rubidium atomic beam in standing wave for blue detuning (δ_L=200 MHz) for first focal spot is shown in Fig. 3.7a. Interaction time required for focusing the atomic beam is 0.35 μs. Fig. 3.7b shows the effect of multiple focusing for longer interaction time of atoms with laser. Fig. 3.8a shows the initially divergent (θ_{dmax} = 5 mrad) cold rubidium atomic trajectories in standing wave for first focal spot. The focus spot size is increased in this case as compared to collimated atomic beam due to

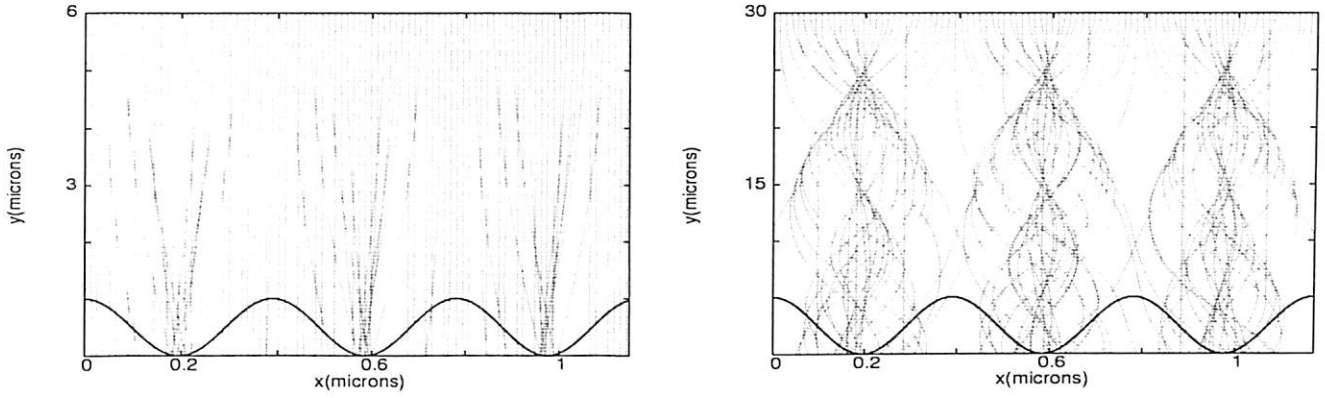

(a) (b)

Figure 3.7: Trajectories of initially collimated cold rubidium atomic beam in optical standing wave at intensity 16.5 W/m^2 showing (a). First focal spot and (b). Multiple focusing due to longer interaction time of atomic beam with laser. Intensity distribution is shown in the bottom of the figure

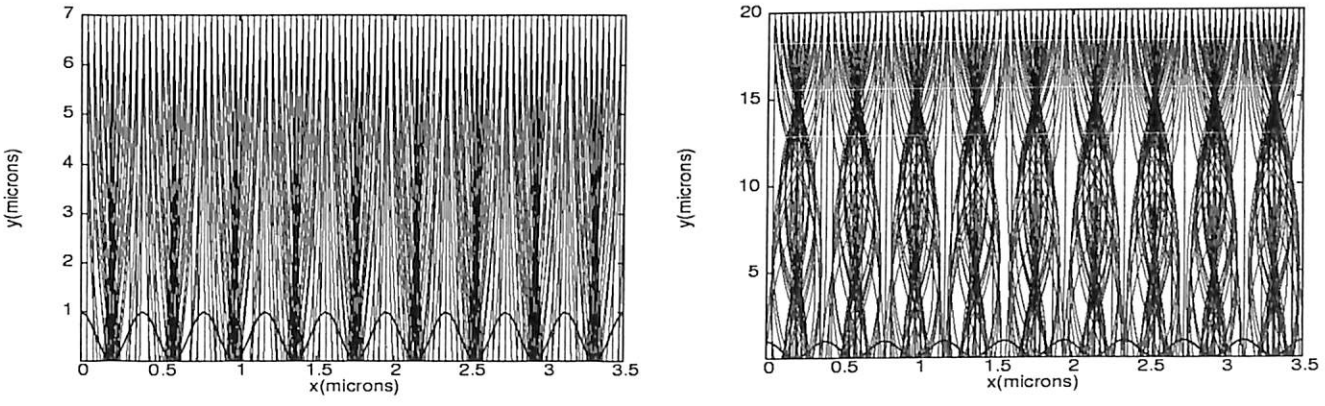

(a) (b)

Figure 3.8: Trajectories of initially divergent cold rubidium atomic beam in optical standing wave at intensity 16.5 W/m^2 showing (a). First focal spot and (b). Multiple focusing due to longer interaction time of atomic beam with laser. Intensity distribution is as shown in the bottom of the figure

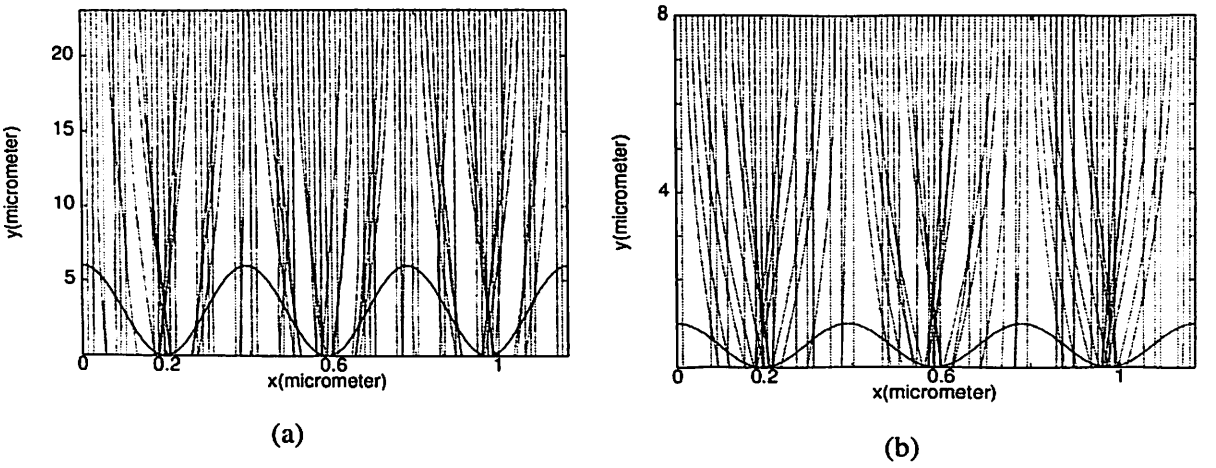

Figure 3.9: Trajectories of initially collimated cold rubidium atomic beam in optical standing wave at intensity (a). I_0=1 W/m^2 and (b).I_0=10 W/m^2. Intensity field is as shown in the bottom of the figure

divergence. Fig. 3.8b shows multiple focusing due to longer interaction time of atoms with the standing wave.

The computed trajectories of cold beam of rubidium in standing wave at intensities 1 and 10 W/m^2 for blue detuning are shown in Fig. 3.9a and b, respectively. At higher intensities atoms are tightly focused with better contrast. From Fig. 3.7a and Fig. 3.9a and b, it is obvious that at lower intensity, the atomic beam has to travel a larger distance, in other words interaction time with the field are required to be large. Interaction time required for the atomic beam for focusing at various intensity are listed in Table. 3.1.

Intensity (W/m^2)	Focusing time (μs)
1	1.35
10	0.47
16.5	0.35

Table 3.1: Focusing time at various intensities of laser

Results for a thermal beam at atomic velocity 1700 m/s are shown in Fig. 3.10. Results are similar to that of cold beam. Thermal beam has to travel a distance longer by two

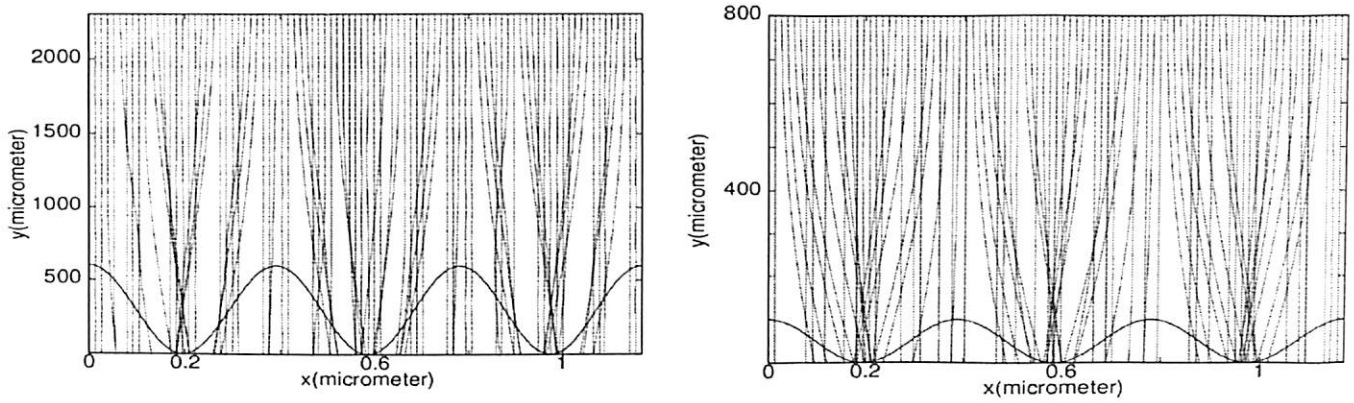

(a) (b)

Figure 3.10: Trajectories of rubidium thermal atomic beam at intensity, I_0=1 W/m^2 and I_0=10 W/m^2.

orders of magnitude before being focused compared to that of cold atomic beam. This confirms that interaction time required for the focusing at any given intensity is constant and is independent of velocity of the atom.

3.4 Interferometric configuration

We proposed a new configuration of multiple atomic lenses formed via interference of four nearly collinear optical beams [130] for writing the square arrays of structures. The interference of four beams results into the square arrays of equally illuminating light spots. These light spots act as the two dimensional periodic potential for the focusing of the atomic beam via dipole force.

3.4.1 Configuration details

Experimental set up used to generate square arrays of equal illuminating light spots is shown in Fig. 3.11 [130]. It comprises of a MachZhander interferometer coupled to Michel-

son interferometer (or two Michelson interferometers in tandem) producing the four nearly collinear beams in the output. The resultant intensity distribution of interference pattern in the transverse plane, generated by using such set up is given by

$$I = I_0[4 + 4\cos(kx) + 4\cos(ky) + 2\cos(kx + ky) + 2\cos(kx - ky)] \quad (3.13)$$

Where $k = 2\pi\mu$ and spatial frequency $\mu = \frac{\sin(\theta)}{\lambda}$, θ is the angular separation between two interfering beams of either of the interferometer and λ is the wavelength of the laser light used. Fig. 3.12a shows the computed plot of intensity distribution of Eq. 3.13 and Fig. 3.12b shows the recorded pattern onto CCD (PCO-Pixelfly-imaging-SVGA) from the set up of Fig. 3.11 using a He-Ne laser. The collimated as well as divergent cold (v=17 m/s) ru-

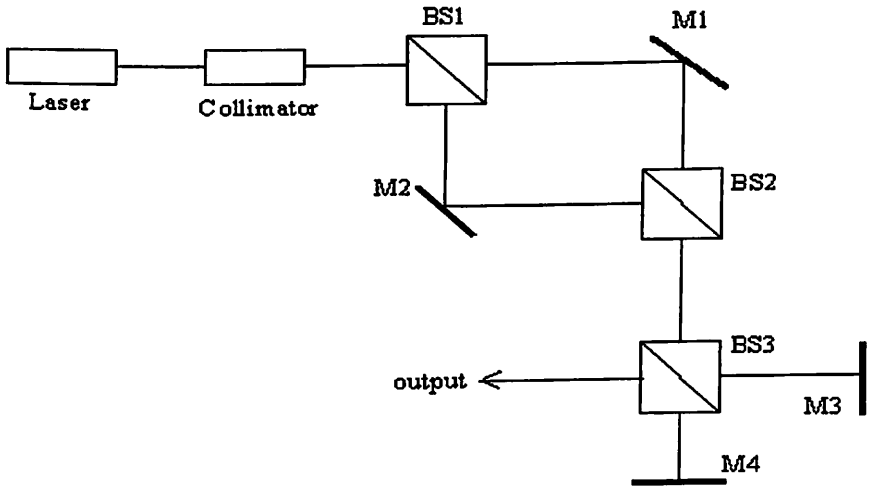

Figure 3.11: Experimental set up for the production of four beam interferometric pattern.

bidium atomic beams traveling in counterpropagating interfering beams along z-axis from the set up of Fig. 3.11 are considered (see Fig. 3.13) for simulation of atomic trajectories via dipole force using Eq. 2.48.

Equations of motion of rubidium atoms traveling in this optical configuration (from

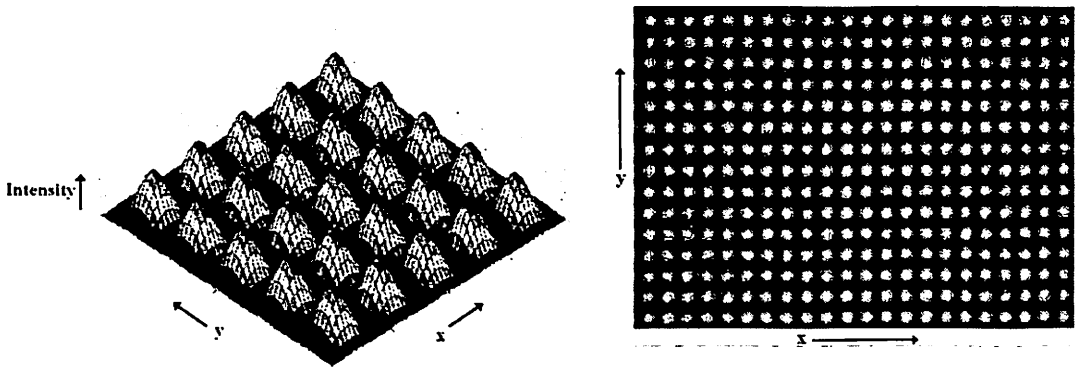

(a) (b)

Figure 3.12: a. Three dimensional plot of intensity distribution of four beam interferometric pattern. b. Recorded four beam interferometric pattern using a He-Ne laser.

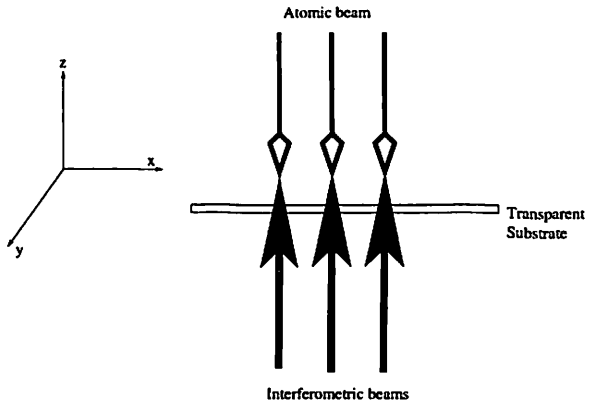

Figure 3.13: Launching position of rubidium atoms in presence of interfering optical beams.

Eq. 2.48) are given by

$$m\frac{\partial^2 x}{\partial t^2} = \frac{\hbar\delta_L I_0 k[2\sin(kx) + \sin(kx + ky) + \sin(kx - ky)]}{1 + \frac{I_0\Gamma^2[4+4\cos(kx)+4\cos(ky)+2\cos(kx+ky)+2\cos(kx-ky)]}{I_{sat}(\Gamma^2+4\delta_L^2)}} \tag{3.14a}$$

$$m\frac{\partial^2 y}{\partial t^2} = \frac{\hbar\delta_L I_0 k[2\sin(ky) + \sin(kx + ky) + \sin(kx - ky)]}{1 + \frac{I_0\Gamma^2[4+4\cos(kx)+4\cos(ky)+2\cos(kx+ky)+2\cos(kx-ky)]}{I_{sat}(\Gamma^2+4\delta_L^2)}} \tag{3.14b}$$

$$m\frac{\partial^2 z}{\partial t^2} = 0 \tag{3.14c}$$

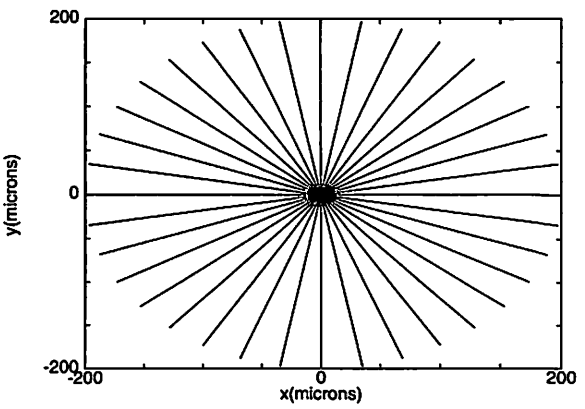

Figure 3.14: Cross sectional view of initial positions of rubidium atoms in the beam.

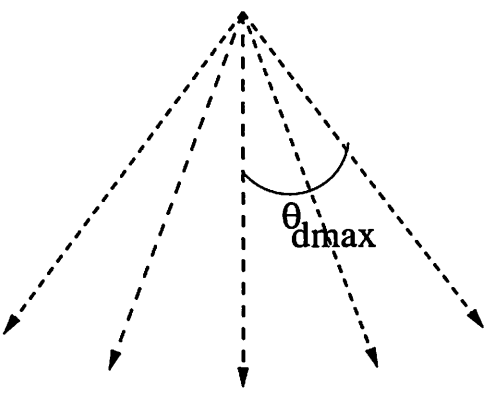

Figure 3.15: Launching coaxial cones of atomic beams for maximum divergence angle θ_{dmax}.

The peak intensity of laser, I_0, was taken to be 16.5 W/m^2, corresponding to the saturation intensity of rubidium transition. The laser wavelength was red detuned (δ_L=-200 MHz) from the resonance line of 780 nm of rubidium. Eqs.3.14 are computed simultaneously for collimated as well as divergent atomic beam for following initial boundary conditions. For the collimated rubidium atomic beams the three boundary conditions at t=0 are

$$\frac{\partial x}{\partial t} = v_x = 0 \tag{3.15a}$$

$$\frac{\partial y}{\partial t} = v_y = 0 \tag{3.15b}$$

$$\frac{\partial z}{\partial t} = v_z = 17\text{m/s} \tag{3.15c}$$

Other three boundary conditions are x, y and z coordinates of the atoms in the beam at t=0, which is given by

$$x = N\epsilon \cos(\phi) \tag{3.16a}$$

$$y = N\epsilon \sin(\phi) \tag{3.16b}$$

$$z = z_0 \tag{3.16c}$$

Where N=-2000, -1900, -1800, ..., 1800, 1900, 2000; ϵ=10^{-9}, ϕ=0,0.174,0.348,...., 2π. Pictorially initial arrangment of the atoms in the transverse plane x-y is shown in Fig. 3.14.

For divergent atomic beams three boundary conditions at t=0 are

$$v_x = \frac{v}{1.41}\sin(\theta_d) \tag{3.17a}$$

$$v_y = \frac{v}{1.41}\sin(\theta_d) \tag{3.17b}$$

$$v_z = v\cos(\theta_d) \tag{3.17c}$$

$$v = (v_x^2 + v_y^2 + v_z^2)^{1/2} = 17\text{m/s} \tag{3.17d}$$

Where θ_d is the divergence angle. The other three boundary conditions are same as shown in Fig. 3.14 (and given by Eq. 3.16) apart from the difference that now from each location 5 atoms are launched in coaxial cones (as shown in Fig. 3.15) with a maximum cone angle (or θ_{dmax}) of 5 mrad.

3.4.2 Result and discussion

The sequence of computed lithographic patterns for collimated cold rubidium atomic beams for interaction time of 82.3 μs and 88.2 μs (corresponding interaction length of 1400 μm and 1500 μm respectively) are shown in Fig. 3.16a and b respectively. It can be seen from

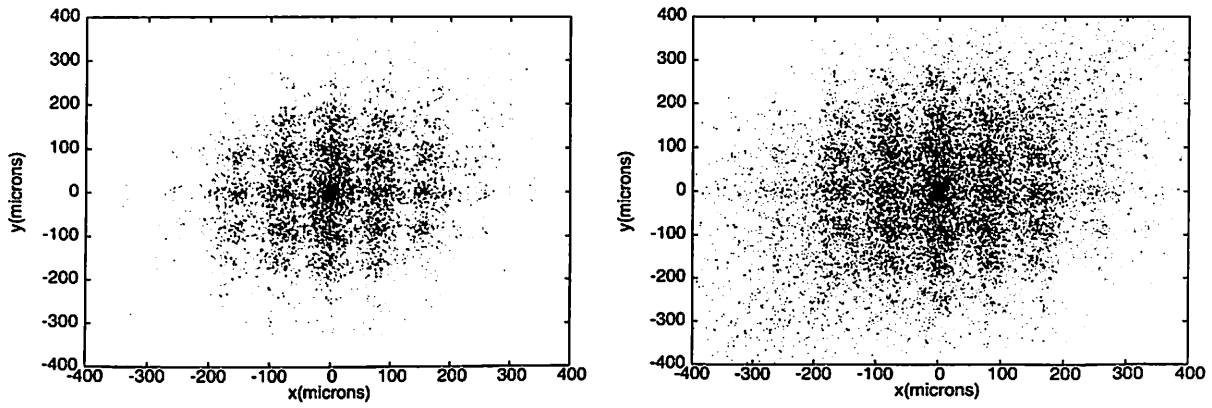

Figure 3.16: Final positions of initially collimated rubidium atoms after interacting with interferometric beams for an interaction length of a. 1400 μm and b. 1500 μm.

the both the lithographic patterns that the atoms have relocated themselves towards the intensity peaks. The effect of divergence of the atomic beam is also considered as the well collimated atomic beam is practically not possible. The starting configuration of atomic beam is shown in Fig. 3.14 and Fig. 3.15. Fig. 3.17 shows the lithographic patterns for such configuration for interaction length of 1400 μm and 1500 μm, corresponding to interaction time of 82.3 μs and 88.2 μs for cold rubidium atoms. These lithographic patterns looks quite similar to that of with the case of collimated atomic beams. In this case also one can see the relocation of atoms around the intensity peaks. The density of the atoms in the center of Fig. 3.16 – 3.17 is large because of the higher density of the atoms in the center of Fig. 3.14 at the initial location. If a uniform distribution of atoms in atomic beam is consider then the focused pattern will also show the same density of atoms in each spot.

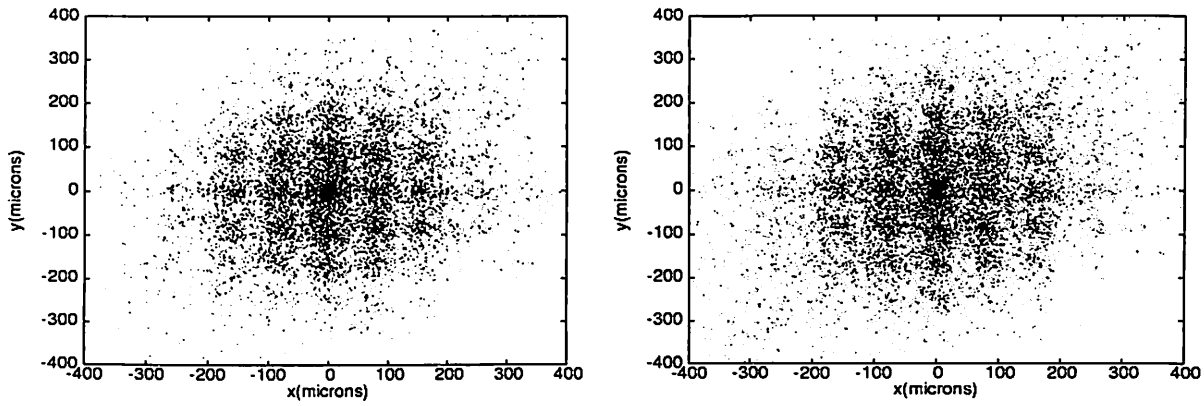

Figure 3.17: Final positions of divergent rubidium atoms after interacting with interferometric beams for an interaction length of a. 1400 μm and b. 1500 μm.

3.5 Matrix of Micro-Ovens for arrays of multiple atomic beams

The periodicity of above two configurations (Sec. 3.3 and 3.4) is limited to $\lambda/2$ though the individual focus spot in the array may be of dimensions tens of nanometer. Therefore a new configuration of using microscopic square arrays of atomic beams (matrix of micro-ovens) in presence of gaussian intensity distribution (TEM_{00} mode) of laser was explored for the first time for reducing the periodicity below $\lambda/2$. This new configuration is equivalent to imaging the large number of discrete atomic beams via single atomic lens. This is the reverse analogy of the above two configurations having single atomic beam traveling in multiple light potentials. One can also draw analogy of this configuration with optics, as shown in Fig. 3.18. In conventional optics large number of periodical light beams can be focused using a convex lens. In our case, light beams are replaced by atoms and lens by TEM_{00} mode of laser. In optics minimum size of focal spot is restricted by wavelength of light. But in case of atoms, the de Broglie wavelength is quite small (<0.1 nm in case of

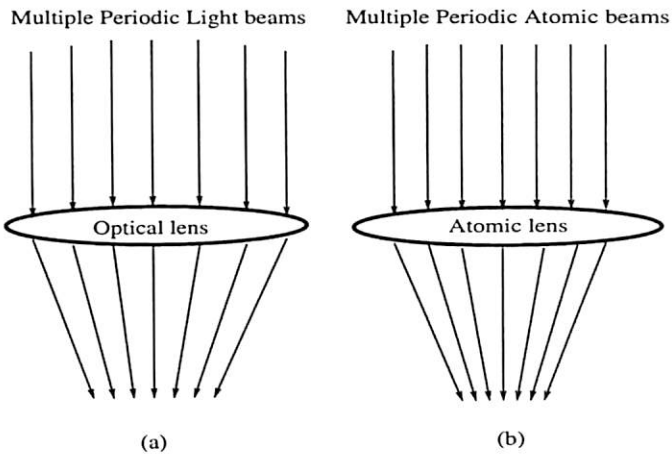

Figure 3.18: Analogy of MMO concept with optics

thermal atoms), so theoretically it is possible to get sub-nanometeric atomic spots with this configuration.

3.5.1 Matrix of micro-ovens

Usually atoms in a beam are having sub-nanometric spacing. Matrix of micro-ovens is a system which can deliver large number of multiple periodic discrete atomic beams well separated from each other.

3.5.2 Configuration details

Intensity distribution of TEM_{00} mode laser traveling along y direction is defined by Eq. 3.1 The collimated as well as divergent atomic beams of rubidium were considered for simulations of trajectories via dipole force using Eq. 2.48. The cross section (z-x plane) of square arrays of atomic beam launched is shown in Fig. 3.19 a. The initial positions of each atomic beam corresponds to the corner of squares of size 2 μm. The diameter of each atomic beam is considered to be 1 μm with 91 atoms placed symmetrically in it (Fig. 3.19b). The direction of propagation of rubidium atomic beam is taken along y axis and that of laser

beam along -y axis as shown in Fig. 3.2. The atoms were assumed to enter in the field at a Rayleigh distance with respect to the location of beam waist (w_0=50 μm) of laser.

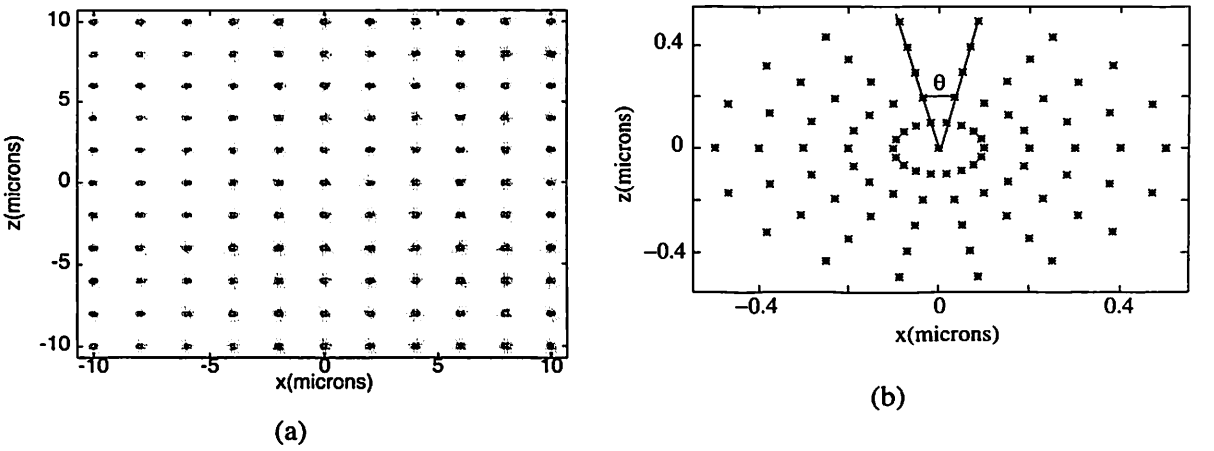

Figure 3.19: (a). Cross sectional view of initial positions of rubidium atomic beam arranged in a square geometry. (b). Arrangements of atoms in each individual beam

From Eq. 2.48 equations of motion of atoms in x, y and z direction are given by

$$m\left(\frac{\partial^2 x}{\partial t^2}\right) = \frac{2x\hbar\delta_L}{\frac{w(y)^2[1+(\frac{y}{y_0})^2]}{I_0 exp[-2(x^2+z^2)/w(y)^2]} + \frac{\Gamma^2}{I_{sat}(\Gamma^2+4\delta_L^2)}} \tag{3.18}$$

$$m\left(\frac{\partial^2 y}{\partial t^2}\right) = 0 \tag{3.19}$$

$$m\left(\frac{\partial^2 z}{\partial t^2}\right) = \frac{2z\hbar\delta_L}{\frac{w(y)^2[1+(\frac{y}{y_0})^2]}{I_0 exp[-2(x^2+z^2)/w(y)^2]} + \frac{\Gamma^2}{I_{sat}(\Gamma^2+4\delta_L^2)}} \tag{3.20}$$

The peak intensity of laser at the center of the beam waist was taken to be 16.5 W/m^2 corresponding to the saturation intensity of rubidium transition. The laser wavelength was red detuned (δ_L=-200 MHz) from the resonance line of 780 nm of rubidium. Eq. 3.18, 3.19 and 3.20 are computed simultaneously for the proposed configuration of atomic beams collimated as well as divergent. For collimated atomic beams three initial boundary conditions

at t=0 are

$$\frac{\partial x}{\partial t} = v_x = 0 \tag{3.21}$$

$$\frac{\partial y}{\partial t} = v_y = 17 \text{ or } 1700 \text{ m/s} \tag{3.22}$$

$$\frac{\partial z}{\partial t} = v_z = 0 \tag{3.23}$$

Other three boundary conditions are x, y and z coordinates at t=0 (Fig. 3.19), which is given by

$$x = ab + cd\cos(\theta) \tag{3.24}$$

$$y = y_0 \tag{3.25}$$

$$z = eb + cd\sin(\theta) \tag{3.26}$$

Where a=-10,-8,.....,8,10, b=1 μm, c=0,1,2,3,4,5, θ=0,0.348,0.696,1.044,.....,2π rad, d=0.1μm, e =-10,-8,.....,8,10.

For divergent atomic beams three initial boundary conditions at t=0 modified to

$$v_x = \frac{v}{1.41}\sin(\theta_d) \tag{3.27}$$

$$v_y = v\cos(\theta_d) \tag{3.28}$$

$$v_z = \frac{v}{1.41}\sin(\theta_d) \tag{3.29}$$

$$\frac{\partial r}{\partial t} = v = (v_x^2 + v_y^2 + v_z^2)^{1/2} = 17 \text{ or } 1700 \text{ m/s} \tag{3.30}$$

Where θ_d is the divergence angle. The other three boundary conditions are same as shown in Fig. 3.19 and (and given by Eq. 3.24- 3.26) apart from the difference that now from each location 41 atoms are launched in coaxial cones (as shown in Fig. 3.20), such that the total

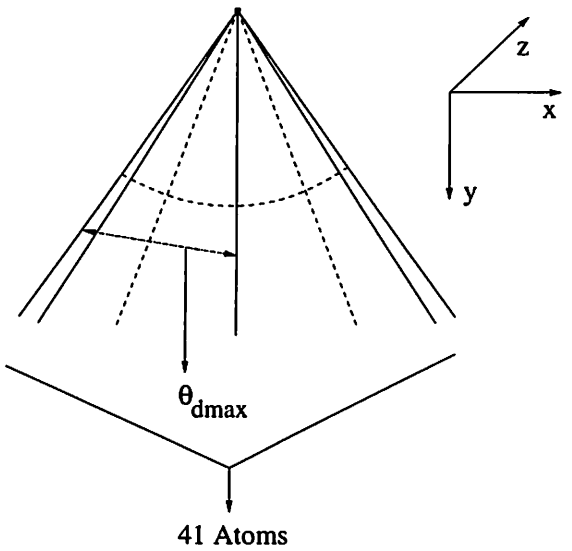

Figure 3.20: Launching coaxial cones of atomic beams for divergence angle θ_d

number of atoms in each beam are now 91×41 with a maximum cone angle (or θ_{dmax}) of 1 mrad and 4.5 mrad.

3.5.3 Result and discussions

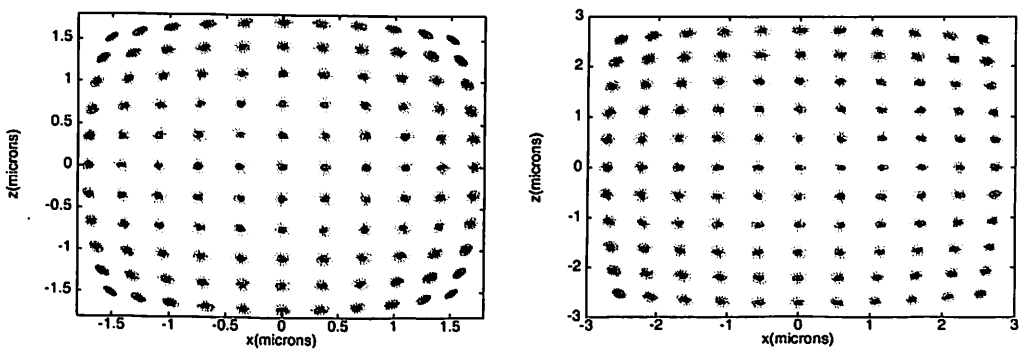

(a) (b)

Figure 3.21: Final positions of cold rubidium atoms after interacting with TEM_{00} mode laser for initially collimated set of atomic beams for time (a). 41.17 μs and (b). 44.11 μs

The sequence of computed lithographic patterns for collimated arrays of cold rubidium beams for interaction time of 41.17 μs and 44.11 μs (corresponding interaction length

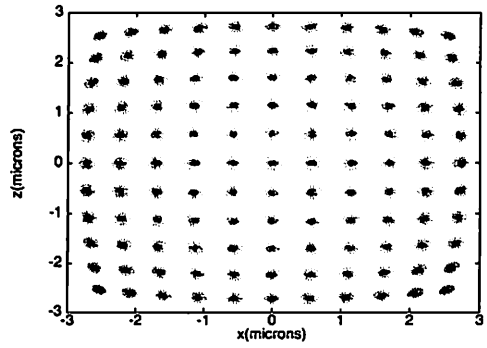

Figure 3.22: Final positions of thermal rubidium atoms after interacting with TEM_{00} mode laser for initially collimated set of atomic beams for time of 44.11 μs.

of 700 μm and 750 μm respectively) are shown in Fig. 3.21a and b respectively. The lithographic pattern of the atoms after an interaction time of 41.17 μs with the field is shown in Fig. 3.21a. Overall pattern compression factor as compared to initial configuration (Fig. 3.19a) is $\approx$ 5.8. The minimum periodicity of this pattern is 380 nm ($<\frac{\lambda}{2}$) and the individual atomic beams compressed to 200 nm in the center of the laser beam. Fig. 3.21b shows the pattern after an interaction length of 750 μm. The compression factor in this case is $\approx$ 3.6. The spot size at the center is expanded to 300 nm with periodicity 580nm ($>\frac{\lambda}{2}$). The astigmatism in the pattern is because of non uniform gradient of intensity distribution of TEM_{00} mode. The lithographic pattern for thermal (1700 m/s) atomic beam for an interaction length of 75000 μm (it is chosen such that to keep the interaction time same with that of Fig. 3.21b ($\frac{75000\mu m}{1700 m/s} = 44.11\mu s$) is shown in Fig. 3.22c. This pattern has the same periodicity, compression factor and individual beam compression factor as that of cold beam (Fig. 3.21b).

The well collimated atomic beams for such lithography is an ideal choice but practically not possible. Therefore we have considered the effect of divergence of the atomic beam. The starting configuration of atomic beam is shown in Fig. 3.19 and Fig. 3.20. Fig. 3.23 and Fig. 3.24 shows the lithographic patterns for such configuration for interaction length of 700 μm and 750 μm, corresponding to interaction time of 41.17 μs and 44.11 μs for cold

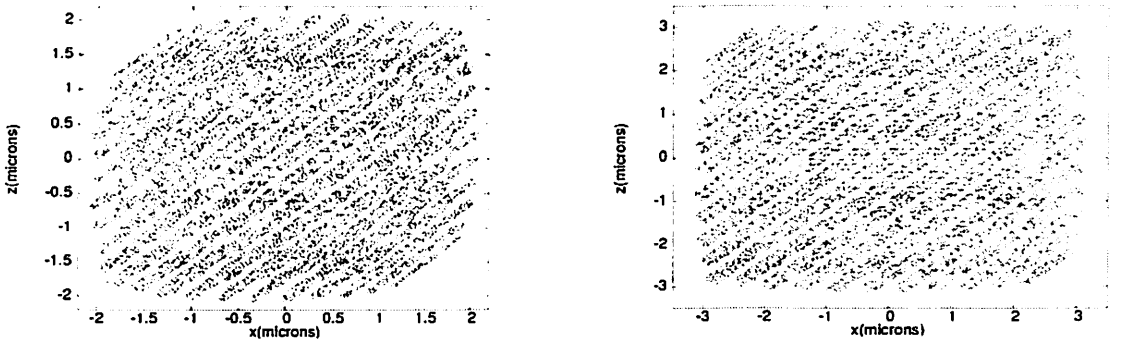

(a) (b)

Figure 3.23: Final positions of cold rubidium atoms after interacting with TEM_{00} mode laser for set of atomic beams having initial cone angle of 1 mrad for time (a). 41.17 μs and (b). 44.11 μs

rubidium atoms. The lithographic patterns of atoms after an interaction time of 41.17 μs

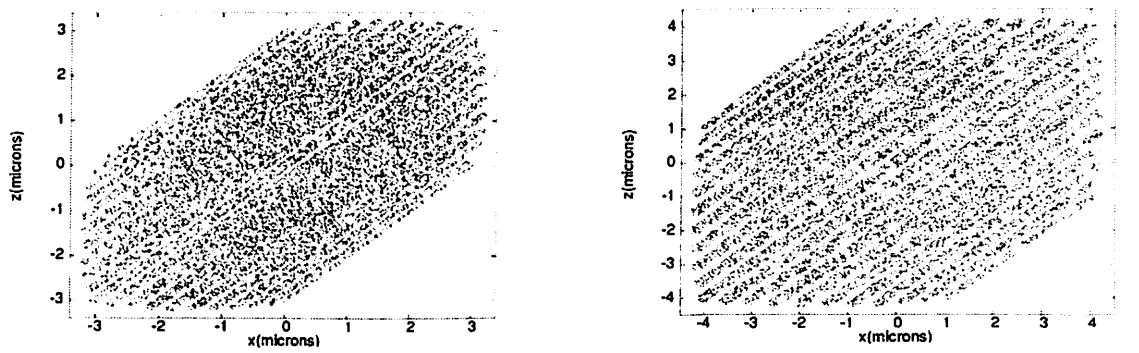

(a) (b)

Figure 3.24: Final positions of cold rubidium atoms after interacting with TEM_{00} mode laser for set of atomic beams having initial cone angle of 4.5 mrad for time (a). 41.17 μs and (b). 44.11 μs

with the field is shown in Fig. 3.23a and Fig. 3.24a. These patterns shows the line structure of atoms with periodicities 320 nm and 300 nm (both $<\frac{\lambda}{2}$) for maximum divergence of 1 mrad and 4.5 mrad respectively at the center of the pattern. The corresponding line thicknesses, at the center are nearly equal to 220 nm and 210 nm respectively. The overall compression factor in this case is $\approx$ 5 and 3.2 respectively. The pattern further expands

after an interaction time of 44.11 μs, as shown in Fig. 3.23b and Fig. 3.24b with overall compression factor $\approx$ 3.3 and 2.4 respectively. The periodicities of these patterns are 490 nm and 500 nm (both $>\frac{\lambda}{2}$) with line thickness 330 nm and 340 nm respectively. The reason for observed line structure can be symmetric atomic distribution along x and z direction of the atomic beams at the launching position. Final positions of thermal rubidium atoms (1700 m/s) after an interacting length of 75000 μm (again it is chosen such that to keep the interaction time same with that of Fig. 3.23b and Fig. 3.24b) for maximum divergence of 1 mrad and 4.5 mrad are shown in Fig. 3.25a and 3.25b respectively. These patterns are

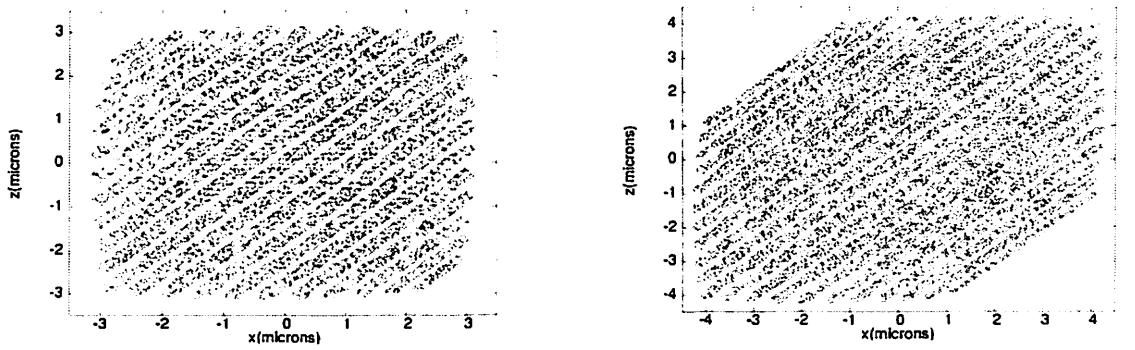

(a) (b)

Figure 3.25: Final positions of thermal rubidium atoms after interacting with TEM_{00} mode laser for set of atomic beams having initial cone angle of (a). 1 mrad and (b). 4.5 mrad for time 44.11 μs

having same periodicity, line thickness and overall pattern compression factor as that of the cold beam (Fig. 3.23b and Fig. 3.24b).

3.6 Isotopic separation of Uranium using dipole force

In the previous sections, we have worked out some novel configurations of atomic beams as well as light fields for the manipulation of trajectories of atoms to focus down to micron and nanometer dimensions for the generation of periodic structures. The trajectories of

atoms depends on the gradient in intensity of the laser field as well as on the atomic species (energy level scheme). Therefore, using the appropriate configuration, the dipole force can also be applied for isotopic separation. In this section, we have taken Uranium as an example to demonstrate the scope of dipole force for isotopic separation.

World consumption of enriched U^{235} (fissile isotope of uranium) has enhanced due to the increase in the number of light water nuclear power reactors. Natural uranium contains about 99.275% of U^{238} and 0.72% of U^{235} remaining 0.005% is U^{234}. It is neccesary to get 2.5–5% concentration of U^{235} in nuclear fuel to start and sustain the chain reaction in nuclear power reactors. There are two commericial processes [131] employed for the enrichment of U^{235}, (a). Gaseous diffusion process and the (b). Centrifuge process. Both these proceses are costly and requires high power, moreover these techniques require cascade stages as one stage can not yield the required concentration of U^{235}. There are some laser enrichment processes [131] which exploits the isotopic shifts of the transition for the selective ionization of isotopes. These ions so formed can be separated by physical or chemical proceses. This technique is still in development stages and hence not applied on a commercial scale. Both commercial processes, mentioned above, become less efficient in separating U^{235} from U^{236} which is generally contained in the recycled nuclear fuel because of almost identical masses .

A new scheme to separate U^{235} from U^{238} and U^{236} by using dipole force from a counter propagating TEM_{00} mode of laser is proposed. The dipole force modifies the trajectories of atoms and with the proper selection of controlling parameters viz; gradient in intensity and detuning, the different isotopes can be made to focus at different location in the transverse plane.

3.6.1 Proposed scheme and configuration details

In the proposed scheme we have exploited isotopic shifts of uranium, but in a more direct way. For the present scheme, $5f^3 6d7s^2\ {}^5L_6 - 5f^3 6d7s7p\ {}^7M_7$ transition of uranium was considered. The energy level diagram depicting the isotopic shifts [132] for U^{235}, U^{236} and U^{238} is shown in Fig. 3.26. The laser was blue detuned by 6746 MHz and 1626 MHz for U^{238} and U^{236} isotopes respectively but it is red detuned by 1626 MHz for U^{235} as shown in Fig. 3.26. Following Eq. 2.48, with this choice of detuning, U^{235} will be attracted towards the positive gradient in intensity where as U^{238} and U^{236} will be attracted towards the negative gradient in the field. The schematics of proposed experimental configuration is shown in Fig. 3.27. Low divergent cold atomic beam can be generated by pulsed laser ablation of thin film is allowed to interact with counterpropagating TEM_{00} laser beam (Fig. 3.27). The different isotopes of uranium in the atomic beam experiences dipole force in different directions owing to the isotopic shifts. The bigger isotopes of uranium viz; U^{238} and U^{236} are thrown away from the laser beam (because of the blue detuning) and U^{235} gets focused at the center of the laser beam (because of the red detuning).

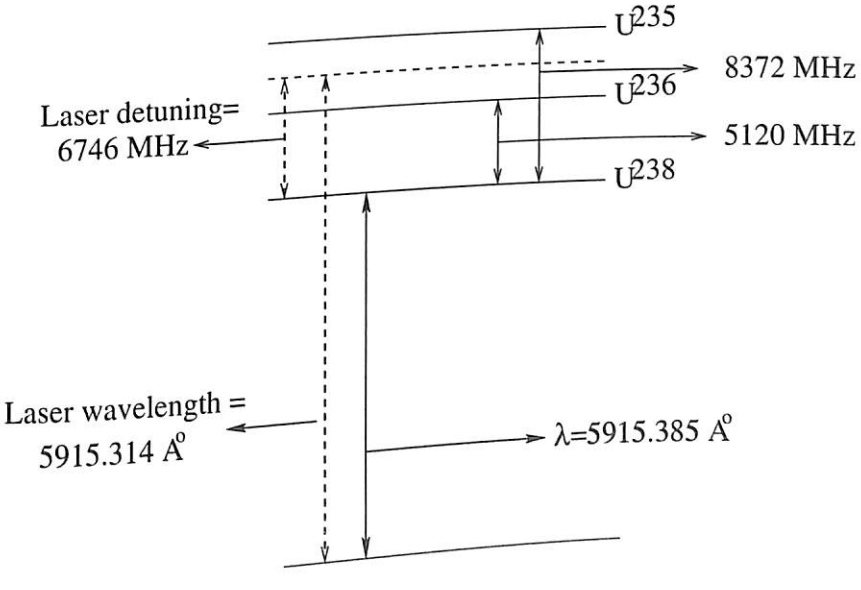

Figure 3.26: Energy level digram of uranium showing isotopic shifts and laser detuning

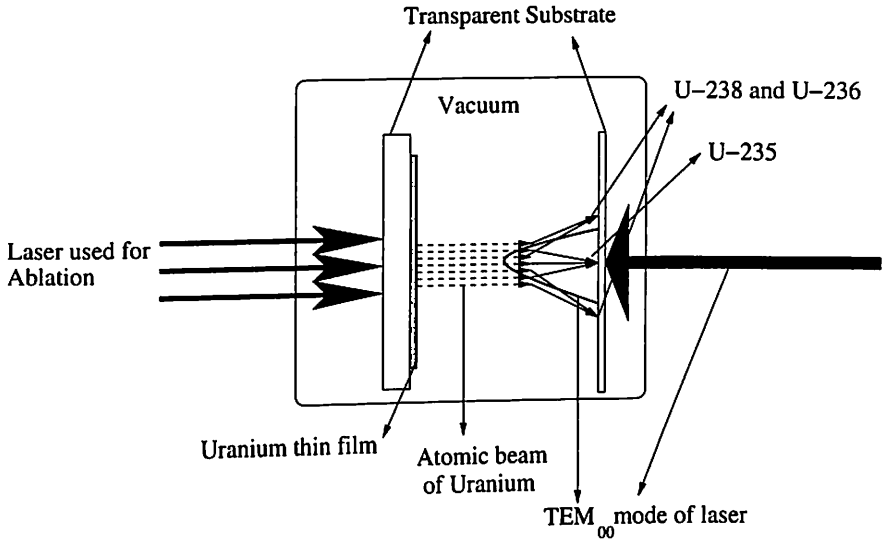

Figure 3.27: Proposed experimental scheme for isotopic separation of uranium

From Eq. 2.48, equations of motion of atoms in x, y and z direction traveling in counter propagating TEM_{00} mode of laser (Eq. 3.1) are given by

$$m\left(\frac{\partial^2 x}{\partial t^2}\right) = \frac{2x\hbar\delta_L}{\frac{w(y)^2[1+(\frac{y}{y_0})^2]}{I_0 exp[-2(x^2+z^2)/w(y)^2]} + \frac{\Gamma^2}{I_{sat}(\Gamma^2+4\delta_L^2)}} \tag{3.31}$$

$$m\left(\frac{\partial^2 z}{\partial t^2}\right) = \frac{2z\hbar\delta_L}{\frac{w(y)^2[1+(\frac{y}{y_0})^2]}{I_0 exp[-2(x^2+z^2)/w(y)^2]} + \frac{\Gamma^2}{I_{sat}(\Gamma^2+4\delta_L^2)}} \tag{3.32}$$

$$m\left(\frac{\partial^2 y}{\partial t^2}\right) = 0 \tag{3.33}$$

The peak intensity of laser at the center of the beam waist was taken to be 4 W/m^2 corresponding to the saturation intensity of uranium transition $5f^3 6d7s^2\ ^5L_6 - 5f^3 6d7s7p\ ^7M_7$ [133]. The laser wavelength is blue detuned (δ_L= 6746 MHz) from the resonance line of 5915.385 A^0 of U^{238}. The natural linewidth of the above transition is 0.7169 MHz [133]. Eq. 3.31, 3.32 and 3.33 are computed simultaneously for the modified trajectories of uranium isotopes for collimated as well as divergent atomic beams under dipole force. The atoms are

assumed to enter in the field at a Rayleigh distance with respect to the location of beam waist (w_0=50 μm) of laser.

Boundary conditions

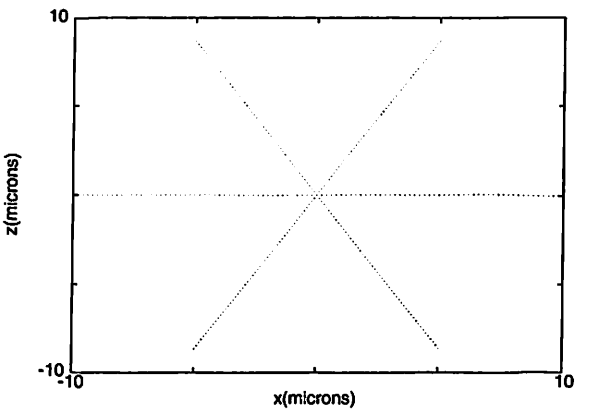

Figure 3.28: Launching position of uranium isotopes in presence TEM_{00} mode of laser

For collimated atomic beams, three initial boundary conditions at t=0 are

$$\frac{\partial x}{\partial t} = v_x = 0 \tag{3.34}$$

$$\frac{\partial y}{\partial t} = v_y = 100 \text{ m/s} \tag{3.35}$$

$$\frac{\partial z}{\partial t} = v_z = 0 \tag{3.36}$$

Other three boundary conditions are x, y and z coordinates at t=0, which is given by

$$x = Rd\cos(\theta) \tag{3.37}$$

$$y = y_i = \text{interaction length} \tag{3.38}$$

$$x = Rd\sin(\theta) \tag{3.39}$$

Where R = 0, 2, 4,....., 98, 100, d = 0.1 μm and θ = 0, 1.04, 2.09,....., 2π rad. Pictorially x-z initial coordinates of atoms are shown in Fig. 3.28. For divergent atomic beams three

boundary conditions at t=0 modified to

$$v_x = \frac{v}{1.41}\sin(\theta_d) \tag{3.40}$$

$$v_y = v\cos(\theta_d) \tag{3.41}$$

$$v_z = \frac{v}{1.41}\sin(\theta_d) \tag{3.42}$$

$$\frac{\partial r}{\partial t} = v = (v_x^2 + v_y^2 + v_z^2)^{1/2} = 100 \text{ m/s} \tag{3.43}$$

Where θ_d is divergence angle. The other three boundary conditions are same as shown in Fig. 3.28 and (and given by Eq. 3.37- 3.39) apart from the difference that now from each location 5 atoms are launched in coaxial cones with a maximum cone angle (or θ_{dmax}) of 5 mrad.

The purpose of these simulations is to show the difference in the dipole force direction experienced by different uranium isotopes, therefore number of atoms of each uranium isotope is taken to be equal regardless of their relative abundances. Also the initial positions of all uranium isotopes is taken to be same.

3.6.2 Simulated results

Modified trajectories of initially collimated cold (100 m/s) uranium atomic beam for an interaction length of 5000 μm are shown in Fig. 3.29. Two dimensional cross sectional view of Fig. 3.29 and it's magnified central portion is shown in Fig. 3.30. One can clearly see from this picture the different paths taken by U^{235}, U^{236} and U^{238} isotopes and subsequently the separation in their final positions. Due to larger blue detuning and hence more repulsive force, U^{238} isotope shoots out of the laser beam much faster than U^{236}. Red detuning makes U^{235} atoms to focus themselves at the center of laser beam having positive gradient with focal spot of U^{235} around 3×3 μm.

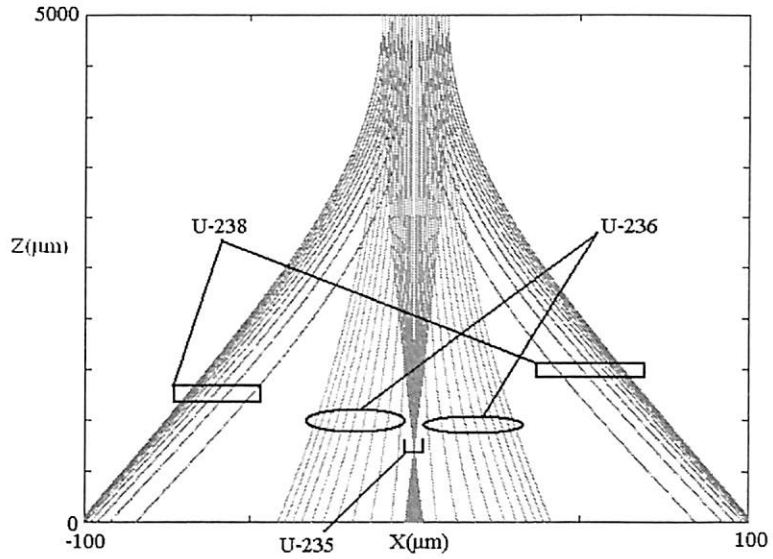

Figure 3.29: Trajectories of initially collimated uranium atoms under dipole force

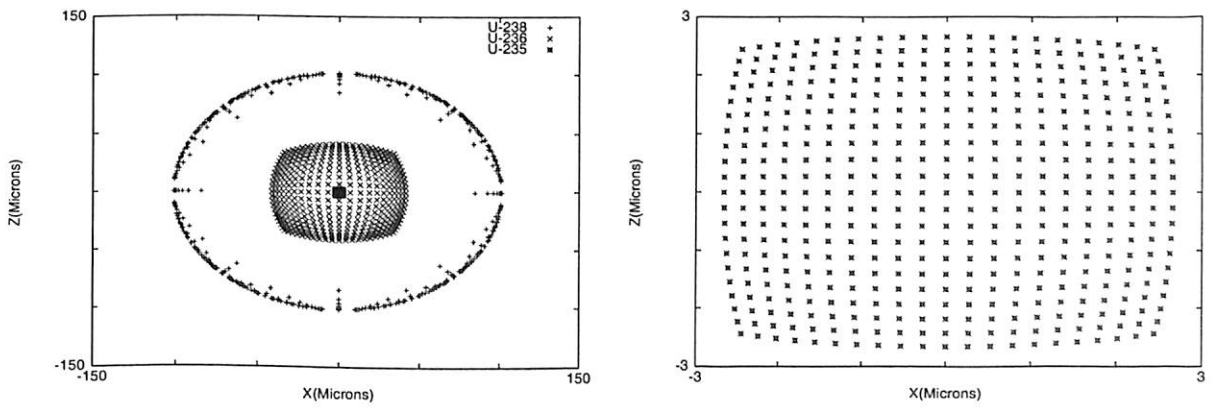

(a) (b)

Figure 3.30: (a). Cross sectional view of final positions of initially collimated uranium isotopes after an interaction length of 5000 μm with TEM_{00} mode of laser (b). Expanded central portion of (a) showing focus spot of U^{235} isotope

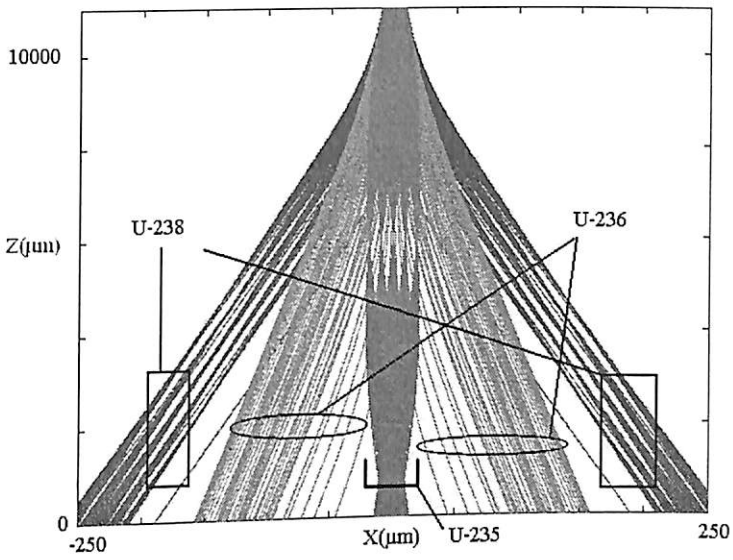

Figure 3.31: Trajectories of initially divergent uranium atoms under dipole force

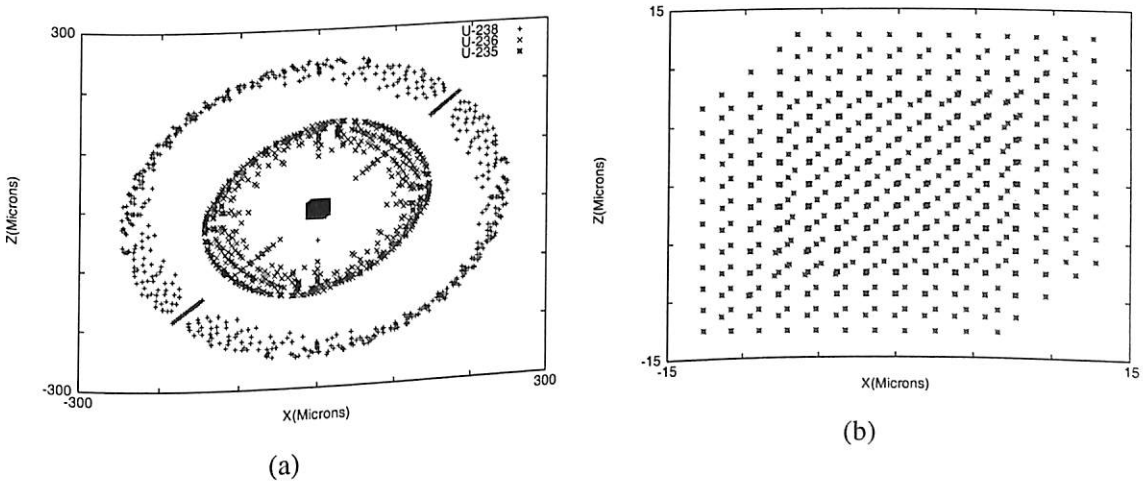

(a) (b)

Figure 3.32: (a). Cross sectional view of final positions of divergent uranium isotopes after an interaction length of 11000 μm with TEM_{00} mode of laser (b). Expanded central portion of (a) showing focus spot of U^{235} isotope

To consider the effect of divergence of the atomic beam, the starting configuration of atomic beam was considered similar to the previous case with a difference that beam is assumed to be launched in a cone, with a cone angle of 5 mrad. Trajectories are simulated for an interaction length of 1100 μm and are shown in Fig. 3.31. Two dimensional cross sectional view of Fig. 3.31 and it's magnified central portion is shown in Fig. 3.32. Besides the smearing effect due to the divergence, the overall concept seems to be valid in this case also. Here the focal spot of U^{235} is found to be around 15×15 μm.

3.7 Conclusion

The simulated rubidium atomic trajectories for TEM_{00} mode of laser and standing wave configuration via dipole force shows multiple focusing of atoms for longer interaction time with the light field. The interaction time required for the focusing of the atomic beam is independent of longitudinal velocity of atoms but decrease with the increase in the intensity of light field. The focused spot of divergent atomic beam is broad compared to the collimated atomic beam.

The computed lithographic patterns for a single atomic beam traveling in counterpropagating two dimensional periodic potentials generated via interference of four optical beams shows the accumulation of atoms towards the center of the potentials. Thus the proposed configuartion may find its application in microfabrication and fabrication of photonics devices.

The computed results for the proposed new configuration of matrix of micro-ovens (cold and thermal) yield interesting patterns with periodicities much less than $\lambda/2$ in presence of single potential from a TEM_{00} mode laser. The proposed configuration is relatively simple because it doesn't require any conditioning of light potential as directly TEM_{00} mode is used. Simulated results confirms that the focusing is independent of the temper-

ature of the beam. It depends only on the interaction time. Thus the idea of using arrays of atomic beams in TEM_{00} mode appears to be a promising configuration for generation of periodic nano structures. The trajectories simulated in this Chapter is for rubidium atoms but this configuartion is very much applicable to other atoms also. The fabrication of such closely spaced micro-ovens delivering large number of discrete atomic beams with small divergence is not very difficult. In Chap.4 we described the technique of producing such large arrays of pulsed atomic beams and results are discussed in Chap.6.

Apart from the nano lithography, dipole force can be applied for isotopic separation of Uranium by choosing laser detuning cleverly. Depending on the experimental arrangement, one can play with the laser detuning for the collection of required isotopes either at the center of the laser beam or outside it. This technique can be applied for isotopic separation of any element which has strong transition lines for which a tunable laser is available. Here, particularly we proposed this scheme for uranium for following reasons.

- This method is cheap and requires very less power compared to already existing techniques.
- It separates the isotopes in a single step.
- It may prove efficient for the enrichment of uranium from natural uranium as well as recycled nuclear fuel.

Chapter 4

Experimental set-up

4.1 Introduction

One of the major requirement for the formation of periodic nano structures via dipole force is low divergence atomic beam. Collimated atomic beams is also a topic of interest because of its importance in the field of atom optics [90, 134], laser spectroscopy [88] and in the fabrication of optoelectronic devices [135]. The most general method for the production of atomic beam is thermal oven. The divergence of atomic beam generated directly from the thermal ovens is in the range of radians. With the help of appropriate set of apertures, the divergence of the beam is reduced and finally fine collimation is performed via laser cooling [134]. Application of thermal oven is restricted to the materials of low melting points only. There have been reports [113, 116, 118] on the generation of pulsed neutral atomic beam over wide range of materials using laser ablation of thin foil, solid target and thin film. The laser ablation for the production of atomic beams can be used for any material irrespective of their melting points. It has ability to produce high atomic flux with energies ranging from cold to super-thermal range. In the earlier report [118], laser is focused from the rear side onto the thin films of the material resulting into the ablation of material from

the thin film, giving atomic beam. Because of the focusing of the laser beam, the laser energy gets concentrated over a small region, the momentum distribution and hence the divergence of the resulting atomic beam is large and the collimation is required for precision application viz; micro/nano lithography. We have reported for the first time [129] production of low energy low divergence pulsed atomic beam via laser ablation using unfocused laser beam. In this chapter, the experimental set-up developed by us for the production of low divergence low energy pulsed atomic beam is described. The beam deflection set-up, divergence measurement and the ablation dynamics via reflectivity measurement, developed in the present work are described for the characterization of atomic beam.

The experimental set-up developed for direct single shot micro-nano lithography via selective laser ablation using two and four beams high power laser interferometry is discussed. The experimental set-up developed for the one and two dimensional arrays of atomic beams via high power laser interferometry is also discussed. This is the technique developed for the first time for the production of matrix of micro ovens for the generation of arrays of atomic beams in square geometry. This matrix of micro oven is a promising configuration for nanolithography via dipole force as proposed in chap.3 for deposition of atoms having periodicity less than $\lambda/2$.

4.2 Experimental set-up for the generation and characterization of pulsed atomic beam

4.2.1 Generation of atomic beam

Thin films of Indium were used for the rear side ablation for the production of cold low divergence pulsed atomic beam. Thin film was deposited on the cleaned microscopic glass

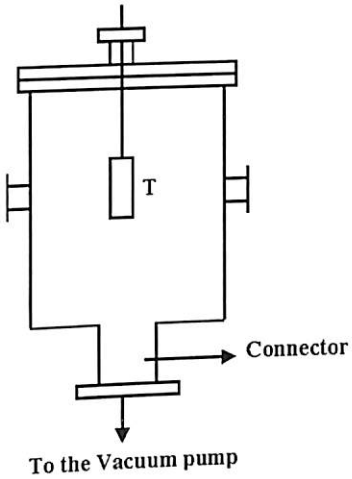

Figure 4.1: Side-view of Vacuum chamber

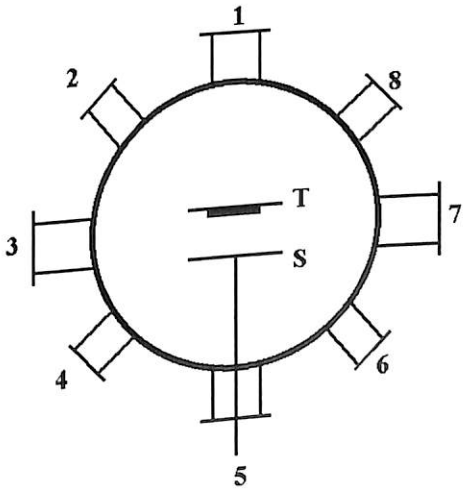

Figure 4.2: Top-view of Vacuum chamber. T; Target (Indium thin film), S; Glass substrate, 1,3,5,7; 50 KF ports, 2,4,6,8; 40 KF ports

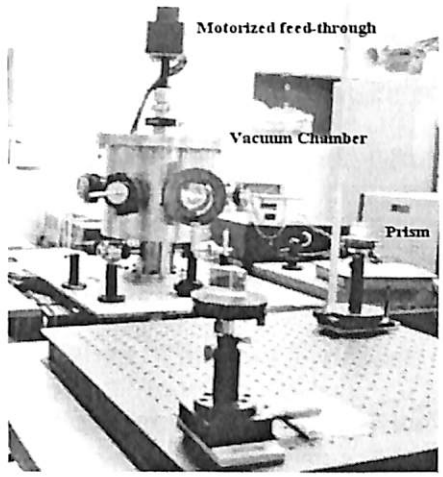

Figure 4.3: Photograph of Vacuum chamber

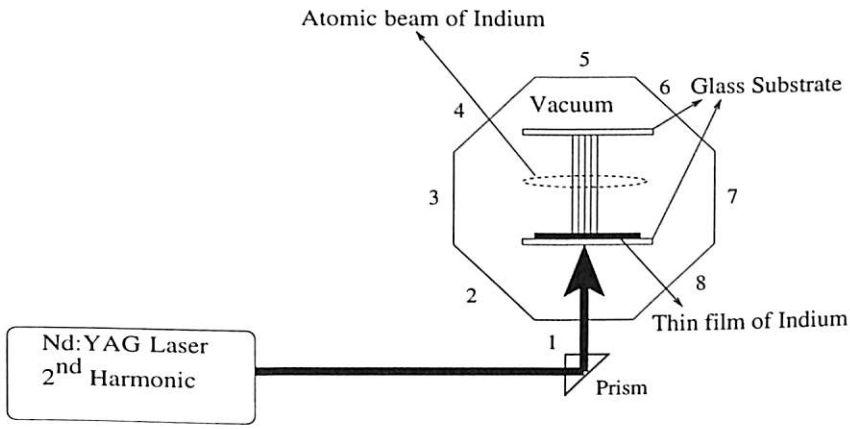

Figure 4.4: Atomic beam generation set-up via rear side unfocused laser ablation of thin film

plates via thermal evaporation coating unit in a base pressure of 10^{-6} Torr. Indium metal used for the deposition was of purity 99.995% , bought from Nuclear Fuel Complex, Hyderabad . The thin film was mounted inside the ablation chamber (make; New Poona Industries, Pune) from the top port as shown in Fig. 4.1. The ablation chamber was cylindrical in shape, made up of stainless steel, internal diameter of 44 cm and length 30 cm, having alternate four 50 KF ports and four 40 KF ports located equidistant on the curved surface as shown in Fig. 4.2. The top flange of the chamber contained a 50 KF port. Thin film was inserted through this port by a motorized translator assembly (Technovac, Bangalore),

as shown in the photograph of Fig. 4.3, such that the thin film can be scanned completely through one of the 50 KF port (port 1). The port 1 was sealed with 50 KF view port containing polished glass window. The thin film was aligned nearly parallel to the glass window. The opposite 50 KF port (port 5) to port 1, a glass substrate was inserted through a wilson feed-through for the deposition of atomic beam. Rest of the ports were sealed with either respective view ports having polished windows for other optical diagnostics or with the blank flanges. The bottom of the chamber was welded with a 100 cm length and internal diameter 100 mm collar (Fig. 4.1). The free bottom end of this collar was connected to the diffusion pump backed by rotary pump. The pirani and penning gauges were mounted at appropriate ports for the measurement of vacuum in the pump as well as in the chamber. The base pressure of the chamber was maintained below 10^{-5} Torr. Thin films of Indium

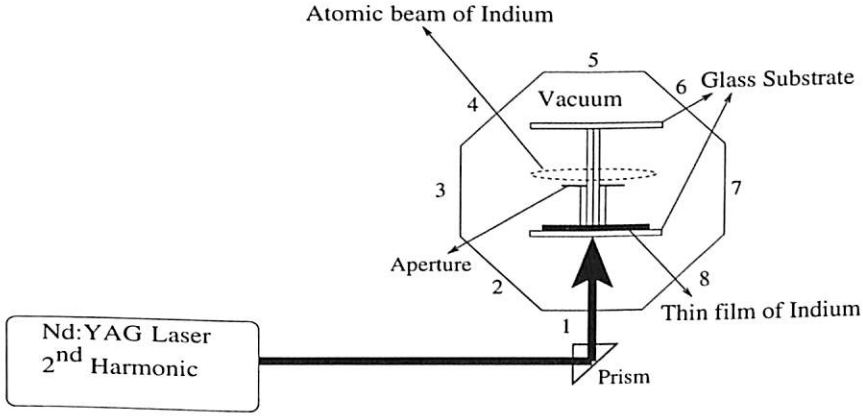

Figure 4.5: Set-up with the aperture for the collimation of atomic beam

were illuminated from the rear side directly by second harmonic of Q switched Nd:YAG laser (400 mJ in fundamental, 8 ns pulse width, beam diameter 8 mm, model HYL101 Quanta System) under high vacuum (10^{-5} Torr). A 90^0 degree prism was used for steering the laser beam into the vacuum chamber as shown in Fig. 4.3 and 4.4. Thin film of Indium was kept slightly slanted to the incoming laser beam to avoid retro-reflection of laser beam going back into the laser head. During the experiment, thin film was moved vertically via

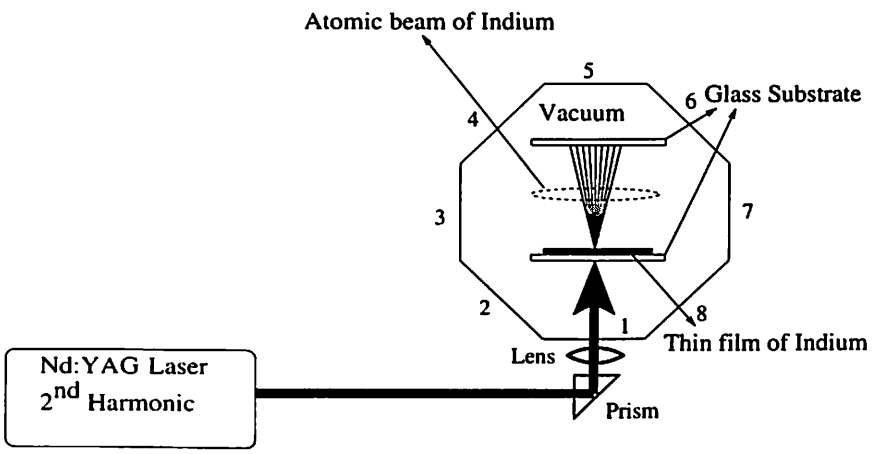

Figure 4.6: Atomic beam generation set-up via focused laser

motorized feed-through to get the fresh region for ablation for each shot. The low divergence low energy atomic beam thus produced was deposited onto the substrate placed few centimeters apart. For curtailing the divergence further, an aperture was inserted into the chamber by wilson feed-through, through 90^0 degree 50 KF port 3 in between the substrate and the target as shown in Fig. 4.5. Experiments were also performed with focused laser beam. For this, instead of direct illumination, laser was focused (f =35 cm) onto the rear side of the thin film, as shown in Fig. 4.6 and atomic beam was deposited onto the substrate inserted through the opposite port.

4.2.2 Divergence measurement

Divergence of the atomic beam was measured by comparing the diameter of the ablated film and the diameter of the atomic beam deposited onto the substrate. For this a glass substrate was placed few centimeters apart from the thin film to deposit the indium atomic beam as shown in Fig. 4.4. The thin film was moved continuously via motorized feed through vertically to get the fresh portion for each shot of laser for ablation. This resulted into the formation of the ablated region in the form of a strip. The divergence was estimated by measuring the diameter of the deposited spot, the width of the ablated strip onto the target

using optical microscope (Zeiss Axiotech 100 HD) and the distance between the target and the substrate. The geometry of the measurement is shown in the Fig. 4.7. In the figure, X is the width of the ablated strip representing the ablated beam diameter at the target during the formation and beam diameter Y at a distance L, estimated by measuring the diameter of the deposition onto the substrate. The maximum angular divergence, θ_d, from Fig. 4.7 is given by.

$$\therefore \text{ Angular divergence} = \theta_d = 2\theta = 2\arctan(\frac{Y-X}{2L}) \tag{4.1}$$

The experiment was also conducted by placing apertures of 0.25 cm and 0.35 cm diameter

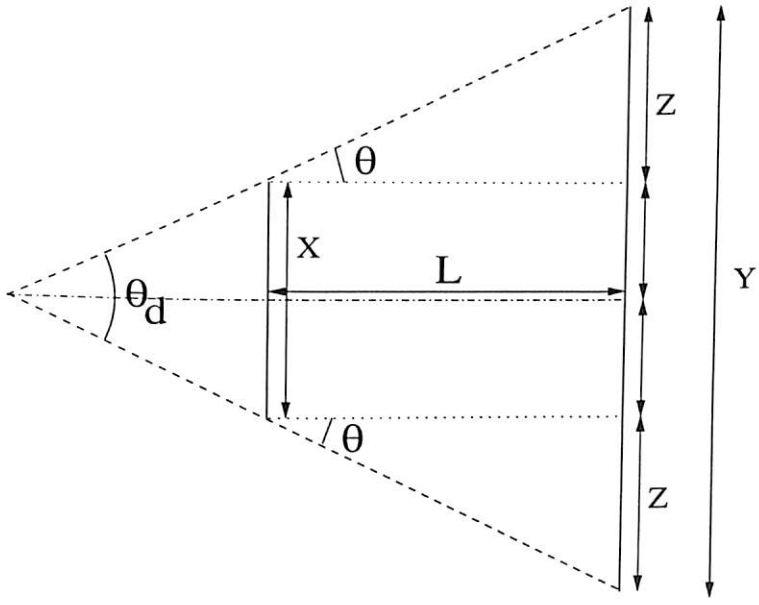

Figure 4.7: Divergence measurement of atomic beam. X; Ablated width of thin film, Y; Diameter of deposited atomic beam onto the substrate, L; Distance between thin film and glass substrate and θ_d; Angular divergence

in between the target and the substrate to curtail the divergence further, as shown in Fig. 4.5. For the divergence measurement with the aperture, X in Eq. 4.1 (and Fig. 4.7) represent the aperture diameter and L denotes the distance between the aperture and glass substrate. The divergence of the atomic beam produced from the focused laser was also measured.

These experiments were conducted number of times at different laser energies for target and substrate distances ranging from 2 to 10 cm.

4.3 Beam deflection set-up for the measurement of axial atomic velocity

The schematics of experimental set-up developed for the measurement of longitudinal velocities of atomic and ionic beam is as shown in Fig. 4.8. An unfocused laser beam from the second harmonic of Nd:YAG laser was used to illuminate the indium thin film from the rear side under high vacuum (10^{-5} Torr). This resulted into the formation of slowly moving ionic and atomic species having low divergence. A 10 mW He-Ne laser (Melles Griot, 05-LHR-991) was aligned parallel to the thin film through a 90^0 port (port 3, Fig. 4.8) terminated with 50 KF view-port of the ablation chamber and detected by a photodiode 1 (PD 1, Melles Griot) placed at the opposite window (port 7). Both, the He-Ne laser and PD1 were mounted on a linear translation stage (least count 10 μm). A part of Nd:YAG laser beam, by taking 4% of 4% reflection from the two microscopic glass plates G1 and G2 illuminated photodiode 2 (PD 2, Melles Griot) and displayed onto Tektronix TDS 2012 Two Channel Digital Storage Oscilloscope (DSO) for the trigger as well as for reference signal. The DSO was used in the single shot acquisition mode. As a result of the production of pulsed atomic beam via rear side laser (Nd:YAG) illumination of thin film, He-Ne laser gets deflected and accordingly the photodiode signal (PD1) undergoes modulation and is recorded onto DSO. Both He-Ne laser and PD1 were moved simultaneously, away from the target so as to record the deflection signals at a different longitudinal position for the time of flight measurement. Both the PD's (1 and 2) were terminated with 50 Ω terminator. By measuring the peak position of the deflection signal at known distances from the

target, the velocity of propagation of the beam was measured for various laser energies per pulse. For the measurement of velocity of pulsed atomic or molecular beams, time of flight measurement by recording mass spectra [136] and fluorescence spectra [116] are reported very well. These techniques are relatively involved compared to time of flight measurement via beam deflection set-up [137, 138]. The measurements are performed directly in beam deflection set-up using TEM_{00} mode He-Ne laser onto the photodiode. Therefore spatial resolution as well as signal to noise ratio are large compared to the other techniques.

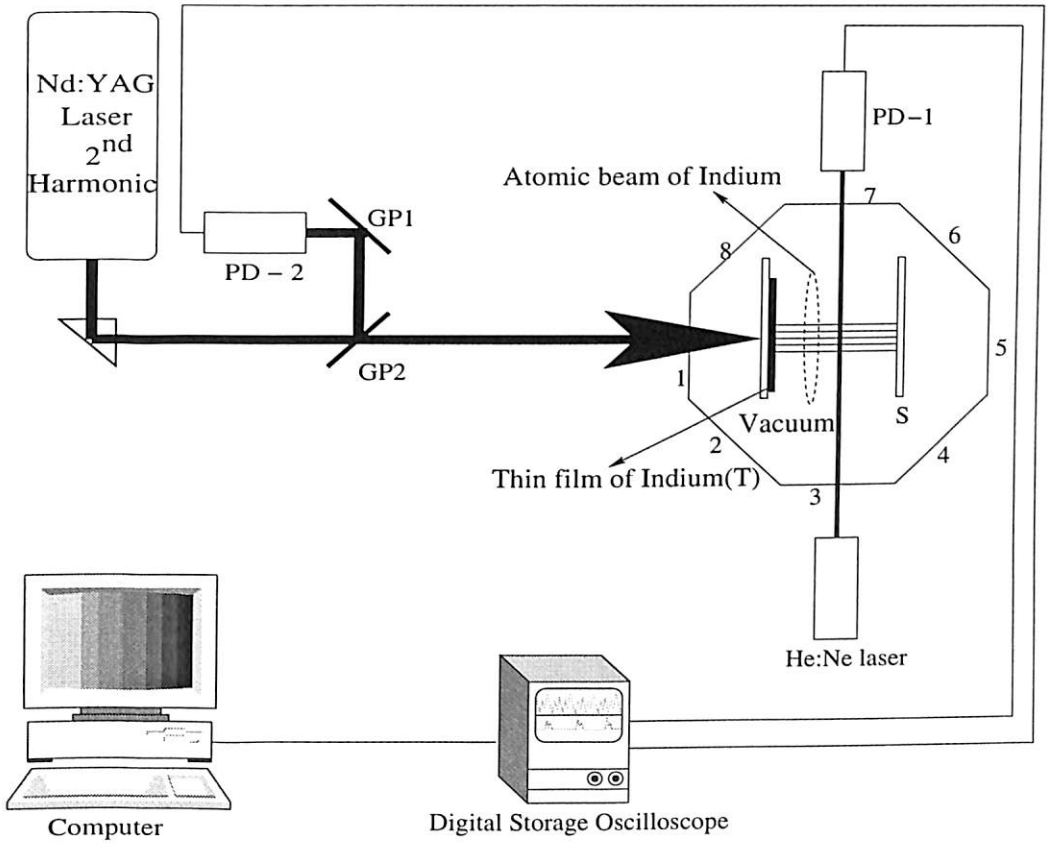

Figure 4.8: Longitudinal atomic velocity measurement set-up. PD1,2; Photodiode, GP1,2; Glass plates, T; Indium thin film, S; Glass substrate

4.4 Reflectivity modulation of thin film during ablation

For recording the ablation dynamics, a 10 mW He-Ne laser (Melles Griot, 05-LHR-991) was launched from port 4 so as to illuminate the target film at 45° as shown in Fig. 4.9. The reflected beam was detected with PD 1 kept at 90° port 6 with respect to that of He-Ne laser. As a result of ablation, reflectivity of the thin film changes, hence the intensity of the He-Ne laser falling onto PD 1 changes and is displayed onto the DSO. The trigger signal was taken from PD2 as described in the Sec. 4.3. These experiments were also performed for various laser energies.

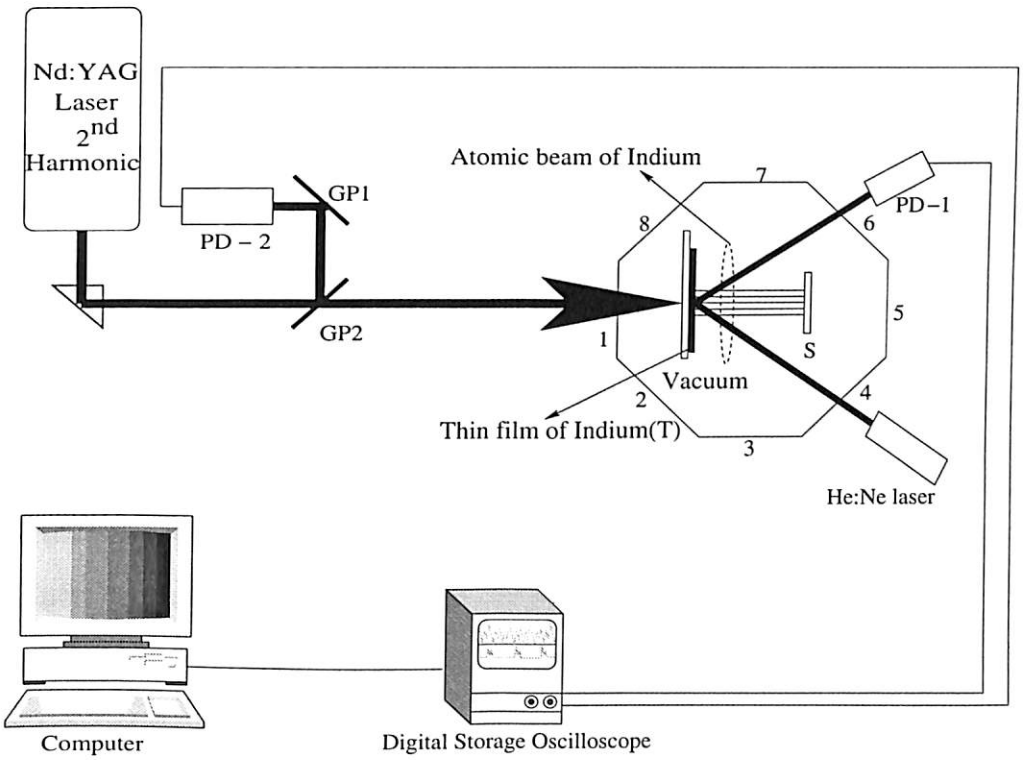

Figure 4.9: Experimental Set-up used to study ablation dynamics of thin film. PD1,2; Photodiode, GP1,2; Glass plates, T; Indium thin film, S; Glass substrate

4.5 Selective laser ablation lithography

The technique of selective laser ablation lithography (SLAL) is based on modifying the surface morphology by selectively ablating the material using high power laser. This is a very general technique and is applicable to any material. In this technique, thin films of metals, semiconductors, polymers or any other complex compound can be ablated selectively by illuminating it with interference pattern formed by high power laser. This results in the ablation of materials in the region of maximum intensity leaving the area exposed to minimum intensity unaffected. The periodicity of the pattern so formed will depend on the spatial frequency of the interference pattern. The width of the line depends on the laser intensity and damage threshold of the material of the thin film. The process can be explain with the help of intensity distribution of the interference pattern shown in Fig. 4.10 with the line marked for the damage threshold. From the figure it is clear that the thin film exposed to the intensities above the damage threshold will be ablated leaving behind rest of the material unaffected and thus by changing the intensity of the laser the writing width can be controlled. This technique is a single step single shot and does not require any mask. In the earlier reported configuration of laser interference lithography for direct write lithography [85], there was no on line control on the pattern geometry. We have developed the Michelson interferometer using high power laser for the single step single shot lithography without mask. The configuration has the advantage of having on line control on the periodic geometry configuration of the nano structures simply by modifying the interference pattern by adjusting tilts of mirror.

4.5.1 Selective laser ablation lithography in one dimension

The experimental set-up used for selective ablation lithography in one dimension is shown in Fig . 4.11. A Michelson interferometer was assembled with two high damage thresh-

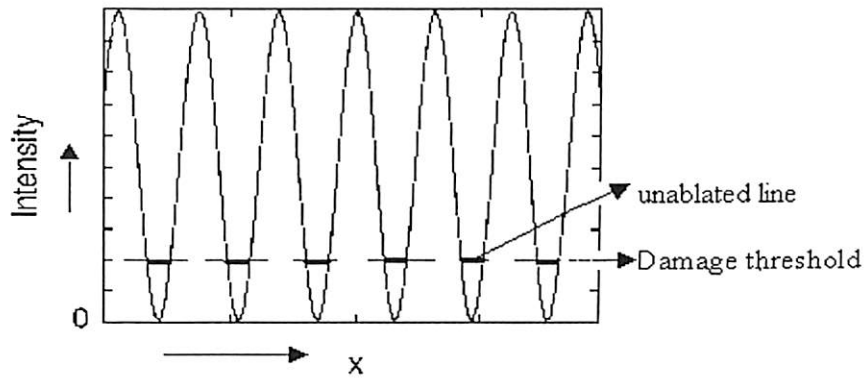

Figure 4.10: Intensity distribution in the interference pattern

old broadband (400 nm - 650 nm) mirrors M_1 and M_2 (Melles Griot) and a anti-reflection coated high damage threshold cube beam splitter BS (Melles Griot, 03BSC009). The interferometer was illuminated with second harmonic of Nd:YAG laser with the help of 90^0 prism P_1. The output of this interferometer results into the straight parallel fringes. the spatial frequency μ of this interference pattern depends on the angular separation of two beams given by [139]

$$\mu = \frac{\sin(\theta)}{\lambda} \tag{4.2}$$

Where θ is the angular separation between two interfering beams and λ is the wavelength of the laser light used. θ can be adjusted with the tilt of mirror M_1 or M_2. The interference pattern was steered with the help of other two 90^0 prism P_2 and prism P_3 into the vacuum chamber through one of the 50 KF port to illuminate the thin film from the rear side. For the fine writing, interference pattern was compressed with the help of a lens L (f=25 cm) such that the distance between the lens and the thin film was 30 cm thereby compressing the pattern by a factor of 0.2. With 8 mm diameter Nd:YAG laser beam, it gives the pattern size of 1.6 mm onto the thin film. The region of indium thin film exposed to the bright fringes was ablated leaving behind the Indium lines in the dark fringe region. The surface morphology of the thin film after selective ablation was scanned with optical microscope.

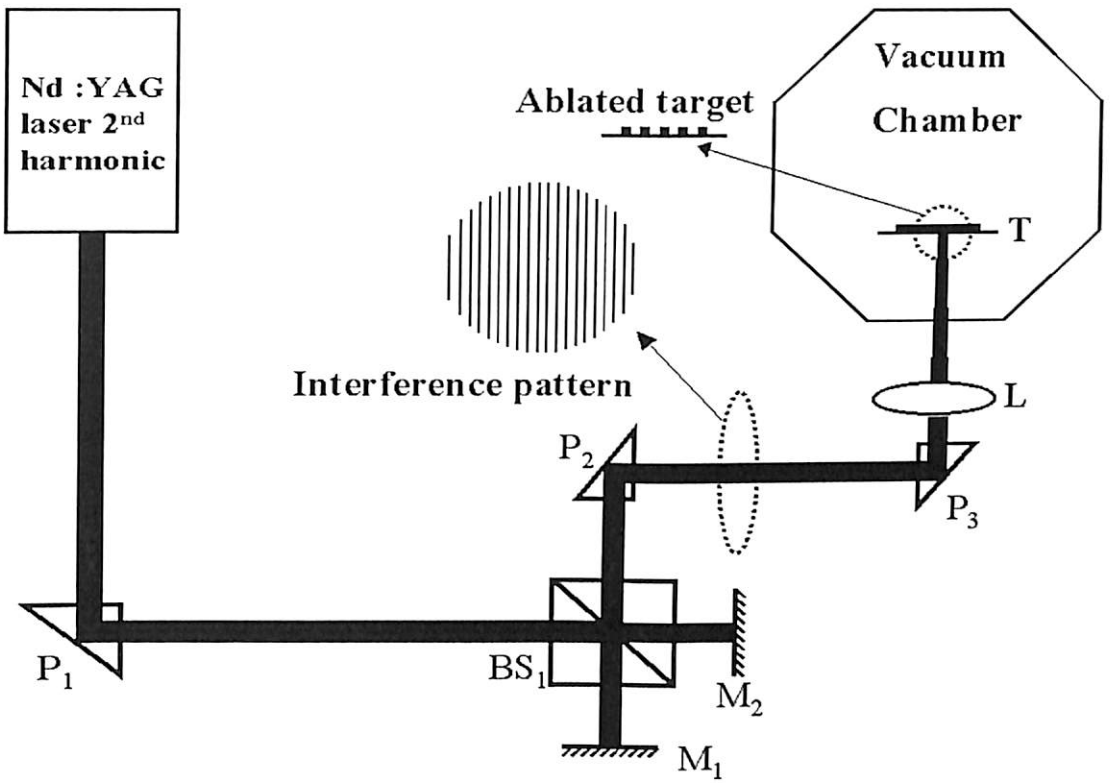

Figure 4.11: Experimental set-up for selective laser ablation lithography in one dimensions. P_{1-3}; Prism, BS_1; Beam Splitters, M_{1-2}; Mirrors, L; Lens, T; Target Indium thin film and S; Substrate

4.5.2 Selective laser ablation lithography in two dimension

For the two dimensional periodic lithography in a single shot, single step, two Michelson interferometer in tandem were aligned, as shown in Fig. 4.12, with the help of four high damage threshold mirrors M_{1-4} (Melles Griot) and two anti-reflected coated high damage threshold cube beam splitters BS_{1-2} (Melles Griot, 03BSC009). Beam splitter BS_1 and mirrors M_1 and M_2 forms the first stage of the interferometer similar to the Fig. 4.11 giving the two interfering beams. These two beams were launched into the second Michelson interferometer comprising of beam splitter BS_2 and mirrors M_3 and M_4. The output of BS_2 consists of four nearly collinear interfering beams. The resultant intensity distribution of these four beam is given by Eq. 3.13. The mirror tilts were adjusted in such a way

that the interference pattern of individual stages were oriented perpendicular to each other. This gives the arrays of equal illuminating light spots in the square geometry as shown in Fig. 3.12 and Fig. 4.12. The interference pattern steered into the vacuum chamber with the help of prism P_2 after compressing it with the lens as describe in Sec. 4.5.1. It finally illuminated the rear side of indium thin film T, kept in the vacuum chamber (10^{-5} Torr) as shown in Fig. 4.12. The region of indium thin film exposed to the bright spot was ablated, imprinting the structures onto the thin film in two dimensional arrays of square geometry.

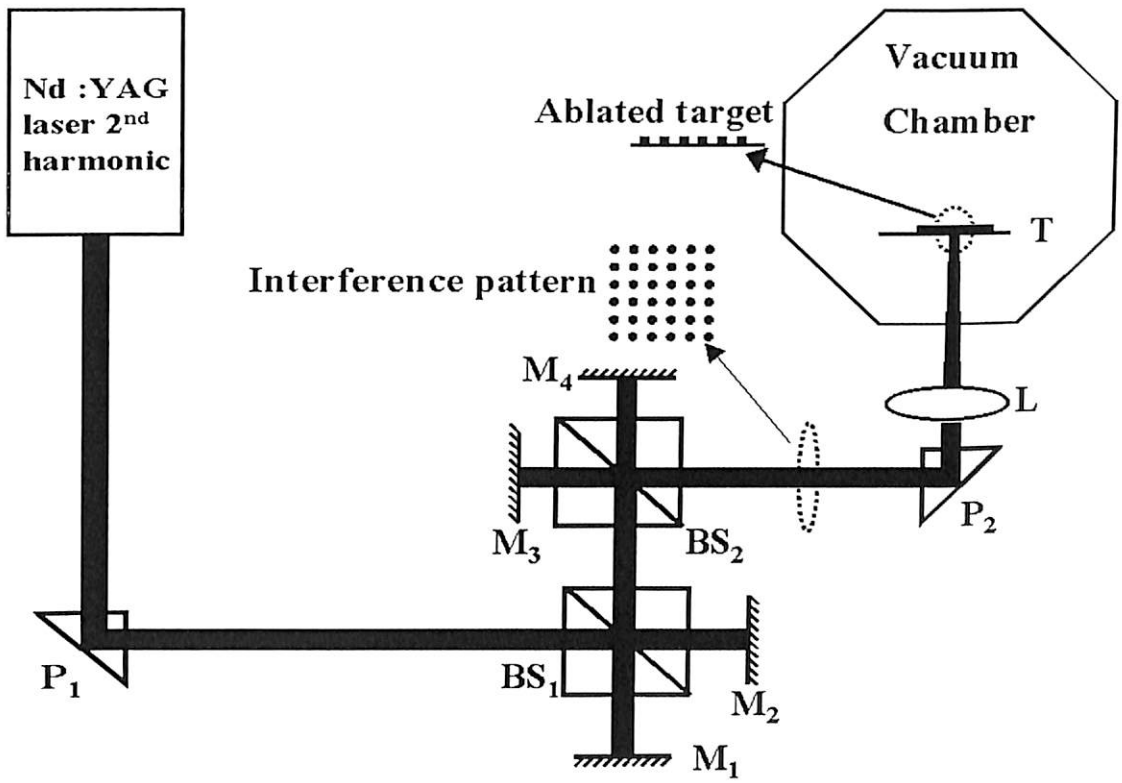

Figure 4.12: Experimental set-up for selective laser ablation lithography in two dimensions. P_{1-2}; Prism, BS_{1-2}; Beam Splitters, M_{1-4}; Mirrors, L; Lens, T; Target Indium thin film and S; Substrate

4.6 Multiple atomic beam in one and two dimension

The experimental set-up developed for the generation of low energy low divergence atomic beam in the present work is described in Sec. 4.2. On the illumination of the thin film with high power laser directly (Fig. 4.4). The material of the thin film is ablated resulting into the generation of the atomic beam. In Sec. 4.5, We have described the selective ablation of the thin film to perform single step single shot lithography via high power laser interferometer. When the thin film was illuminated with the interference pattern formed by high power laser the region of the bright fringes was ablated leaving behind the large arrays of structure written on the film (Fig. 4.10). The material which is selectively ablated results into the atomic beam. Thus, by illuminating the thin film from the rear side by interferometric pattern, one can not only perform the lithography but also large number of parallel atomic beams get evolved. In other words, large number of sculpted atomic beams can be generated via selective laser ablation. With the one Michelson interferometer sculpting is in one dimension and with two Michelson interferometer in tandem, sculpting is in two dimension resulting into large number of discrete atomic beams in square array geometry in a single shot. This system can also be called as matrix of micro-ovens. These set-ups are reported for the first time by us for the generation of large number of periodic atomic beams.

4.6.1 Sculpted atomic beams in one dimensions

Experimental set-up for the generation of Sculpted atomic beam in one dimensions is shown in Fig. 4.13. A Michelson interferometer was aligned using second harmonic of Q-Switched Nd:YAG laser. Various optical components used in the set-up (prisms, mirrors, beam splitter) reduces the intensity of laser beam. Therefore intensity of the interference pattern is very small compared to the direct laser beam. The intensity of unfocused pattern

was not sufficient to ablate the material of the thin film. Therefore a lens of focal length 25 cm is used to increase the intensity of the pattern by compressing it and thereby increasing the spatial frequency of the interference pattern also. This focused interference pattern was allowed to fall onto the rear side of Indium thin film (target) kept in high vacuum (10^{-5} Torr). This set-up is similar to that of Fig . 4.11, with the addition of a glass substrate (S) inserted through the opposite port via wilson feed-through kept few millimeter apart from the Indium thin film to collect the ablated atomic beam for the topographical analysis of atomic beams. The rear side illumination of thin film by second harmonic of Nd:YAG laser

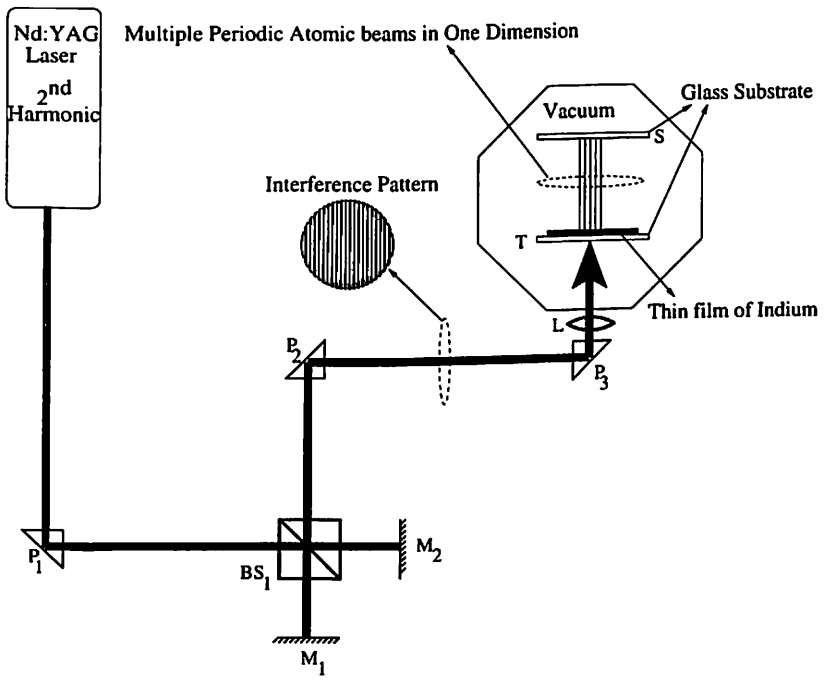

Figure 4.13: Schematics of experimental set-up used for generation of sculpted atomic beam in one dimension. P_{1-3}; Prism, BS_1; Beam Splitters, M_{1-2}; Mirrors, L; Lens, T; Target Indium thin film and S; Substrate

results into the ablation of indium in the region of maximum intensity (bright fringe) leaving the area of minimum intensity (dark fringe) unaffected. The morphology of the planer parallel atomic beams will be similar to as that of the interference pattern. The substrate and target were scanned with the optical microscope.

4.7 Matrix of micro-ovens

Experimental set-up for the generation of Sculpted atomic beam in two dimensions is shown in Fig. 4.14. Two Michelson interferometer were aligned in tandem using second harmonic of Q-Switched Nd:YAG laser and the focused interference pattern was allowed to fall onto the rear side of Indium thin film kept in high vacuum (10^{-5} Torr). This set-up is similar to that of Fig . 4.12, only difference here is the one glass substrate (S) kept few millimeter apart from the Indium thin film to collect the ablated material for the topographical analysis of beams. The interference pattern of this four beam set-up is shown in Fig. 4.14 as

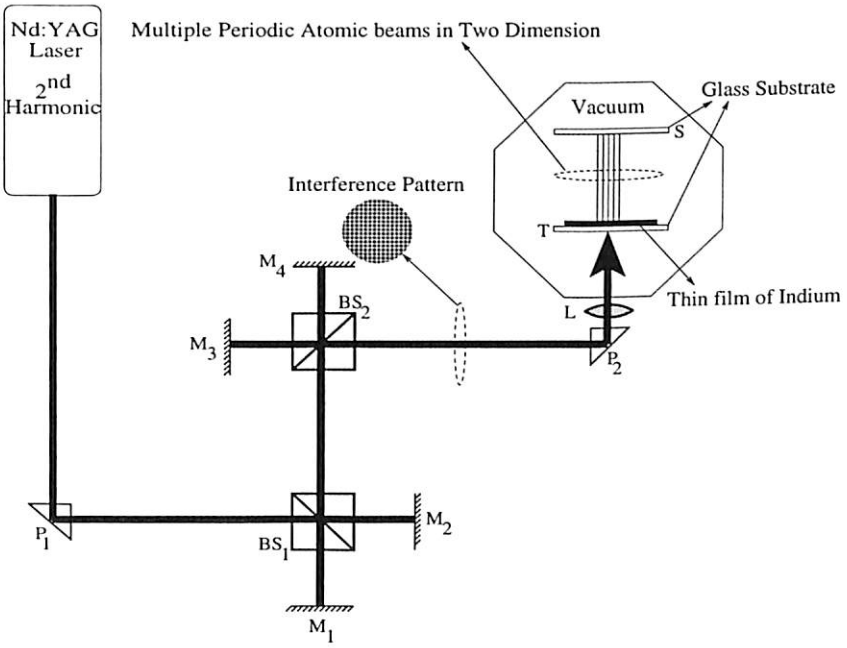

Figure 4.14: Schematics of experimental set-up used for generation of sculpted atomic beam in two dimension. P_{1-2}; Prism, BS_{1-2}; Beam Splitters, M_{1-4}; Mirrors, L; Lens, T; Target Indium thin film and S; Substrate

well as in Fig. 3.12 containing equal illuminating bright spots in square geometry. The rear side illumination of thin film by second harmonic of Nd:YAG laser results into the ablation of indium in the region of maximum intensity (bright spot) leaving the area of minimum intensity (dark spot) unaffected. The periodicity and geometry of the resultant atomic beams

will have similar two dimensional morphology as that of the interference pattern. These atomic beams were deposited on the glass substrate placed a few millimeters apart from the target for the topographical analysis of beams. The substrate and target was scanned with the AFM (Smena B, NTMDT).

4.8 Conclusion

Experimental set-up developed for the production and characterization of low-energy low-divergence pulsed atomic beam of Indium via rear side ablation of thin film is described. A novel technique of single-shot single-step selective laser ablation lithography in one and two dimension is presented. The experimental set-up for the application of selective laser ablation lithography for the generation of multiple arrays of atomic beams in one and two dimension is discussed for the first time.

Chapter 5

Low-divergence low-energy pulsed indium atomic beam via laser ablation

5.1 Introduction

The generation of pulsed atomic beam via laser ablation have been reported on variety of pure metals [111–118]. The laser ablation technique for the atomic beam can be used for any material irrespective of melting point and chemical reactivity. It has the ability to produce high atomic flux having energies from cold to super-thermal range. In most of the earlier reports, a high power laser is focused onto the desired target. The ablation of the material takes place resulting into the formation of the atomic beam. The intensities at the focal point are very large and therefore substantial portion of the material is converted into the plasma and more over expansion of the ablated material is hemispherical. Therefore the divergence of the atomic beam generated by focused laser ablation is very large.

In the present work, we report the generation of low-divergence low-energy pulsed atomic beam of Indium by using an unfocused laser. The divergence measurement and the

velocity measurements are reported as a function of laser energy.

5.2 Atomic beam generation

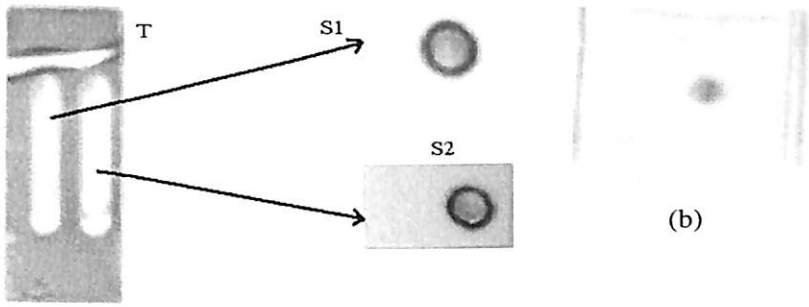

(a)

Figure 5.1: (a). Ablated Target (T) and the deposited ablated beams on substrates S1 and S2 without aperture (b). Deposited Indium beam with aperture of size 0.35 cm.

The experimental set-up for the generation of pulsed atomic beam of indium via rear side ablation of thin film using second harmonic of high power Nd:YAG laser under high vacuum (10^{-5} Torr) is shown in Fig. 4.4. A glass substrate was kept few centimeters apart from the thin film to deposit ablated atomic beam for divergence measurement, XRD and EDAX studies. Fig. 5.1a shows the ablated target of indium thin film (T) and the substrate S1 and S2 obtained by depositing the ablated Indium atomic beam for ten shots. The target T was moved vertically so that the fresh portion of the Indium thin film was available for every shot of laser. On illumination with Nd:YAG laser continuously (10 pps), the material of the thin film was ablated from the target at every shot resulting into the region of transparent strip of width almost equal to the size of the laser beam (8 mm diameter), as shown in Fig. 5.1a. The central region of the deposited atomic beam onto S1 and S2 shown in Fig. 5.1a have lesser density than outer portion, this is due to the ablation of the material from this region by the left over energy of Nd:YAG laser which comes out from the ablated

portion of the target (T). Fig. 5.1b shows the deposited atomic beam for ten consecutive shots of laser onto the glass substrate with aperture of size 0.35 cm kept in between the target and substrate

5.2.1 X-ray diffraction and EDAX spectrum

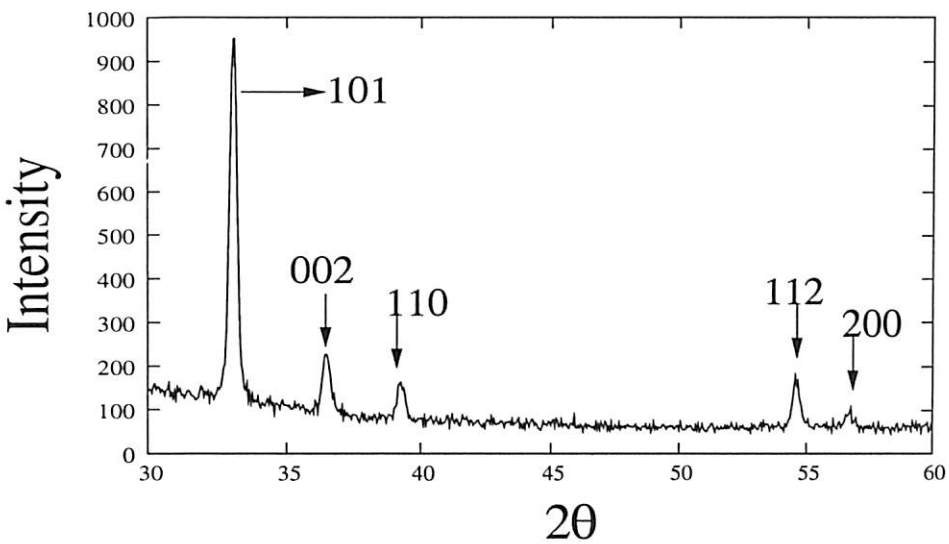

Figure 5.2: X-ray diffraction pattern of deposited indium atomic beam

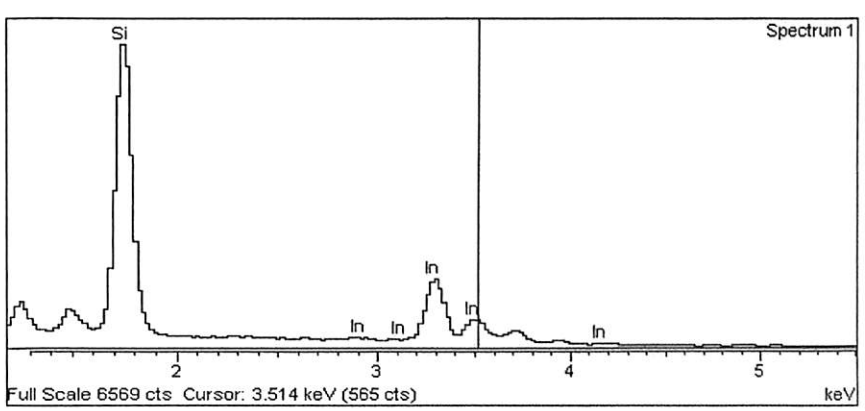

Figure 5.3: EDAX spectrum of deposited indium atomic beam

Powder X-ray diffraction (XRD) (SEIFERT, XRD 3003 TT, Cu K_α radiation, λ=1.5418

A^0) and Energy dispersive X-ray analysis (EDAX) (LEO 1430 VP, OXFORD Instruments, T353) were performed on the thin film obtained by depositing the ablated pulsed atomic beam of Indium for ten consecutive shots at laser fluence of 242.7 mJ/cm^2 per pulse. X-ray diffraction pattern (XRD) and EDAX spectrum are shown in Fig. 5.2 and Fig. 5.3 respectively. The XRD pattern matches with standard reference of indium given in the literature [140]. Particle size is measured using FWHM of 101 peak and is found to be 26.5 nm. From the EDAX spectrum, Fig. 5.3, the weight percentage of indium is found to be equal to 58.03%, the rest of being is that of glass (Si) substrate. This confirms that the ablated beam is made up of indium only.

5.3 Divergence of atomic beam

The divergence of the atomic beam generated via laser ablation is measured by comparing the size of the beam at the target and the diameter of the beam deposited onto the substrate kept few centimeters apart. The experiments were performed with and without aperture for unfocused laser beam. Typically 8-10 shots of atomic beam were deposited onto the glass substrate. The divergence was also recorded with the focused beam without any aperture. The geometry of the measurement is shown in Fig. 4.7. The results of divergence measurement for unfocused and focused laser beam and with and without aperture are listed in table. 5.1. In table. 5.1, θ and θ_1 are the average angular divergence with unfocused laser without aperture and with aperture respectively. θ_2 is the average angular divergence with focused laser and without aperture. The laser energy per pulse listed in table 5.1 and in subsequent sections were measured with the broad band power/energy meter (Model 13 PEM001, Melles Griot). The fluence was calculated from this by considering the size of the laser beam (focused or unfocused). The divergence of the atomic beam was found to increase with the laser fluence. The lowest divergence was found to be equal to 23 mrad

without using any aperture or collimation atom optics with laser energy on the target 43 mJ/pulse and corresponding fluence of 85.5 mJ/cm^2. This is the lowest divergence reported probably without the use of any collimated atom optics. The presence of aperture curtails the wings of the atomic beam and reduces the divergence. The experimental set-up with the aperture is shown in Fig. 4.5. With the aperture of 0.25 cm, the divergence of the atomic beam was 75 mrad and with that of 0.35 cm the divergence was 88 mrad. Both the measurement were performed at the laser fluence of 242.7 mJ/cm^2 (corresponding laser energy of 122 mJ/pulse). Smaller size aperture results into the low divergent atomic beam but simultaneously it will reduce the atomic flux.

The divergence with unfocused beam is about one orders of magnitude less than that of produced with focused laser at same (unfocused) energy per pulse 122 mJ, table. 5.1. This is because of increase in the divergence of the incidence light as well as the intensity drastically which gives more random kicks to the atoms forming the thin film, hence to greater divergence.

Laser fluence per pulse (mJ/cm^2) (unfocused)	Laser energy per pulse (mJ)	θ (mrad)	θ_1 (mrad) Aperture size= 0.35cm	0.25cm	θ_2 (rad) at 3.8 J/cm^2
242.7	122	237±9.3	88±3.5	75±3	2.3±0.9
169.1	85	81±3.2			-
85.5	43	23±0.9			-

Table 5.1: Comparison of angular divergence of Indium atomic beam at different laser powers, with/without apertures and with unfocused/focused laser beam. θ is the average angular divergence with unfocused laser and without aperture, θ_1 is the average angular divergence with aperture and unfocused laser and θ_2 is the average angular divergence with focused laser and without aperture.

This is the simplest possible technique of divergence measurement with an estimated error of 4%. For very low divergence, below 1 mrad, achieved via laser cooling [134] the

fluorescence measurement are more accurate.

5.4 Longitudinal velocity of Indium atomic and ionic beam

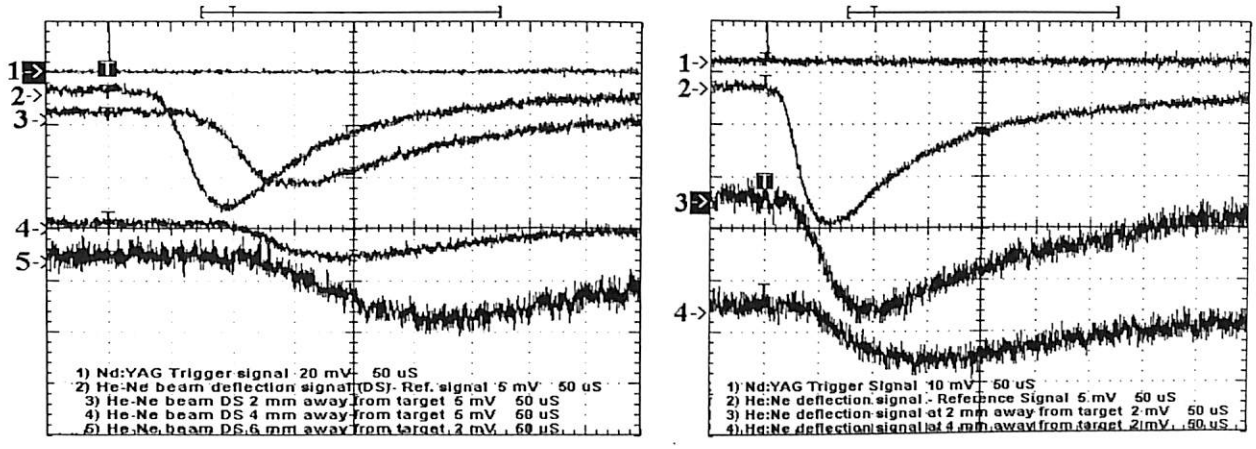

(a) (b)

Figure 5.4: Deflection signals for time of flight measurement of indium atomic beam at (a). 43 mJ and (b). 85 mJ laser energy per pulse. Trace-1; Nd:YAG signal from PD2. He-Ne deflection signal at: Trace-2; Close to the target, Trace-3; At 2 mm away from the target, Trace-4; At 4 mm away from the target and Trace-5; at 5mm away from the target.

The beam deflection set-up used for the measurement of velocity of neutrals and ions of Indium via time of flight detection is shown in Fig. 4.8. A He-Ne laser is launched perpendicular to the atomic beam detected by a photodiode PD1 and displayed onto Digital storage oscilloscope with 50Ω terminator. The photodiode registered a dip in the signal as a result of formation of the pulsed atomic and ionic beam via laser ablation. The beam velocity was measured by recording the PD1 signals at different distances in longitudinal direction. If t_1 and t_2 are the time for maximum dip in the signals with respect to the arrival of the laser pulse and d_1 and d_2 are their corresponding locations at which beam deflection

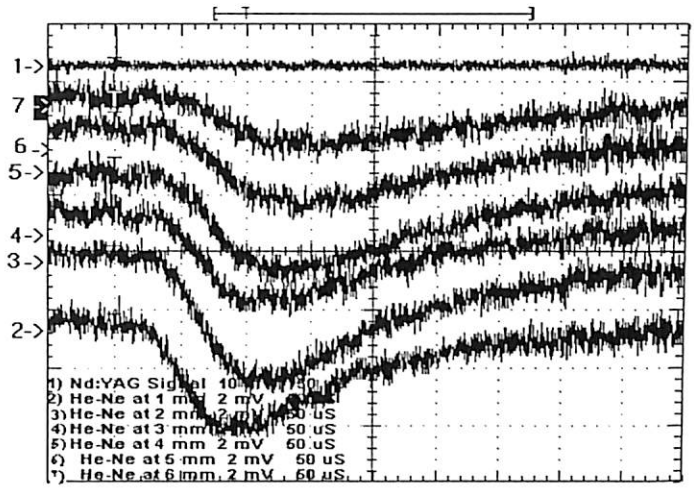

Figure 5.5: Deflection signals for time of flight measurement of indium atomic beam for 122 mJ laser energy per pulse. Trace-1; Nd:YAG signal. He-Ne deflection signal: Trace-2; Close to the target (1 mm away), Trace-3; 2 mm away, Trace-4; 3 mm away, Trace-5; 4 mm away, Trace-6; 5 mm away, Trace-7; 6 mm away from the target

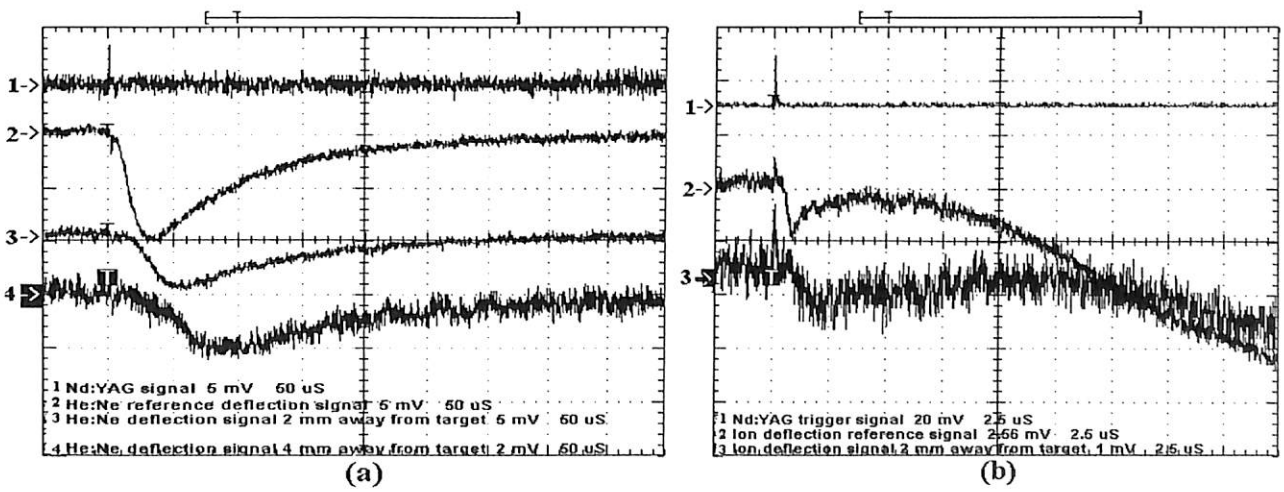

Figure 5.6: Deflection signals corresponding to (a) Atomic beam and (b) Ionic beam at various distances from the target at 160 mJ laser energy per pulse. Trace-1; Nd:YAG signal. He-Ne deflection signal: Trace-2; Close to the target, Trace-3; 2 mm away, Trace-4; 4 mm away.

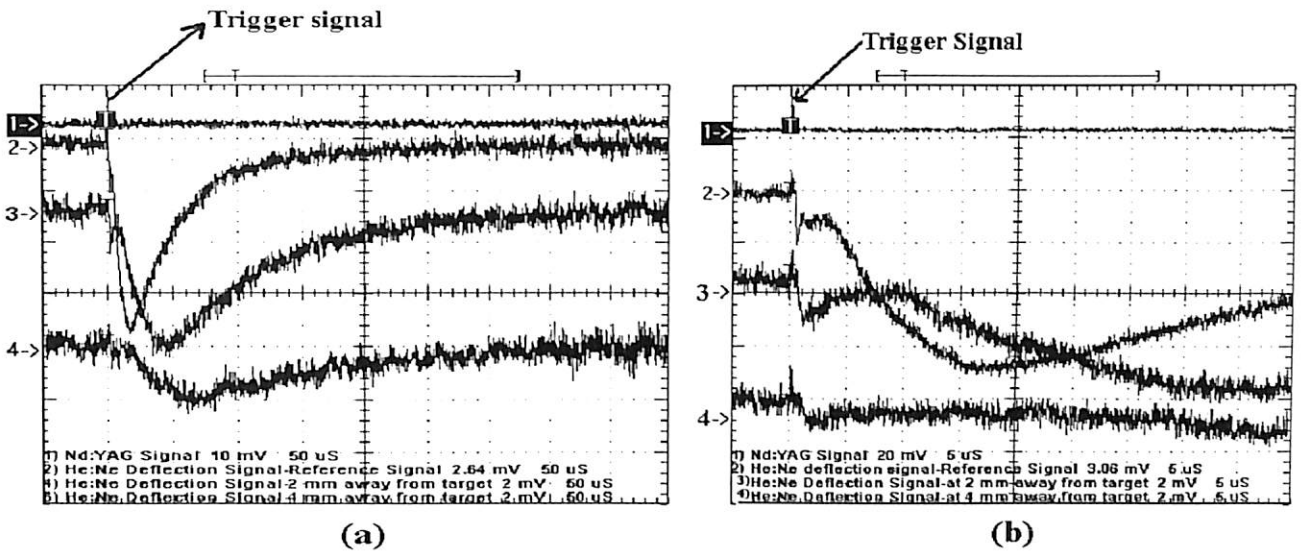

Figure 5.7: Deflection signals corresponding to (a) Atomic beam and (b) Ion beam at various distances from the target at 175 mJ/pulse. Trace-1; Nd:YAG signal. He-Ne deflection signal: Trace-2; Close to the target, Trace-3; 2 mm away, Trace-4; 4 mm away.

signals were recorded, then the velocity of the atomic beam is given by

$$v = \frac{d_2 - d_1}{t_2 - t_1} \tag{5.1}$$

The oscilloscope traces, recorded from the beam deflection set-up at various laser energies are shown in Fig. 5.4, 5.5, 5.6 and 5.7. The trace 1 of all the figures corresponds to the Nd:YAG signal used for triggering the DSO from PD 2 (Fig. 4.8). All other traces corresponds to He-Ne beam deflection signal from PD 1 (Fig. 4.8) at various distances from the target thin film.

Fig. 5.4a and b were recorded for the laser fluence of 85.5 mJ/cm^2 (43 mJ/pulse) and 169.1 mJ/cm^2 (85 mJ/pulse) respectively. Fig. 5.5 and 5.6 corresponds to laser fluence of 242.7 mJ/cm^2 (122 mJ/pulse) and 318.3 mJ/cm^2 (160 mJ/pulse) respectively. Oscillogram of Fig. 5.7 corresponds to that of 348.1 mJ/cm^2 (175 mJ/pulse). The velocity of the neutral

Laser fluence (mJ/cm^2)	Laser energy per pulse (mJ)	Axial Atomic velocity (m/s)	Axial Ionic velocity (m/s)
85.5	43	44±0.33	-
169.1	85	47±0.35	-
242.7	122	96±0.72	-
318.3	160	100±0.75	1333±10
348.1	175	100±0.75	3333±25

Table 5.2: Variation of axial atomic and ionic velocities with laser energy per pulse

atomic beam was estimated by measuring the shift in the peak position (dip) of the beam deflection signal for the known distances at same laser energy. Fig. 5.6a and Fig. 5.7a shows the two peaks. The first peak is very narrow and therefore signals at 318.3 mJ/cm^2 and 348.1 mJ/cm^2 were also recorded at the fast time scale of 2.5 and 5 μs respectively.

The first peak, corresponding to the higher velocity component, may be attributed to the ionic species and that of the second peak being slow corresponds to the neutrals. The average velocities of the atomic beam and ionic beam measured as a function of laser energy per pulse are listed in table. 5.2. Initially the velocities of atomic beam increases with the laser energy per pulse owing to the large momentum transfer with the higher and higher energies. No traces of ion peak was observed (Fig. 5.4, 5.5). After energy of around 122 mJ/pulse, no significant changes in neutral energy was observed. At higher energies, ionization of material of the thin film takes place as confirmed by the appearance of an additional peak in the early phase of the signal and so more and more laser energy is dissipated in the ion

formation rather than increasing the kinetic energy of the neutrals. Hence the ion energy increases beyond certain threshold as listed in table. 5.2. The percentage error estimated in these measurement is 0.75%.

5.5 Reflectivity modulation of thin film during ablation

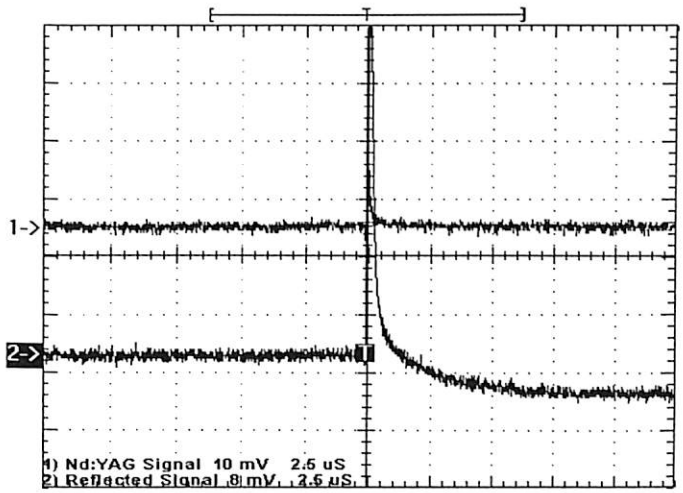

Figure 5.8: Reflectivity modulation of thin film at 43 mJ laser energy per pulse

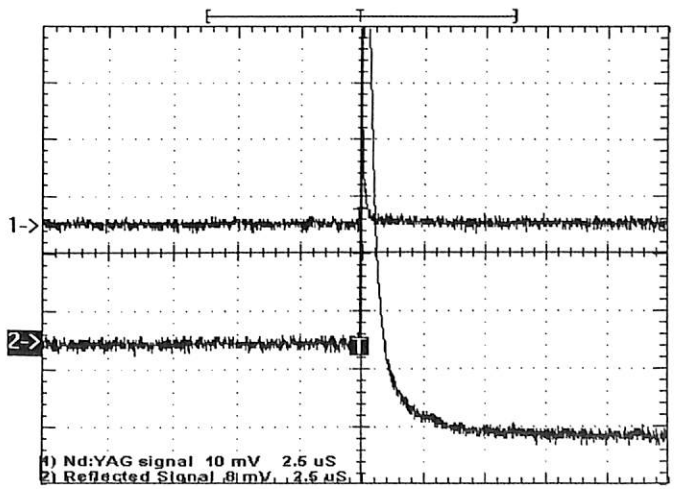

Figure 5.9: Reflectivity modulation of thin film at 85 mJ laser energy per pulse

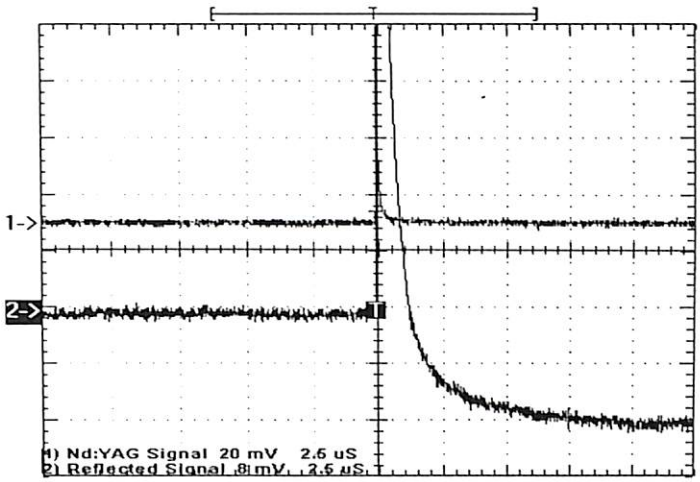

Figure 5.10: Reflectivity modulation of thin film at 122 mJ laser energy per pulse

For recording the temporal evolution of the ablation of thin film via nanosecond high power laser, the reflectivity of the thin film as a function of time was recorded with the experimental set-up of Fig. 4.9. Signals from PD 1 (Fig. 4.9) for the reflectivity measurement during the ablation process are shown in Fig. 5.8- 5.10 corresponding to laser fluence of 85.5 mJ/cm^2, 169.1 mJ/cm^2 and 242.7 mJ/cm^2 respectively. Trace 1 corresponds to the PD 2 signal and trace 2 is the signal from PD 1 which is directly proportional to the reflectivity of the target thin film. The initial dc level of the PD1 signal, V_{uab}, corresponds to the unablated thin film and is proportional to the reflectivity R_{uab} of the unablated target. The first positive peak of PD 2 signal corresponds to scattered Nd:YAG laser falling onto it. The slowly decaying signal with respect to the initial dc level corresponds to the changing reflectivity of the thin film during the ablation of Indium. Therefore the signal, $V_{ab}(t)$, at any instant of time t after firing of the laser shot is directly proportional to the reflectivity, $R_{ab}(t)$, of thin film at that instant of time during ablation. By comparing the signal $V_{ab}(t)$ and V_{uab}, we get an idea about the relative reflectivity at any instant of time during ablation process. In other words

$$\frac{R_{ab}(t)}{R_{uab}} = \frac{V_{ab}(t)}{V_{uab}} \tag{5.2}$$

The measured ratio of the ablated reflectivity to that of unablated thin film $\frac{R_{ab}(t)}{R_{uab}}$ from the signal of Fig. 5.8- 5.10 at 2.5 μs and 12.5 μs are listed in table. 5.3. As indium is a highly reflecting material therefore low reflectivity of the target after the completion of the ablation process at high fluence of single shot of Nd:YAG laser confirms the complete ablation of the material of the thin film, where as at low laser fluence (85.5 mJ/cm^2), the reflectivity of the substrate after the ablation is large (70%) and so the fluence is not high enough to blow off the complete material of the thin film in the region exposed to Nd:YAG laser. Ablation process is also fast at higher laser fluence owing to the deposition of larger and larger energy onto the target thin film.

Laser fluence (mJ/cm^2)	Laser energy per pulse (mJ)	$\frac{R_{ab}(t)}{R_{uab}}$ after 2.5 μs	$\frac{R_{ab}(t)}{R_{uab}}$ after 12.5 μs
242.7	122	0.5	0.17
169.1	85	0.5	0.2
85.5	43	0.9	0.7

Table 5.3: Ratio of the ablated reflectivity and unablated reflectivity, $\frac{R_{ab}(t)}{R_{uab}}$, of the target at 2.5 μs and 12.5 μs for various laser fluence.

5.6 Conclusion

We have successfully generated low divergence low energy pulsed indium atomic beam via rear side ablation of thin film of Indium by unfocused laser. The lowest divergence of 23 mrad was observed by this technique at a fluence of 85.5 mJ/cm^2 (43 mJ/pulse). Below this energy, no ablation of the material of the thin film was observed. With the help of apertures, divergence of atomic beam was further curtailed. It was found that divergence of atomic beam increases with increase in laser energy and is about one order of magnitude less than that of produced with focused laser. Longitudinal velocity of atomic beam was measured

as a function of laser energy by time of flight measurement using beam deflection set-up. It was found that the velocity of atomic beam increases with laser energy upto 160 mJ/pulse with the maximum velocity of 100 m/sec. Beyond this energy, no significance increase in atomic velocity was observed. We have observed the formation of ion of the indium at laser energy of 160 mJ/pulse and at higher energies. Longitudinal velocity of ionic beam was found to be one order of magnitude more than that of the atoms. To the best of our knowledge such slow pulsed atomic beams having beam divergence down to 23 mrad without any collimated atom optics is not reported earlier. The reflectivity measurement shows that the ablation process is fast for the higher laser energies and certain minimum energy is needed to blow off the full material of the thin film. These slow beams of atoms and ions may find their applications in lithography where host sites are very sensitive to the kinetic energy of the implanted beams.

Chapter 6

Selective laser ablation lithography and generation of multiple atomic beams

6.1 Introduction

In Chap.1, we reviewed various schemes for lithography. We also discussed two upcoming lithographic techniques of atom lithography using dipole force [28–31] and direct writing via laser interference lithography [83–85]. These two techniques show lot of advantages over other existing techniques as both are single step and do not require any material mask.

We have developed a new configuration of laser interference lithography technique to modify the surface morphology of a thin film in a single step. This technique utilizes the selective ablation of material of the thin film on illumination with the delocalized interference patterns obtained from the interference of two and four beams of pulsed high power laser. We have reported probably for the first time, using this technique, the direct writing of two dimensional periodic arrays of spots in square geometry having periodicity of the order of wavelength. This is a single step direct technique and performs the complete

writing in a single shot of laser.

In Chap.3, we proposed a promising new configuration of multiple periodic atomic beams focused by TEM_{00} mode of laser to obtain the periodic structure of periodicity much below $\lambda/2$. The main requirement of this configuration is the source of atomic beam which can deliver the arrays of discrete atomic beams in two dimension. We have developed the experimental set-ups, described in Chap.4, to obtained such periodic discrete atomic beams. The results obtained with the set-ups of Fig . 4.13 and 4.14 for the multiple discrete atomic beams are discussed in Sec. 6.3.

6.2 Selective laser ablation lithography

6.2.1 One dimensional lithography

For one-dimensional Selective laser ablation lithography (SLAL), a Michelson interferometer was aligned and adjusted for periodic parallel straight fringes. The spatial frequency of interference pattern depends on the angular spacing between the two interfering beams (Eq. 4.2) and can be controlled by adjusting the tilt of mirror M_1 or M_2. The interference pattern was compressed down by a lens of focal length 25 cm for increasing the intensity and then illuminated the thin film of Indium placed inside the vacuum chamber as shown in Fig . 4.11. The two beams coming out of the interferometer were not exactly collinear. However, the angular separation was kept sufficiently small for all the observations so as to maintain the good overlap of the two beams till distances of four to five meters. Therefore, interference pattern from the interferometer was observed to be de-localized up to a distance of couple of meters. But with a lens, at the focal plane and near to the focal point (depth of focus), the two beams were imaged individually at different transverse location, thereby no overlap and the resultant pattern was just two distinct closely spaced

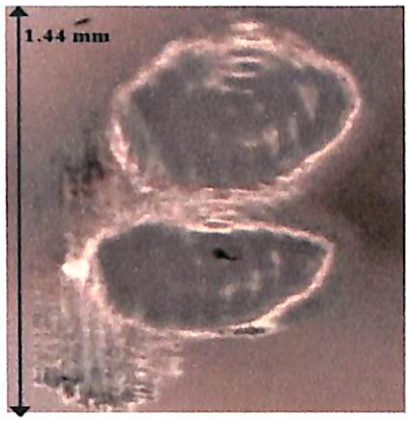

Figure 6.1: Micrograph of Indium thin film showing two distinguish ablated spots obtained by exposing with non overlapping beams after lens. Distance between the lens and the thin film was 22.5 cm.

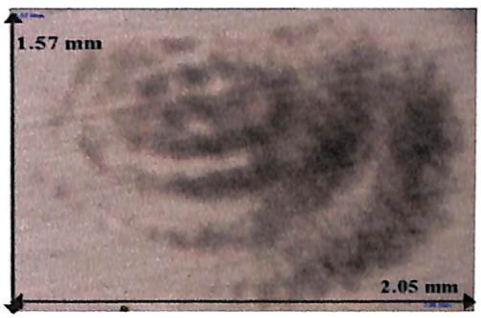

Figure 6.2: Micrograph of Indium thin film exposed by two beam interferometric pattern showing single ablated spot. Distance between the lens and the thin film was 31 cm.

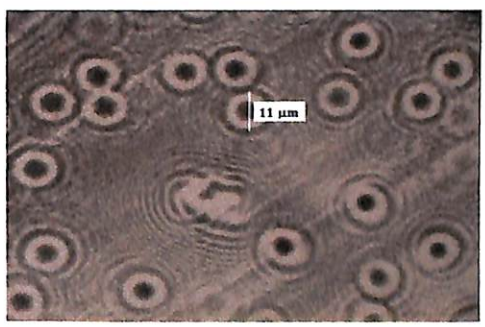

Figure 6.3: Micrograph of Indium thin film exposed to Nd:YAG laser directly.

bright spots. When the thin film was placed at the focus or near to the focus, the material was ablated from the region of these two distinct spots without giving any periodic writing. Micrograph of the Indium thin film ablated selectively by placing it at a distance of 22.5 cm from the lens is shown in Fig. 6.1 at laser energy (measured after prism P_3, Fig . 4.11) of 17.2 mJ. It clearly shows the two dark patches confirming the ablation of the thin film by two well separated beams. As the film was moved away from the focal spot, the beams started overlapping and the interference pattern was imprinted via selective ablation of the material from the region of bright fringe (Sec. 4.5.1). Therefore for one-dimensional periodic patterning in a single step, the location of the thin film from the lens should be such that there is sufficient overlap of the two beams for the formation of the interference pattern as well as the intensity in the bright fringe should be above the ablation threshold. We have observed that complete overlap of the two interfering beams onto the thin film can be obtained around 30 cm from the lens (Fig . 4.11). Micrograph shown in Fig. 6.2 was obtained after ablation by keeping the thin film at a distance of 31 cm from the lens at a laser energy of 17.2 mJ/pulse. It shows the complete overlap of the two beams. The ablated region of Fig. 6.2 is not of the perfect circular geometry as well as not uniformly distributed. The reason for this is the poor quality of laser beam. The Nd:YAG laser used for the experiment was not delivering perfect TEM_{00} mode of laser beam. A micrograph picture of Indium thin film, which was directly exposed to Nd:YAG laser is shown in Fig. 6.3, reveals the non uniform distribution of intensity with in the laser beam. Fig. 6.4 shows a series of micrograph pictures of Indium thin film exposed to two beam interference pattern with different spatial frequencies and laser energies. The fine variation in the spatial frequencies was obtained by adjusting the mirror tilts. The distance between the lens and the thin film was maintained at 31 cm for all the pictures of Fig. 6.4. The multiple diffraction pattern in the form of concentric rings in the laser beam (Fig. 6.3) was also imprinted in the background

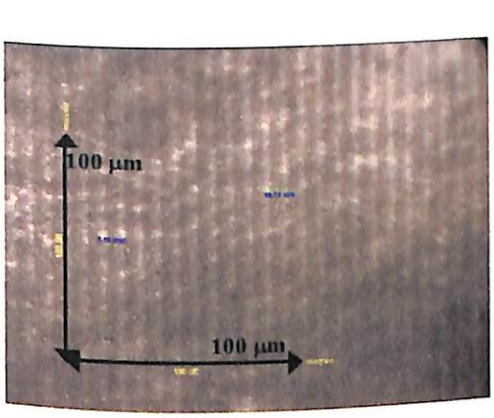

(a) Λ = 10.11 μm, d = 2.19 μm

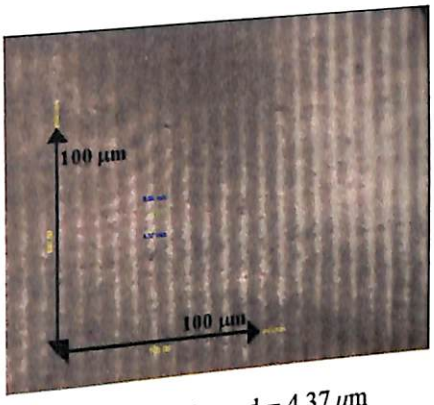

(b) Λ = 9.56 μm, d = 4.37 μm

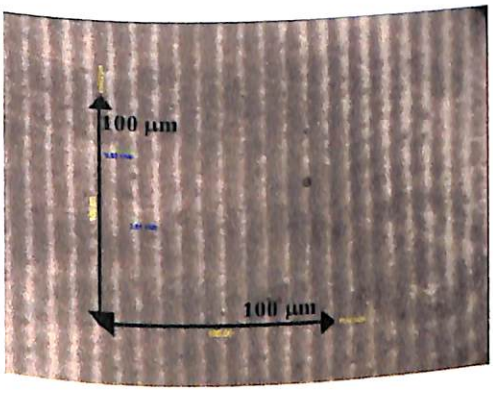

(c) Λ = 9.02 μm, d = 3.01 μm

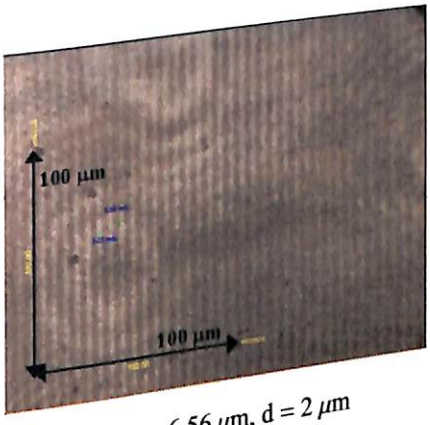

(d) Λ = 6.56 μm, d = 2 μm

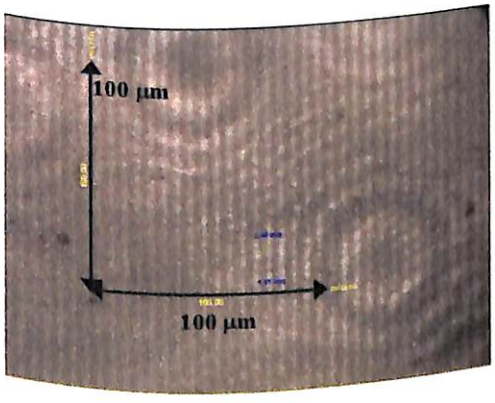

(e) Λ = 5.46 μm, d = 2 μm

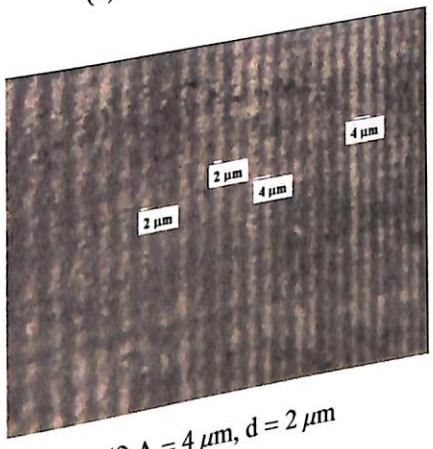

(f) Λ = 4 μm, d = 2 μm

Figure 6.4: Micrograph of Indium thin film showing formation of gratings of different periodicities (Λ) and line-widths (d)

of all the samples of Fig. 6.4. For Fig. 6.4(a), output energy of interferometer measured after prism P_3 (Fig. 4.11) was 16.5 mJ per pulse. The periodicity in this case was found to be equal to 10.11 μm with a width of 2.19 μm of the leftover Indium. For Fig. 6.4(b), 6.4(c) and 6.4(d), output energy of interferometer was 18 mJ per pulse and the periodicities were found to be equal to 9.56 μm, 9.02 μm and 6.56 μm with a width of 4.37 μm, 3.01 μm and 2 μm respectively of the remaining Indium. Fig. 6.4(f) was recorded by ablating the thin film with 17 mJ per pulse, measured after prism P_3 (Fig. 4.11). The periodicity of this pattern is 4 μm and linewidth 2 μm. These micrograph clearly shows that the complete lithography in the form of parallel lines of Indium can be perform in a single shot and the periodicity as well as the line width can be altered with simply changing the orientation of the mirrors.

6.2.2 Two-dimensional lithography

The two dimensional lithography by SLAL was performed by illuminating the thin film with the interference pattern obtained by aligning the two Michelson interferometer in tandem. The experimental set-up is shown in Fig. 4.12. The four beams from the interferometer were adjusted to result into periodic tiny spots of light in square geometry as shown in Fig. 3.12. The spatial frequency of the interference pattern depends on the angular spacing between the four interfering beams (Sec. 3.4.1). Angular spacing between the four beams was controlled by adjusting the tilt of mirrors M_1 or M_2 and M_3 or M_4. The alignment in this set-up was more critical than two beam interferometer as it involves handling of four beams simultaneously. Finally, the interference pattern was compressed with the lens of focal length 25 cm and the thin film was illuminated from the rear side under vacuum with this compressed pattern. As discussed in the previous section, the distance between film and lens was kept at 30 cm so as to obtain the complete overlap of all the four beams on the thin film to form the interference pattern in the form of arrays of light spots in the square

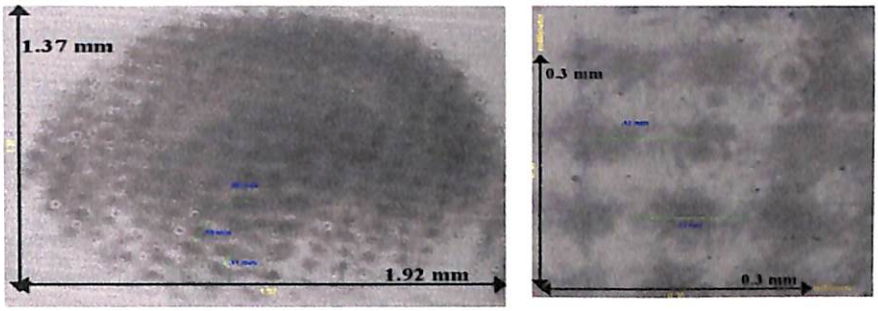

(a) Total exposed area

(b) Micrograph at higher magnifi cation

Figure 6.5: Micrograph of Indium thin film showing formation of holes

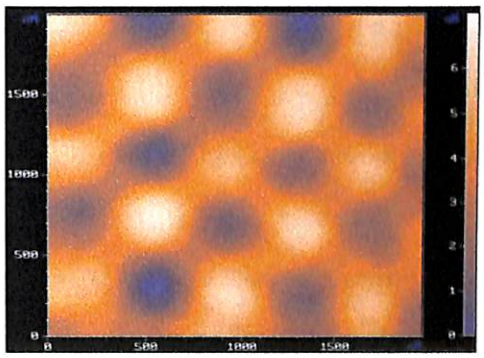

Figure 6.6: Atomic force microscope picture of Indium thin film exposed to four beam interference pattern

geometry. The region of the thin film exposed to bright spot was ablated resulting into imprinting large arrays of holes in the square geometry in one shot. Fig. 6.5 shows micrograph of Indium thin film exposed by four beams interference pattern having smaller spatial frequency. In this case, the laser energy at the output plane of interferometer (after prism P_2, Fig. 4.12) was 13.5 mJ per pulse. Fig. 6.5a shows the formation of around 200 holes in an area of approximately 3 mm^2 in a single shot onto the thin film. The micrograph of this ablated portion at higher resolution is shown in Fig. 6.5b. It shows formation of holes with periodicity 0.13 mm. The blame for poor quality of this pattern goes to quality of Nd:YAG laser beam again which was not exactly TEM_{00}. For performing the lithography at nano scales, the mirrors of the interferometer of Fig. 4.12 were further adjusted so as to increase the angular separation between the beams for higher spatial frequency (or small periodicity). The laser energy at the output of the interferometer (after P_2) was kept same (13.2 mJ/pulse) and the thin film was located at the same distance of 30 cm from the lens. The fresh portion of the thin film was exposed by a single shot of laser under vacuum with the modified compressed pattern for the SLAL. The exposed portion was scanned with Atomic force microscope. The scanned AFM picture is shown in Fig. 6.6. It clearly shows formation of periodic holes on Indium thin film leaving behind the nano hillocks of Indium in square geometry. The periodicity of this pattern is 593 nm with FWHM of holes 263 nm. The periodicity of this pattern is almost touching the wavelength of light (532 nm), used for selective ablation lithography which is the ultimate minimum periodicity obtained by this technique.

6.3 Multiple periodic atomic beams

In the last section, we have demonstrated how selective ablation of indium thin film with two beams and four beams interference pattern from the high power laser yields into one

and two dimensional periodic structures at micron and nano scales. The material selectively ablated from the thin film evolves in the form of large number of discrete periodic atomic beams. These multiple periodic discrete atomic beams are analyzed in this section. The motivation behind the analysis of the morphology of these atomic beam is the requirement of matrix of micro-ovens, a novel configuration proposed in Sec. 3.5 for the atom lithography using dipole force having periodicity less than $\lambda/2$.

6.3.1 Multiple atomic beams in one dimension

Straight line fringes obtained from Michelson interferometer of Fig. 4.13 were used for the generation of parallel planer pulsed multiple atomic beams. Thin films of Indium (T) was ablated with a single shot of compressed two beam interference pattern from the rear side using second harmonic of Nd:YAG laser under high vacuum (10^{-5} Torr). The lens was kept at a distance of 31 cm from the thin film and the energy recorded at the output of interferometer (after P_3) was 17.2 mJ/pulse. Thin film was moved vertically to obtain the fresh region of material of the thin film for ablation for each shot of Nd:YAG laser. The ablated material in the form of atomic beam of Indium was deposited on the glass substrate (S) kept at a distance of 14.5 mm away from the thin film as shown in Fig. 4.13. Six consecutive shots of pulsed atomic beams were deposited onto the substrate (S). Then the substrate (S) was taken out of the vacuum chamber and scanned with optical micrograph for the topographical analysis of atomic beams. The target T and substrate S were scanned using optical microscope. Scan images of T and S are shown in Fig. 6.7. Fig. 6.7a shows the complete pattern imprinted onto the target and Fig. 6.7b shows the corresponding micrograph at higher resolution. It clearly shows the formation of line structures of Indium having periodicity 9 μm with width of 3 μm on the target.

Optical microscopic images of the glass substrate is shown in Fig. 6.7c and d. Fig. 6.7c

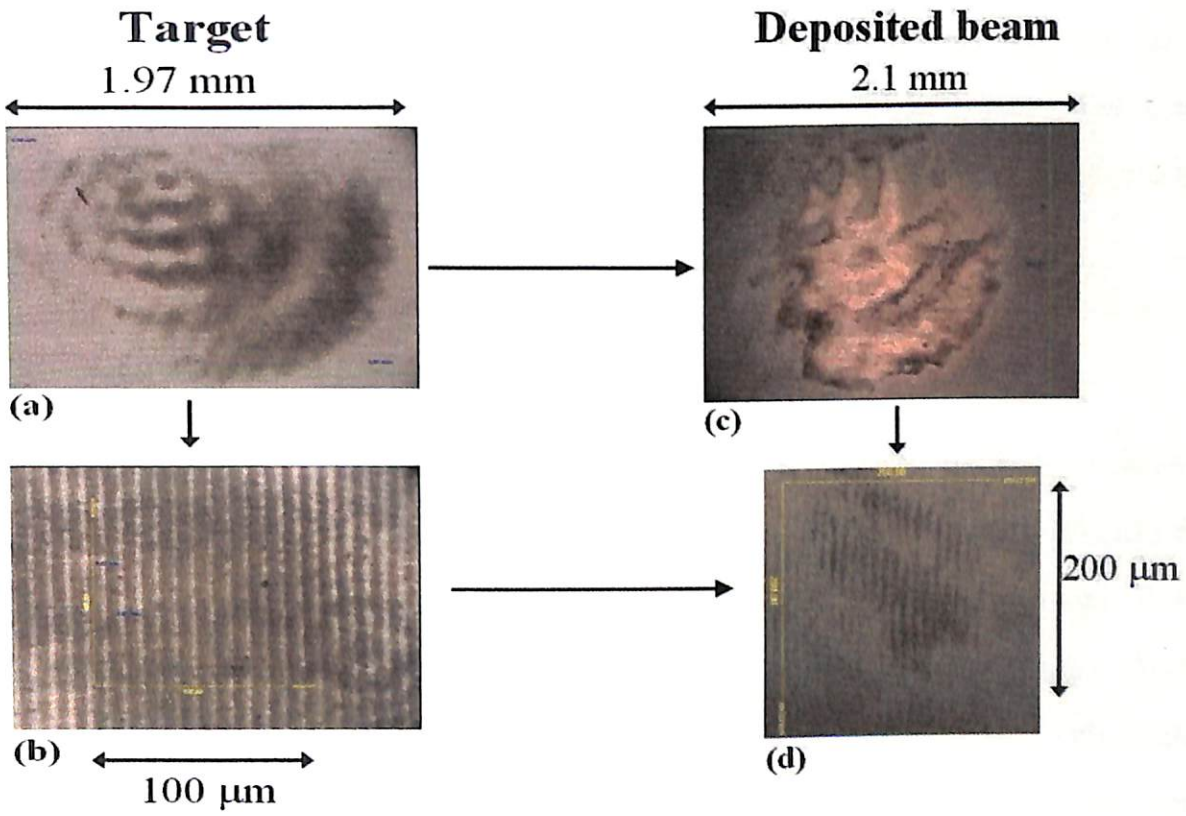

Figure 6.7: Optical micrograph of target and deposited atomic beam

shows the complete deposition of material emitted from the target thin film and Fig. 6.7d shows the corresponding periodic structure at higher resolution. It shows the similar periodic line pattern with periodicity 10.2 μm and deposited linewidth 8.2 μm . This confirms that the sculpting of the atomic beam in one dimension can be performed by interference pattern for the generation of large number of parallel pulsed atomic beams in a single shot. The overall size of the system of atomic beams as well as the periodicity of the deposited beam onto the substrate (Fig. 6.7c and d) are slightly more than that of the material ablated from the target (Fig. 6.7a and b). This is because of some divergence of ablated atomic beam.

6.3.2 Matrix of micro-ovens

After successfully sculpting the atomic beam in one dimension, we have conducted experiment for sculpting the atomic beam in two dimension to generate the discrete atomic beams arranged in a square geometry. This serves as a matrix of micro-ovens. To obtain the multiple periodic atomic beams in two dimensions, the interference pattern also has to be periodic in two dimension. Therefore thin film of indium was ablated with single shot of four beams interference pattern using second harmonic of Nd:YAG laser under high vacuum (10^{-5} Torr), Fig 4.14. The thin film was moved vertically with the help of motorized feed-through to expose the fresh region of thin film for every shot of laser. The ablated material was deposited on the glass substrate for five consecutive shots. The separation between the substrate and the target was kept at 15 mm. The target thin film and deposited atomic beam on the glass substrate were scanned using atomic force microscope. Fig. 6.8a and b show AFM scan images of target indium thin film in two and three dimensional view respectively. Height profile of these images along the line AB and CD are shown in Fig. 6.8c and d. These images clearly shows formation of nano sized periodic holes and

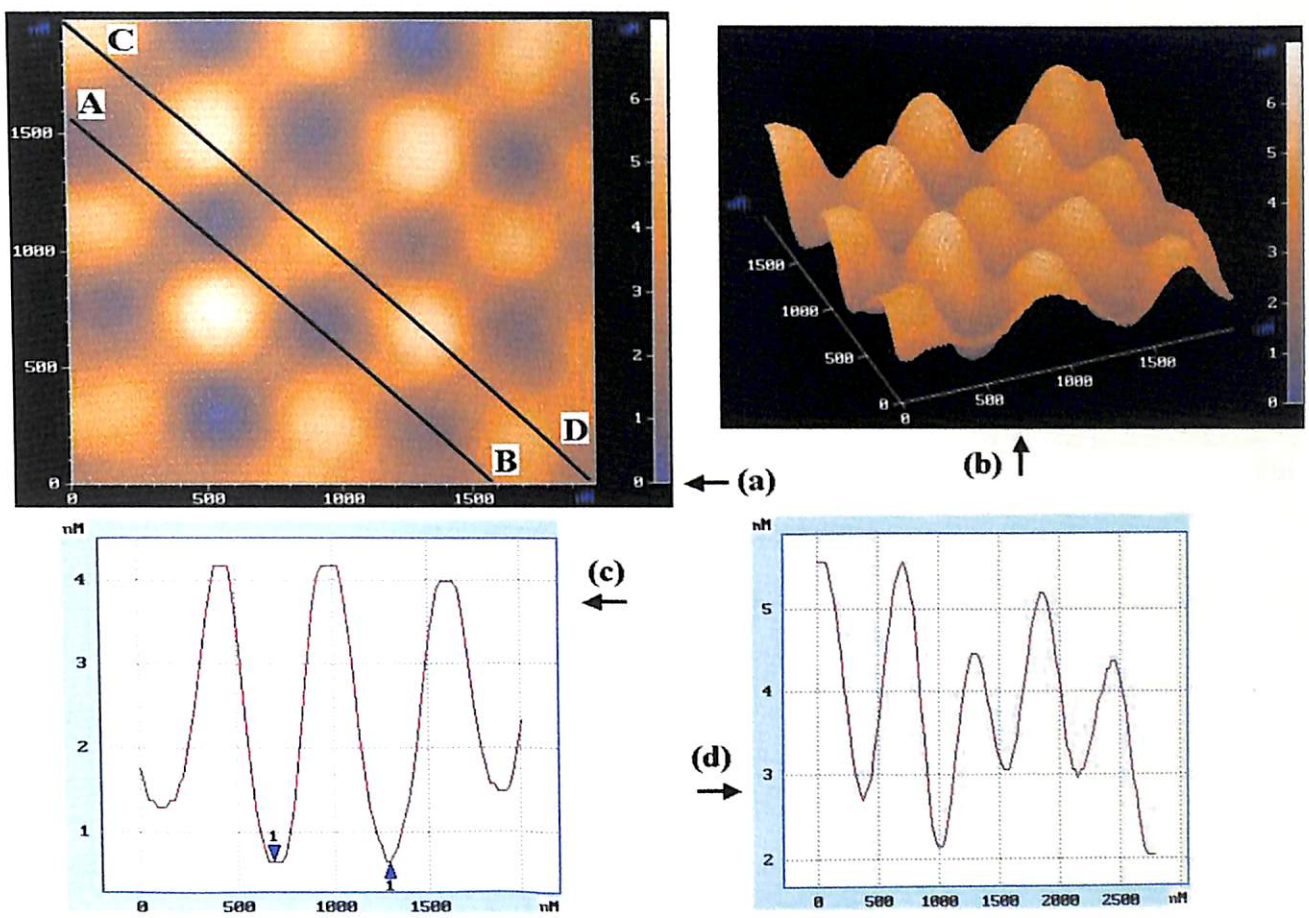

Figure 6.8: AFM scan pictures of target (a). 2-d view (b). 3-d view (c). Oscilloscope trace along line AB (d). Oscilloscope trace along line CD.

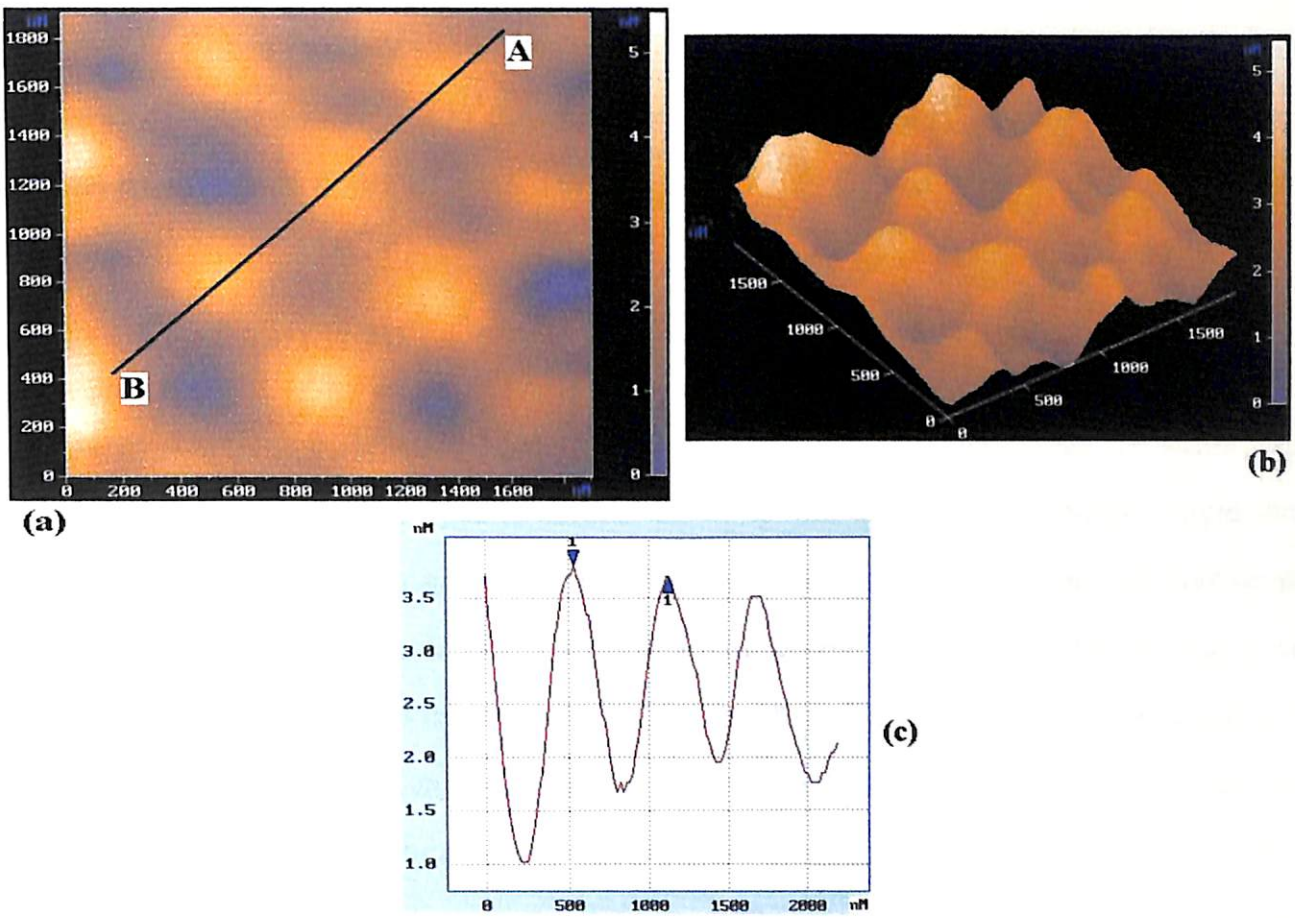

Figure 6.9: AFM scan pictures of deposited atomic beam (a). 2-d view (b). 3-d view (c). Oscilloscope trace along line AB.

hillocks of Indium on the thin film having periodicity 593 nm and FWHM of hole equal to 263 nm. This confirms the periodic ablation of thin film in two dimension.

Fig. 6.9a and b shows the AFM scans of deposited atomic beam in two and three dimensional view respectively. Height profile of these images along the line AB is shown in Fig. 6.9c. These images shows the nano sized dots on the substrate with periodicity 630 nm and FWHM equal to 294 nm confirming the production of arrays of multiple atomic beams having bidirectional periodicity.

6.4 Conclusion

We have developed the technique of selective laser ablation lithography for writing one and two dimensional periodic structures onto the thin film, in a single-step, single-shot. Michelson interferometer as well as two Michelson interferometers in tandem were developed using second harmonic of Q-switched high power Nd:YAG laser for generating the one and two dimensional interference pattern for selective ablation. The Indium thin film was imprinted via selective laser ablation into periodic lines and dots on illuminating with this high power interference pattern. Using this technique, we could perform the complete periodic writing with only one shot of laser. The minimum periodicity obtained in the present experiment was 593 nm, very close to the wavelength limit of 532 nm. The laser array pattern is highly delocalized in the present configuration, so its transportation at the site of the target is not difficult and pattern can be compressed without distortion onto the target by the lens for the fine writing. The spatial frequency of the pattern can also be changed on line by adjusting the orientation of the mirrors. The structure obtained by this technique was found to be stable even after a period of four months.

The technique of selective laser ablation also results into the generation of large number of pulsed discrete atomic beams simultaneously having one and two dimensional periodic-

ity. We could successfully observed the parallel, planer atomic beams having periodicity 10 μm and the two dimensional arrays of discrete atomic beams having periodicity 630 nm with FWHM of 294 nm. This novel configuration of atomic beams is required for the atom lithography for writing periodic structure below $\lambda/2$ as proposed in Chap.3.

Chapter 7

Conclusion

7.1 Atom lithography using dipole force

Semi-classical trajectories were simulated for various configuration of light fields and atomic beams for atom lithography using dipole force. New configurations of atomic beam and light field were proposed for atom lithography for micro and nano periodicity.

7.1.1 TEM_{00} mode of laser

Most simplest light configuration is TEM_{00} mode of a laser. Gaussian variation of intensity in the transverse plane of TEM_{00} laser beam acts as a single atomic lens for the focusing of atomic beam to a single spot. The trajectories of the uniformly distributed atomic beam in counter propagating TEM_{00} mode of laser were computed for cold and thermal atomic beam for one and two dimensional structures. The trajectories were simulated for collimated as well as divergent atomic beams. The focus spot and the contrast was found to be dependent on the intensity as well as on the divergence of the atomic beam but it is independent of the longitudinal velocity of the atoms. Multiple focusing of the atomic beam for

longer interaction time with the light field was observed.

7.1.2 Optical standing wave

The TEM_{00} mode of laser beam gives only one single focus spot of atoms of micron dimensions. Therefore simulations were performed with standing wave of light which gives series of periodic micro-lenses with period $\lambda/2$ for atom lithography. Trajectories of rubidium atoms were simulated for thermal and super thermal atomic beams (collimated as well as divergent) interacting with standing wave light configuration. Sharpness of focus spot and the contrast found to be dependent on the intensity and divergence of the atomic beam. Multiple focusing of the atomic beam was also observed for longer interaction time with the light field. In this case also interaction time required for focusing at a given intensity was found to be independent of axial velocity of atoms.

7.1.3 Interferometric Configuration

The standing wave configuration is equivalent to one dimensional periodic potential and the focus spots of the atoms in such potential is in the form of grating structure (or periodic line). For writing the two dimensional arrays a new scheme of two dimensional periodic potentials via multiple beam interferometry, resulting into two dimensional arrays of tiny spots in square geometry, for atom lithography using dipole force was proposed. Simulated lithographic patterns of single atomic beam in such periodic potential shows formation of periodic square arrays of atoms having the spatial frequency same as that of the interference pattern. The spatial frequency of this proposed lithography technique can be controlled easily, on line, by orientation of the mirrors of the interferometer.

7.1.4 Matrix of Micro-Ovens

The periodicity of above two configurations is limited to $\lambda/2$ though the individual focus spots in the array may be of dimensions tens of nanometer. Therefore a new configuration of using microscopic square arrays of atomic beams, matrix of micro-ovens, in presence of counter propagating Gaussian intensity distribution (TEM_{00} mode) of laser was explored for reducing the periodicity below $\lambda/2$. This new configuration is equivalent to imaging the large number of discrete atomic beams via single atomic lens. This is the reverse analogy of the above two configurations having single atomic beam traveling in multiple light potential. Lithographic patterns for such square arrays of rubidium atomic beams (cold as well as thermal) in the TEM_{00} field were simulated for collimated as well as divergent atomic beams for different interaction time and divergence. The individual beam was assumed to be located at the corner of a square of size 2 μm and the atomic beam diameter was 1 μm. The lithographic patterns generated using this configurations was found to have periodicity much less than $\lambda/2$ for collimated as well as divergent atomic beams. Nano size periodic dots and lines were seen in the simulated lithographic pattern for collimated and divergent case respectively. The geometry of the pattern was observed to be dependent on the interaction time. The maximum compression factor was found to be of the order of 6 as compared to initial configuration of atomic beam.

7.2 Generation of atomic beam via laser ablation

A new technique was developed to produce fairly collimated cold beam of indium by illumination of the thin films of indium from the rear side directly by (unfocused) second harmonic of Q switched Nd:YAG laser under high vacuum (10^{-5} Torr). We could produce the atomic beam having divergence down to 23 mrad without using any additional atom

optics for collimation. The divergence of the atomic beam was found to increase with increase in laser energy. From the time of flight measurement of beam deflection set-up, the maximum longitudinal atomic beam velocity was observed to be 100 m/s and minimum 44 m/s at laser fluence of 318 mJ/cm^2 and 85.5 mJ/cm^2 per pulse respectively. It was found that initially beam velocity increases with laser energy. After a fluence of around 242.7 mJ/cm^2 no significant increase in axial atomic velocity was observed. Axial velocities of ionic species were also measured at different laser powers. Longitudinal velocity of ionic beam was found to be one order of magnitude more than that of the atoms. From the reflectivity modulation measurement during ablation, it was found that ablation process is slow at lower laser energies and certain minimum energy of laser is needed to blow off the material of the thin film completely.

7.3 Selective laser ablation lithography

Experimental set-up for the selective laser ablation lithography was developed using two and four beam high power laser interference pattern for obtaining line and dot structures with periodicities ranging from micron level to down to wavelength order. This is a direct single-shot, single-step lithographic technique. This technique has an advantage over previously reported techniques as the target position is not critical in this case due to the use of delocalized interference pattern. Also, as all the four beams are entering into the vacuum chamber through the same port, the modification in the interference pattern due to relative wavefront distortion of various interfering beam is minimum. The thin films of Indium was ablated selectively under vacuum via two and four beams delocalized interference pattern. The Indium lines and large number of arrays of dots in the thin film having periodicity from micron to 593 nm ($\approx \lambda$) were imprinted in a single-shot.

7.4 Experimental realization of matrix of micro-ovens

The simulated result of MMO configuration has shown its potential toward the periodic lithography in a single shot having period much less than $\lambda/2$. One of the major requirement for this configuration is the periodic arrays of atomic beams. We have generated these periodic arrays of atomic beams in one dimension as well as two dimensions via rear side ablation of indium thin film by focused high power two and four beams laser interferometer. Micrograph images and AFM scan pictures confirms the formation of periodic one and two dimensional atomic beams having periodicity ranging from 10 μm to the 630 nm with size of the individual beams ranging from 8.2 μm to 294 nm. The periodicity and the size of individual beam depends on the spatial frequency of the interferometric pattern and the beam energy.

7.4.1 Three birds in a single stone

The advantages of rear side selective laser ablation of thin film developed by us and reported in this thesis are three fold.

Selective laser ablation lithography

First the target used for ablation gets imprinted with periodic micro-nanoscopic information of light beams via ablation by two and four beam interference pattern. So this part itself acts as a single-step single-shot lithographic technique.

Multiple atomic beams for atom lithography using dipole force

Secondly the ablated material from above results in the generation of the multiple atomic beam which can be focus down with the help of TEM_{00} mode of laser, acting as an atomic

lens, for obtaining structures with periodicities less than $\lambda/2$ by atom lithography using dipole force.

Multiple atomic beams for direct lithography

Thirdly, the multiple atomic beam deposited directly onto the substrate serves as micro-nano fabrication of periodic structure.

7.5 Uranium enrichment

Application of dipole force in isotopic separation was also explored. As an example, a new scheme was proposed for the enrichment of U^{235} using dipole force generated by a red detuned TEM_{00} mode of laser with respect to U^{235} transition. This technique may prove to be efficient for the enrichment of uranium from natural uranium as well as recycled nuclear fuel. This is also a general technique and can be applied for the isotopic separation of any element.

7.6 Future scope

7.6.1 Selective laser ablation lithography

SLAL is a Promising lithographic technique which can be used for both micro and nano fabrication simultaneously. With the availability of pulsed laser in UV range having the good beam quality the periodicities and structure dimensions can be further reduced.

7.6.2 Atom lithography using dipole force

Microlithography

Proposed configuration of square arrays of multiple atomic lens produced by interference of four nearly collinear optical beams can be implemented experimentally for atom lithography via dipole force to write large number of periodic structures in square arrays in a single step.

Sub $\lambda/2$ lithography

Experimentally 8.2 μm to 294 nm size discrete multiple atomic beams having periodicities ranging from 10 μm to 630 nm respectively was reported in the thesis for the first time. As the minimum periodicities are already in nano scales, further compressing them by factor of 6 with the help of TEM_{00} mode of laser (as discussed in Chap.3) can yield 67 nm size spots with periodicity 131 nm. Compression factor can be further reduced by choosing the higher intensity light fields gradients and proper interaction time.This technique can be used for selective doping of the material for engineering photonic bandgap devices.

7.7 Isotopic separation

In Chap.3, we have proposed a scheme to separate the isotopes of Uranium using dipole force arising from counter propagating TEM_{00} mode of laser. Experimental implementation of this scheme to be realized for testing the feasibility of this process for large scale production. As the dipole force concept is valid for any element, this technique can be implemented for isotopic separation of any material.

Bibliography

[1] M. Wilson et al. Nanotechnology basic science and emerging technologies. *Chapman & Hall/CRC, A CRC press company*, 2002. Boca Raton.

[2] M.G. Tanner et al. Geometry dependence of the energy levels in silicon isolated double quantum-dots. *Microelec. Eng.*, 78-79:195–200, 2005.

[3] Y. Gu et al. Quantum confinement in ZnO nanorods. *App. Phy. Lett.*, 85:3833–3834, 2004.

[4] G.F. Cerofolini et al. Strategies for nanoelectronics. *Microelec. Eng.*, 2005. In press.

[5] T. Borzenko et al. Building and testing submicrometer metallic (gold) air–bridges for nanotransport applications. *Microelec. Eng.*, 78-79:374–380, 2005.

[6] K. Brugger et al. Nanofabricated atom optics: atom chips. *J. Mod. Opt*, 47:2789–2809, 2000.

[7] E. te Sligte et al. Progress towards atom lithography on iron. *Microelec. Eng.*, 67-68:664–669, 2003.

[8] D.K. Wood et al. Submicron giant magnetoresistive sensors for biological applications. *Sensors and Actuators A Physical*, 120:1–6, 2005.

[9] P. Candeloro et al. SnO_2 sub-micron wires for gas sensors. *Microelec. Eng.*, 78-79:178–184, 2005.

[10] C. Moormann. Spatial phase–locked combination lithography for photonic crystal devices. *Microelec. Eng.*, 73-74:417–422, 2004.

[11] R. Houbertz. Laser interaction in sol-gel based materials – 3-d lithography for photonic applications. *Appl. Sur. Sci.* In press.

[12] S.B. Wang et al. Fabrication of 128×128 element optical switch array by micromachining technology. *Microproce. & Microsys.*, 29:21–25, 2005.

[13] C.C. Chang and C.S. Chang. Site–specific growth to control ZnO nanorods density and related field emission properties. *Solid State Communication.* In press.

[14] J. Wang et al. A continuously tunable organic DFB laser. *Microelec. Eng.*, 78-79:364–368, 2005.

[15] H. Ahmed. Single atom scale lithography for single electron devices. *Physica B*, 227:259–263, 1996.

[16] M. Madou. Fundamentals of microfabrication. *CRC press, Boa Raton*, 1997.

[17] G. L.-T. Chiu and J.M. Shaw. Optical lithography. *IBM J. Res. and Devel.*, 41:1/2, 1997.

[18] M. Rothschild. Projection optical lithography. *Materials Today*, 8:18–24, 2005.

[19] R. Klauser et al. Patterning and imaging of self-assembled monolayers with a focused soft X-ray beam. *J. Elec. Spec.& Rel. Phen.*, 144-147:393–396, 2005.

[20] F. Perennes et al. Fabrication of refractive X-ray focusing lenses by deep X-ray lithography. *Microelec. Eng.*, 78-79:79–87, 2005.

[21] W. Weber et al. Electron beam lithography for nanometer–scale planar double–gate transistors. *Microelec. Eng.*, 78-79:206–211, 2005.

[22] S. Cabrini et al. Focused ion beam lithography for two dimensional array structures for photonic applications. *Microelec. Eng.*, 78-79:11–15, 2005.

[23] C. F. Quate. Scanning probes as a lithography tool for nanostructures. *Surface Science*, 386:259–264, 1997.

[24] J.R. Tucker and T.-C. Shen. Prospects for atomically ordered device structures based on STM lithography. *Sol. Sta. Elec.*, 42:1061–1067, 1998.

[25] J. Park and H. Lee. Specific immobilization of nanospheres on template fabricated by using atomic force microscope lithography. *Collids and Surface A: Physicochem. Eng. Aspects*, 257-258:133–135, 2005.

[26] Run-Wei Li et al. Nanopatterning of perovskite manganite thin films by atomic force microscope lithography. *Nanotechnnology*, 16:28–31, 2005.

[27] S. C. Minne et al. Automated parallel high-speed atomic force microscopy. *Appl. Phys. Lett.*, 72:2340–2342, 1998.

[28] V.S. Letokhov et al. Laser Science and Technology An International Handbook: Atom optics with laser light. *Harwood academic publishers*, 1995.

[29] D. Haubrich et al. Atomlithographie. *Phys. Bl.*, 53:523–528, 1997.

[30] D. Meschede and H. Metcalf. Atomic nanofabrication: atomic deposition and lithography by laser and magnetic forces. *J. Phys. D: Appl. Phys.*, 36:R17–R38, 2003.

[31] J.J. McClelland et al. Nanotechnology with atom optics. *Sci. and Tech. of Adv. Mat.*, 5:575–580, 2004.

[32] Claude Cohen-Tannoudji et al. Atom-Photon Interactions. *John Wiley & Sons, New York*, 1992.

[33] H.J. Metcalf and P. van der Straten. Laser Cooling and Trapping. *Springer–Verlag New York, Inc.*, 1999.

[34] T. Muther et al. Three-dimensional nanolithography with light forces. *Microelec. Eng.*, 57-58:857–863, 2001.

[35] M. K. Oberthaler and T. Pfau. One-, two- and three-dimensional nanostructures with atom lithography. *J. Phys.: Condens. Matter*, 15:R233–R255, 2003.

[36] M. Mutzel et al. Atom lithography with a holographic light mask. *Phys. Rev. Lett.*, 88:083601–1–4, 2002.

[37] M. Mutzel et al. Atomic nanofabrication with complex light fields. *Appl. Phys. B*, B77:1–9, 2003.

[38] A. Ashkin. Atomic-beam deflection by resonance-radiation pressure. *Phys. Rev. Lett.*, 25:1321–1324, 1970.

[39] A. Ashkin. Acceleration and trapping of particles by radiation pressure. *Phys. Rev. Lett.*, 24:156–159, 1970.

[40] J. E. Bjorkholm et al. Observation of focusing of neutral atoms by the dipole forces of resonance-radiation pressure. *Phys. Rev. Lett.*, 41:1361–1364, 1978.

[41] J. E. Bjorkholm et al. Experimental observation of the influence of the quantum fluctuations of resonance-radiation pressure. *Opt. Lett.*, 5:111–113, 1980.

[42] T.Sleator et al. Imaging and focusing of an atomic beam with a large period standing light wave. *Appl. Phys. B*, B54:375–379, 1992.

[43] G. Timp et al. Using light as a lens for submicron, neutral-atom lithography. *Phys. Rev. Lett.*, 69:1636–1639, 1992.

[44] J.J. McClelland et al. Laser-focused atomic deposition. *Science*, 262:877–880, 1993.

[45] R.J. Celotta et al. Nanostructure fabrication via laser-focused atomic deposition. *J. Appl. Phys.*, 79:6079–6083, 1996.

[46] J.J. McClelland et al. Nanofabrication via atom optics with chromium. *In Proceedings of the SPIE San Jose CA*, page 90, 1997.

[47] V. Sandoghdar et al. Lithography using nano-lens arrays made of light. *J. Mod. Opt.*, 44:1883–1898, 1997.

[48] U. Drodofsky et al. Nanometerscale lithography with chromium atoms using light forces. *Microelec. Eng.*, 35:285–288, 1997.

[49] F. Lison et al. Nanoscale atomic lithography with a cesium atomic beam. *Appl. Phys. B.*, 65:419–421, 1997.

[50] R.W. McGowan. Light force cooling, focusing, and nanometer-scale deposition of aluminum atoms. *Opt. Lett.*, 20:2535, 1995.

[51] R. Ohmukai et al. Atom lithography with ytterbium beam. *Appl. Phys. B*, B77:415–419, 2003.

[52] E. te Sligte et al. Atom lithography of Fe. *Appl. Phys. Lett.*, 85:4493–4495, 2004.

[53] G. Myszkiewicz et al. Laser manipulation of iron for nanofabrication. *Appl. Phys. Lett.*, 85:3842–3844, 2004.

[54] R. Gupta et al. Nanofabrication of a two-dimensional array using laser-focused atomic deposition. *Appl. Phys. Lett.*, 67:1378–1380, 1995.

[55] J.J. McClelland et al. Laser focusing of atoms for nanostructure fabrication. *Aust. J. Phys.*, 49:555, 1996.

[56] W.R. Anderson et al. Minimizing feature width in atom optically fabricated chromium nanostructures. *Phy. Rev. A*, 59:2476–2485, 1999.

[57] S.J. Rehse et al. Optical manipulation of group III atoms. *Appl. Phys. B*, 70:657–660, 2000.

[58] R. Gupta et al. Raman-induced avoided crossings in adiabatic optical potentials: Observation of $\lambda/8$ spatial frequency in the distribution of atoms. *Phys. Rev. Lett.*, 76:4689–4692, 1996.

[59] B. Brezger et al. Polarization gradient light masks in atom lithography. *Europhys. Lett.*, 46:148–153, 1999.

[60] Th. Schulze et al. Sub-100 nm structures by neutral atom lithography. *Microelec. Eng.*, 46:105–108, 1999.

[61] Th. Schulze et al. Structured doping with light force. *Appl. Phys. Lett.*, 78:1781–1783, 2001.

[62] M. Mutzel et al. Nanoscale focusing of atoms with a pulsed standing wave. *Appl. Phys. B*, 70:689–694, 2000.

[63] W. H. Oskay et al. Observation of cumulative spatial focusing of atoms. *Phys. Rev. Lett.*, 89:283001–1–4, 2002.

[64] D.V. Strekalov et al. Periodic structures generated in a cloud of cold atoms. *Phys. Rev. A*, 66:023601–1/11, 2002.

[65] R. E. Scholten et al. Calculating trajectories for atoms in near-resonant light fields. *Aust. J. Phys.*, 52:493–514, 1999.

[66] J.J. McClelland and M.R. Scheinfein. Laser focusing of atoms: a particle-optics approach. *J. Opt. Soc. Am. B*, 8:1974–1986, 1991.

[67] J.J McClelland. Atom-optical properties of a standing-wave light field. *J. Opt. Soc. Am. B*, 12:1761–1768, 1995.

[68] S.J.H. Petra et al. Numerical simulations on the motion of atoms traveling through a standing-wave light field. *Eur. Phys.J.D*, 27:83–91, 2003.

[69] J. Arlt et al. Atom guiding along Laguerre-Gaussian and Bessel light beams. *Appl. Phys. B*, 71:549–554, 2000.

[70] J. Dalibard et al. Wave-function approach to dissipative processes in quantum optics. *Phys. Rev. Lett.*, 68:580–583, 1992.

[71] K. Molmer and Y. Castin. Monte carlo wavefuntions in quantum optics. *Quantum Semiclass. Opt.*, 8:49–72, 1996.

[72] F.E. van Dorsselaer and G. Nienhuis. Quantum trajectories. *J. Opt. B:Quantum Semiclass. Opt.*, 2:R25–R33, 2000.

[73] C. J. Lee. Quantum-mechanical analysis of atom lithography. *Phys. Rev. A*, 61:063604–1/9, 2000.

[74] K.K. Berggren et al. Microlithography by using neutral metastable atoms and self-assembled monolayers. *Science*, 269:1255–7, 1995.

[75] S. Nowak et al. Writing nanostructures with a metastable helium beam. *Microelec. Eng.*, 35:427–430, 1997.

[76] A.S. Bell et al. Atomic lithography. *Microelec. Eng.*, 41/42:587–590, 1998.

[77] A.S. Bell et al. Nano-lithography with atoms. *Surface Science*, 433-435:40–47, 1999.

[78] A. Fioretti et al. Atomic lithography with barium atoms. *Appl. Sur. Sci.*, 2005. In Press.

[79] M. C. Lemme et al. Triple-gate metaloxide-semiconductor field effect transistors fabricated with interference lithography. *Nanotechnology*, 15:S208–S210, 2004.

[80] C. J. M. van Rijn et al. Microsieves made with laser interference lithography for micro-filtration applications. *Micromech. Microeng.*, 9:170–172, 1999.

[81] R. Murillo. Fabrication of patterned magnetic nanodots by laser interference lithography. *Microelec. Eng.*, 78-79:260–265, 2005.

[82] S. Pau et al. Writing an arbitrary non-periodic pattern using interference lithography. *J. Mod. Opt.*, 48:1211–1223, 2001.

[83] A. Khare et al. Application of laser matter interaction for generation of small-sized material. *Rad. Phy. and Chem.*, 70:553–558, 2004.

[84] Y. Nakata et al. Lithographical laser ablation using femtosecond laser. *Appl. Phys. A*, 79:1481–1483, 2004.

[85] Y. Nakata et al. Fabrication of dot matrix, comb, and nanowire structures using laser ablation by interfered femtosecond laser beams. *App. Phy. Lett.*, 81:4239–4241, 2002.

[86] I. V. Hertel and K. J. Ross. An atomic beam oven with very low associated magnetic field. *J. Sci. Instru. (J. Phys E)*, 1:1245–1246, 1968.

[87] V Samm et al. Structure of the scrap off layer and particle flux in a limiter tokamak. *J. Nucl. Mat.*, 145-147:206–209, 1987.

[88] V. Gerginov and C. E. Tanner. Fluorescence of highly collimated atomic cesium beam: theory and experiment. *Opt. Comm.*, 222:17–28, 2003.

[89] T. Halfmann et al. A source for a high-intensity pulsed beam of metastable helium atoms. *Meas. Sci. Technol.*, 11:1510–1514, 2000.

[90] R.M.S. Knops et al. Design and construction of a high-precision atomic beam machine for quantum optics and atom optics experiments. *Laser Physics*, 9:286–292, 1999.

[91] J. C. Miller. Laser ablation, principle and applications. *Springer verlag*, 1994.

[92] I. W. Boyd. Laser Processing of the films and microstructures, Springer series in material science. *Springer-verlag, Berlin Heidelberg*, 1987.

[93] R. Akhter et al. Modification of the composition of laser weld in electrogalvanized steel and the effect on corrosion properties. *Materials & Manufacturing Processes*, 6:67–86, 1991.

[94] S. Bruneau et al. Ultra-fast laser ablation applied to deep-drilling of metals. *Appl. Sur. Sci.*, 248:299–303, 2005.

[95] Edi. by D. B. Chrisey and G. K. Hubler. Pulsed laser deposition of thin films. *John Wiley & Sons*, 1994.

[96] T. Sato et al. Deposition of diamond-like carbon films by pulsed-laser evaporation. *Japanese J. Appl. Phys.*, 26:L1487–L1488, 1987.

[97] R. K. Dwivedi and R. K. Thareja. Optical emission diagnostics of C_{60}-containing laser-ablated plumes for carbon film deposition. *Phys. Rev. B*, 51:7160–7167, 1995.

[98] R. K. Dwivedi and R. K. Thareja. Laser-ablated carbon plasmas: emission spectroscopy and thin film growth. *Surface & Coatings Technology*, 73:170–176, 1995.

[99] A. Suzuki et al. Transparent conducting Al-doped ZnO thin films prepared by pulsed laser deposition. *Japanese J. Appl. Phys.*, 35:L56–L59, 1996.

[100] I. Apostol and R. Stoian. Pulsed-laser deposition of thin-film process characterization by optical spectroscopy. *Opt. Eng.*, 35:1334–1338, 1996.

[101] A. Misra and R. K. Thareja. Laser ablation deposition of metal oxides/nitrides films at room temperature. *J. Appl. Phys*, 86:3438–3441, 1999.

[102] V. Khomchenko et al. Laser processing and characterization of ZnS-Cu thin film. *Appl. Sur. Sci.*, 247:434–439, 2005.

[103] S. J. Henley et al. The growth of transparent conducting ZnO films by pulsed laser ablation. *Surface and Coatings Technology*, 177-178:271–276, 2004.

[104] M. Okoshi et al. Optical waveguides fabricated by pulsed-laser deposition of SiO_2 films with different refractive indices. *Appl. Phys. Lett.*, 81:789–791, 2002.

[105] M. Park et al. Ultrafast laser ablation of indium tin oxide thin films for organic light-emitting diode application. *Optics and Lasers in Engineering*, 2005. In press.

[106] E. Cappelli et al. Surface characterisation of nano-structured carbon films deposited by Nd:YAG pulsed laser deposition. *Thin Solid Films*, 482:305–310, 2005.

[107] M. Vitiello et al. The emission of atoms and nanoparticles during femtosecond laser ablation of gold. *Appl. Sur. Sci.*, 248:163–166, 2005.

[108] S. Eggins et al. ^{238}U,^{232}Th profiling and U-series isotope analysis of fossil teeth by laser ablation-ICPMS. *Quaternary Science Reviews*, 22:1373–1382, 2003.

[109] M. V. Zoriy et al. Determination of uranium isotopic ratios in biological samples using laser ablation inductively coupled plasma double focusing sector field mass spectrometry with cooled abaltion chamber. *International J. of Mass Spectrometry*, 242:297–302, 2005.

[110] J. Porter et al. Separate effects of the microkeratome incision and laser ablation on the eye's wave aberration. *Am J Ophthalmol*, 136:327–337, 2003.

[111] J. F. Friichtenicht. Laser-generated pulsed atomic beams. *Rev. Sci. Instrum.*, 45:51–56, 1974.

[112] E. S. Marmar et al. System for rapid injection of metal atoms into plasmas. *Rev. Sci. Instrum.*, 46:1149–1154, 1975.

[113] C. Breton et al. Low energy neutral beam production by laser vaporization of metals. *Revue Phys. Appl.*, 15:1193–1200, 1980.

[114] R. Viswanathan and Ingo Hussla. Ablation of metal surfaces by pulsed ultraviolet lasers under ultrahigh vacuum. *J. Opt. Soc. Am. B*, 3:796–800, 1986.

[115] J.S. Bakos et al. Absolute measurement of velocity distribution of neutrals in sodium laser blow-off beam. *Optics Communications*, 74:374–379, 1990.

[116] H. Chae and S. M. Park. Expansion dynamics of laser-generated Si atomic beam. *Bull. Korean Chem. Soc.*, 18:448–450, 1997.

[117] A. B. Bullock and P. R. Bolton. Laser-induced back ablation of aluminium thin films using picosecond laser pulses. *J. Appl. Phys.*, 85:460–465, 1999.

[118] M. A. Kadar-Kallen and K. D. Bonin. Generation of dense, pulsed beams of refractory metal atoms using two-stage laser ablation. *Appl. Phys. Lett.*, 64:1436–1438, 1994.

[119] J. Gonzalo et al. Influence of laser energy density on the plasma expansion dynamics and film stoichiometry during laser ablation of BiSrCaCuO. *J. Appl. Phys.*, 79:8042–8046, 1996.

[120] S. M. Park and J. Y. Moon. Laser ablation of $YBa_2Cu_3O_{7-x}$: the wavelength dependence. *Appl. Phys. A Materials Science and Processing*, 69:S695–S698, 1999.

[121] J. F. Ready. Effect of high power laser radiation. *Academic, New York*, 1971.

[122] A. M. Prokhrov et al. Laser heating of materials. *Alan Hilger Bristol*, 1990.

[123] S. Amoruso. Modeling of UV pulsed-laser ablation of metallic targets. *Appl. Phys. A Materials Science and Processing*, 69:323–332, 1999.

[124] M. A. Kadar-Kallen and K. D. Bonin. Focusing of particle beams using two-stage laser ablation. *Appl. Phys. Lett.*, 54:2296–2298, 1989.

[125] O. B. Anan'in et al. Investigation of laser plasma expansion in an ambient gas by high-speed photography. *Sov. J. Quantum Electron.*, 21:787–789, 1991.

[126] I. Weaver and C. L. S. Lewis. Polar distribution of ablated atomic material during the pulsed laser deposition of Cu in vacuum: Dependence on focused laser spot size and power density. *J. Appl. Phys.*, 79:7216–7222, 1996.

[127] A. Misra and R. K. Thareja. Investigation of laser ablated plumes using fast photography. *IEEE Transactions on Plasma Science*, 27:1553–1558, 1999.

[128] G. Gal et al. Velocity angular distribution of ground level atomic silicon in the plume of laser ablated silica. *J. Appl. Phys.*, 89:1927–1932, 2001.

[129] K. Alti and A. Khare. Generation of cold low divergent atomic beam of indium by laser ablation. Communicated.

[130] A. S. Patra and A. Khare. Interferometric array generation. *Opt. & Laser Tech.* In Press.

[131] www.urenco.com. Manufacturer of enriched uranium for the nuclear power utilities worldwide.

[132] M. Oba et al. Isotope shift and hyperfine structure of the highly excited atomic uranium. *Eur. Phys. J. D*, 21:255–260, 2002.

[133] http://physics.nist.gov/PhysRefData/Handbook/Tables/uraniumtable3.html. National institute of standards and technology (NIST) website.

[134] A. Camposeo et al. A laser-cooled atom beam for nanolithography applications. *Mat. Sci. and Eng. C*, 23:217–220, 2003.

[135] T. Kubota and M. Takeda. Array illuminator using grating couplers. *Opt. Lett.*, 14:651–652, 1989.

[136] P. K. Wu et al. Time-of-flight study of the ionic and neutral particles produced by pulsed-laser ablation of frozen glycerol. *J. Appl. Phys.*, 90:3623–3631, 2001.

[137] P. L. G Ventzek et al. Laser-beam deflection measurements and modeling of pulsed laser ablation rate and near-surface plume densities in vacuum. *J. Appl. Phys.*, 70:587–593, 1991.

[138] T. X. Phuoc. An experimental and numerical study of laser-induced spark in air. *Optics and Lasers in Engineering*, 43:113–129, 2005.

[139] M. Born and E. Wolf. Principles of optics. *Pergamon Press*. Sixth Edition.

[140] Swanson and Fuyat. *Natl. Bur. Stand. (U.S)*, Circ 539:12, 1954.

List of Publications

Journal Publications

1. Alika Khare, **Kamlesh Alti**, Susanta Das, Ardhendu Sekhar Patra and Monisha Sharma, "Application of laser matter interaction for generation of small sized materials", J. Radiation Physics and Chemistry, **Vol 70** 4-5, (553) 2004.

2. **Kamlesh Alti** and Alika Khare, "Generation of cold low divergent atomic beam of indium by laser ablation," Review of Scientific Instruments (In Press).

3. **Kamlesh Alti**, Ardhendu Sekhar Patra and Alika Khare, "Two dimensional periodic potentials via multiple beam interferometry for atom lithography," Journal of Microlithography Microfabrication and Microsystems (In Press).

4. **Kamlesh Alti** and Alika Khare,"Low-energy low-divergence pulsed indium atomic beam via laser ablation," Laser and Particle beams (In Press).

5. **Kamlesh Alti** and Alika Khare, "Simulated lithographic patterns for periodic arrays of atomic beams focused with a single atomic lens," (Revised).

6. **Kamlesh Alti** and Alika Khare, "A novel single shot technique for micro-nano patterning in single step via selective laser ablation," (Submitted).

7. **Kamlesh Alti** and Alika Khare, "Sculpted pulsed Indium atomic beams via selective laser ablation of thin film (Submitted).

8. **Kamlesh Alti** and Alika Khare, "Discrete arrays of atomic beams for sub-$\lambda/2$ lithography via dipole force," (Submitted).

9. **Kamlesh Alti** and Alika Khare, "High power laser interferometry for micro and nano lithography," (under preparation).

10. A. S Patra, **Kamlesh Alti** and Alika Khare, "Patterning of micro-nano lines/dots of indium in single step lithography via selective laser ablation in air," (under preparation).

National and International Conference Publications

1. **Kamlesh Alti** and A. S. Patra and Alika Khare, "A novel technique of direct patterning via high power laser interfreometry" accepted in International Conference on Optics & Optoelectronics, ICOL-2005 (XXXI Symposium of Optical Society of India) Instruments Research and Development Establishment Dehradun, Uttaranchal (INDIA) 12-15 December 2005.

2. **Kamlesh Alti** and Alika Khare, "Measurement of axial velocities of atomic and ionic species produced by laser ablation of indium thin film," presented at Fourth DAE-BRNS National laser symposium (NLS-4), Mumbai, India, 10-13 Jan., 2005.

3. **Kamlesh Alti**, Ardhendu Sekhar Patra and Alika Khare, "Simulated lithographic patterns from a single atomic beam in two dimensional periodic potential generated via interference of four optical beams," presented at Photonics-2004, Seventh International conference on Optoelectronics, Fiber optics and Photonics, Cochin, India,8-11 Dec., 2004.

4. **Kamlesh Alti**, Susanta Das, Bulumani Kalita, Pratima Agarwal and Alika Khare, "Low divergence atomic beam using laser ablation of thin film," presented at Photonics-2004, Seventh International conference on Optoelectronics, Fiber optics and Photonics, Cochin, India,8-11 Dec., 2004.

5. **Kamlesh Alti** and Alika Khare,"Computed lithographic patterns using new configuration of atomic beams," proc. Golden Jubilee DAE-BRNS National laser symposium Ed. by A.K. Nath, K.S. Bartwal, Allied Publishers, pp. 593-594 (2003).

6. **Kamlesh Alti** and Alika Khare, "Atomic trajectories in presence of dipole force for thermal and super thermal beams," presented at Photonics-2002, Sixth International Conference on Optoelectronics, Fiber optics and Photonics, Mumbai, India, 16-18 Dec., 2002.